

Title	Control of the magnetic plproperties in the perovskite-type oxide artificial superlattices
Author(s)	Ueda, Kenji
Citation	大阪大学, 2000, 博士論文
Version Type	VoR
URL	https://doi.org/10.11501/3169124
rights	
Note	

Osaka University Knowledge Archive : OUKA

<https://ir.library.osaka-u.ac.jp/>

Osaka University

博士論文

ペロブスカイト型酸化物人工超格子による
磁気特性制御の研究

**Control of the magnetic properties in the
perovskite-type oxide artificial superlattices**

The Institute of Scientific and Industrial Research
Osaka University

植田 研二

Kenji Ueda

①

ペロブスカイト型酸化物人工超格子による
磁気特性制御の研究

**Control of the magnetic properties in the
perovskite-type oxide artificial superlattices**

Dissertation

Submitted to Department of Chemistry, Osaka University
for the Degree of Doctor of Science

March 2000

The Institute of Scientific and Industrial Research
Osaka University

Kenji Ueda

Contents

Chapter 1 General introduction	1
1.1 General introduction	2
1.2 Perovskite-type oxides	5
1.3 References	7
Chapter 2 Experimental apparatus	9
2.1 Pulsed laser deposition technique for the formation of thin film	10
2.1-1 Characteristic features of pulsed laser ablation technique	10
2.2 References	12
Chapter 3 Control of atomic arrangement and magnetic properties in LaFeO₃-LaCrO₃ artificial superlattices	15
3.1 Ferromagnetism in LaCrO ₃ -LaFeO ₃ superlattices	16
3.1-1 Introduction	16
3.1-2 Experimental	17
3.1-3 Results and Discussion	18
3.1-4 Conclusions	20
3.1-5 References	21
3.2 Artificial control of spin order and magnetic properties in LaCrO ₃ - LaFeO ₃ superlattices	26
3.2-1 Introduction	26
3.2-2 Experimental	28
3.2-3 Results and Discussion	29
3.2-4 Conclusions	34
3.2-5 References	35
Chapter 4 Atomic arrangement and magnetic properties of LaFeO₃-LaMnO₃ artificial superlattices	51
4-1 Introduction	52
4-2 Experimental	54
4-3 Results and Discussion	54

4-4	Conclusions	62
4-5	References	64
Chapter 5 Low dimensional magnets in (110) superlattices		76
5.1	Control of the magnetic and electric properties of low dimensional SrRuO ₃ -BaTiO ₃ superlattices	77
5.1-1	Introduction	77
5.1-2	Experimental	80
5.1-3	Results and Discussion	81
5.1-4	Conclusions	85
5.1-5	References	87
Chapter 6 General conclusions		101
Chapter 7 Appendix		105
7.1	Coexistence of ferroelectricity and ferromagnetism in BiFeO ₃ -BaTiO ₃ thin films at room temperature	106
7.1-1	Introduction	106
7.1-2	Experimental	107
7.1-3	Results and Discussion	108
7.1-4	Conclusions	111
7.1-5	References	113
List of publications		121
Acknowledgements		125

1.1 General Introduction

A large part of the progress of modern semiconductor technology is due to the development of new materials and structures.

Chapter 1

General introduction

The development of new materials and structures has led to the development of new devices and circuits.

The development of new materials and structures has led to the development of new devices and circuits.

The development of new materials and structures has led to the development of new devices and circuits.

The development of new materials and structures has led to the development of new devices and circuits.

The development of new materials and structures has led to the development of new devices and circuits.

The development of new materials and structures has led to the development of new devices and circuits.

The development of new materials and structures has led to the development of new devices and circuits.

The development of new materials and structures has led to the development of new devices and circuits.

The development of new materials and structures has led to the development of new devices and circuits.

The development of new materials and structures has led to the development of new devices and circuits.

The development of new materials and structures has led to the development of new devices and circuits.

The development of new materials and structures has led to the development of new devices and circuits.

The development of new materials and structures has led to the development of new devices and circuits.

1.1 General Introduction

It is one of the dreams of material scientists to make new materials by the control of the arrangements of ions with an atomic or molecular scale. The concept of "superlattices" which is proposed by Esaki and Tsu [1] is one of the ways to achieve this dream. By this method one can make materials that do not exist in nature. The composition of the material is periodically changed by depositing several unit layers of materials alternately with an atomic or molecular scale. A lot of novel materials have been formed by this method of the artificial superlattice and this method can be applied to various fields. The giant magnetoresistance (GMR) effect was observed in metal superlattices [2], and new transistor called high electron mobility transistor (HEMT) [3], has been developed and put into practical use in the field of semiconductor superlattices.

However, in the field of metal oxides (ceramics), the artificial superlattice method is in its preliminary stage and has just started. This is because there are problems such as the control of valence, diversity of constitutions and so on. Recently, it has been become possible to make thin films of metal oxides by controlling the atomic arrangement on an atomic or molecular scale using pulsed laser deposition (PLD) method combined with reflection high energy electron diffraction (RHEED) [4-5].

Actually, Tabata et al. succeeded in forming new materials that have large dielectric constants by making the artificial superlattices with the deposition of perovskite-type ferroelectric oxides (BaTiO_3) and dielectric oxides (SrTiO_3) layers alternately with an atomic or molecular scale so as to introduce lattice strain artificially at the interface [6]. Also in the field of magnetism, artificial superlattices of manganese oxides which show large colossal magnetoresistance (CMR) effect was made [7-12].

Until now, almost all the artificial superlattices of perovskite-type materials have been epitaxially formed on the perovskite-type substrates such as SrTiO_3 (100) substrate, LaAlO_3 (100) substrate, etc., which have the same perovskite-type crystal structure as that of its films deposited [7-12]. The control of stacking direction, which is well used in semiconductor artificial superlattices, has not been performed in the perovskite-type superlattices. This means that the control of stacking has been performed only in one direction ($\langle 001 \rangle$ direction).

In my research, I have tried to form novel magnetic materials by the method of the artificial superlattice combined with the control of stacking directions in perovskite-type material.

In chapter 2, the method of pulsed laser deposition (PLD) is briefly described as a

technique for the film formation. In chapter 3, the attempt to construct new magnetic materials (LaFeO_3 - LaCrO_3 superlattices) by the method of the artificial superlattice combined with the control of stacking directions is reported. Especially, the double perovskite structure (NaCl - type structure of Fe and Cr ions) were obtained in the superlattice formed on SrTiO_3 (111) substrate with one-layer by one-layer sequence, and the material showed ferromagnetism for the first time. Though the total number of magnetic ions (Fe and Cr) are same in (100), (110) and (111) superlattices, quite different magnetic properties can be created in the artificial superlattices. In chapter 4, the concept of artificial introduction of the spin frustration effect is reported. The spin-glass like state which is caused by the frustration effect between antiferromagnetic and ferromagnetic layers is observed. In chapter 5, the proposal for the formation of low dimensional perovskite-type magnetic materials is given. The anisotropy of perovskite (110) surfaces was taken into account and I tried to form one-dimensional magnets by the formation of magnetic-nonmagnetic artificial superlattices on SrTiO_3 (110) substrates. The low dimensional effects has appeared remarkably in the two layers by five layers magnetic-nonmagnetic superlattice.

I have also established the relation between the position of spin and the magnetic properties by creating superlattices of two magnetic layers, where the nearest neighbor

interactions between the layers determine the physical properties, with control of the stacking direction.

1.2 Perovskite-type oxides

The crystal structure of perovskite-type oxides (ABO_3) is shown in Figure 1-1. Its physical properties largely depends on its electronic state of its B-site ions. For example, in 3d transition metal oxides (strongly correlated electron system), the material that includes Ti or V at the B-site (eg. $BaTiO_3$, $SrTiO_3$, Bi_2VO_5 , etc.) shows dielectricity (or ferroelectricity), that includes Mn or Fe (eg. $La_{1-x}Sr_xMnO_3$, $La_{1-x}Sr_xFeO_3$ etc.) shows ferromagnetism, and that includes Cu (eg. $YBa_2Cu_3O_{7-\delta}$, $La_{1-x}Sr_xCuO_4$ etc.) shows superconductivity.

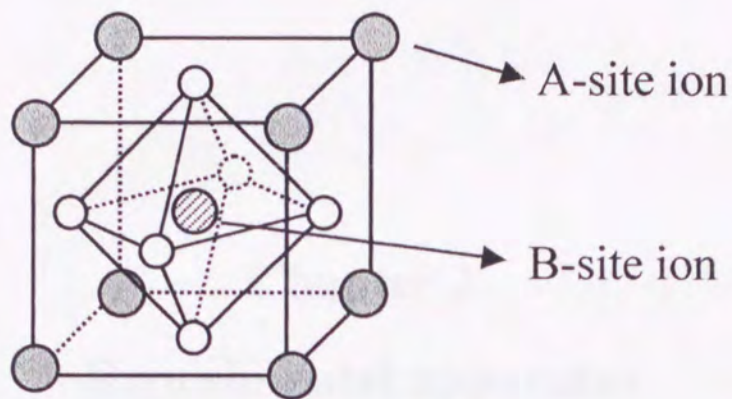
A-site ions, on the other hand, play important role in controlling the valence of B-site ions and the overlap of orbitals, that is one-electron band width, of each B-site ions.

The perovskite-type structure is firm to the substitution of A- and B-site ions and the crystal structure remains almost same. That is, it is easy to change the number of electrons and the correlation strength of electron by the selection of proper ions without changing the crystal structure in perovskite-type materials.

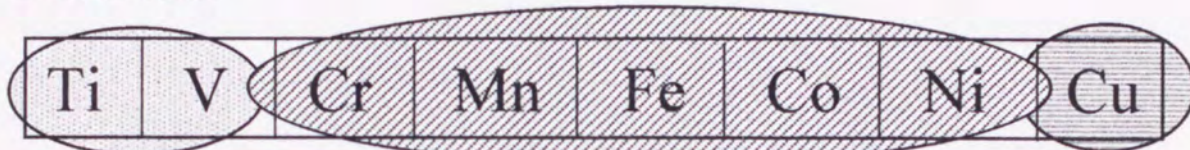
Due to the similarity of the crystal structure and various physical properties of perovskite-type oxides, attempts have been made to make novel materials using the method of the artificial superlattice by combining two (or several) of these materials as described in this chapter.

1.3 References

- [1] L. Esaki and R. Tsu, IBM J. Res. Develop **14**, 61 (1970).
- [2] M. N. Baibich, et al., Phys. Rev. Lett. **61**, 2472 (1988).
- [3] T. Mimura, S. Hiyamizu, T. Fujii and K. Nanbu, Jpn. J. Appl. Phys. **19**, L225 (1980).
- [4] M. Kanai, T. Kawai and S. Kawai, Appl. Phys. Lett. **65**, 1970 (1994).
- [5] M. Yoshimoto et al., Physica C, **190** (1991) 43.
- [6] H. Tabata, H. Tanaka and T. Kawai, Appl. Phys. Lett. **65**, 1970 (1994).
- [7] H. Tanaka and T. Kawai, Solid State Comm. **112**, 201 (1999).
- [8] G. Q. Gong et al., Phys. Rev. B **54**, R3742 (1996).
- [9] M. Izumi et al., Phys. Rev. B **60**, 1211 (1999).
- [10] G. Jakob, V. V. Moshchalkov, and Y. Bruynseraede, Appl. Phys. Lett. **66**, 2564 (1995).
- [11] K. R. Nikolaev, et al., Appl. Phys. Lett. **75**, 118 (1999).
- [12] M. Sahana, M. S. Hegde, V. Prasad and S. V. Subramanyam, Appl. Phys. Lett. **85**, 1058 (1999).



B-site ions



(ferro)electrics
 $\text{BaTiO}_3, \text{SrTiO}_3,$
 $\text{Pb}(\text{Zr}, \text{Ti})\text{O}_3 \dots$

(ferro)magnets
 $(\text{La}, \text{Sr})\text{MnO}_3$
 $(\text{La}, \text{Sr})\text{FeO}_3 \dots$

superconductors
 $(\text{La}, \text{Sr})\text{CuO}_4 \dots$

Figure 1-1 Schematic illustrations of the crystal structure of perovskite oxides (ABO_3).

2.1. Pulsed laser deposition technique for the formation of thin films

Chapter 2

Experimental apparatus

The experimental apparatus used for the deposition of thin films by pulsed laser deposition is shown in Figure 2.1. An Nd:YAG laser beam (wavelength 1064 nm) is focused on the target to ablate it, and the ablated species and ions are deposited on the substrate. The PLD technique has several advantages, such as the possibility of depositing films of various compositions (O₂, N₂, Ar etc.) because the laser light is focused from outside of the chamber. The vacuum degree of the chamber and the substrate temperature are controlled by a computer.

The schematic diagram of the experimental apparatus is shown in Figure 2.1. An Nd:YAG laser beam (wavelength 1064 nm) is focused on the target to ablate it, and the ablated species and ions are deposited on the substrate. The PLD technique has several advantages, such as the possibility of depositing films of various compositions (O₂, N₂, Ar etc.) because the laser light is focused from outside of the chamber. The vacuum degree of the chamber and the substrate temperature are controlled by a computer.

2.1 Pulsed laser deposition technique for the formation of thin films

2.1-1 The characteristic features of pulsed laser ablation technique

In these studies, the pulsed laser ablation (PLD) technique has been used to make transition metal oxides films and superlattices. The PLD technique is one of the most effective film formation technique to make materials such as metal oxides that includes several elements. Smith and Tuner [1] first applied this PLD technique to make thin films in 1965 and the success for making superconducting films provides new development in this field. The technique have been widely applied to form variety of materials such as high T_C superconductors, ferroelectric and ferromagnetic materials, III-V (II-VI) semiconductors, and so on [2-7].

The schematic diagram of laser ablation phenomena is shown in Figure 2-1. An ArF excimer laser pulse ($\lambda = 193\text{nm}$) is focused on the targets to induce ablation, and the ablated atoms and ions are deposited on the substrates. The PLD technique has several merits ; 1, It is possible to form films in various atmospheres (O_2 , N_2 , Ar etc.) because the laser light is introduced from outside of the chamber. 2, The excess energy of ablated ions and atoms are effective to make high quality films. 3, It is

possible to make even films with several elements and high melting points in exact stoichiometry.

The schematic diagram of the apparatus for PLD is shown in Fig. 2-2. An ArF excimer laser pulse ($\lambda = 193$ nm) was focused on the targets, which are sintering pellets placed at the center of the chamber, to induce ablation and the ablated atoms and ions are deposited on the substrates. The energy density of the pulsed laser beam was 0.5 – 1.5 mJ/cm². The substrate is heated by flowing electric current to Si (or PBN) heater. The film thickness was monitored by a quartz crystal oscillator during the film formation. An atomic scale control of crystal growth to make artificial superlattices is also possible using the PLD method combined with in situ reflection high energy electron diffraction (RHEED) observations. The details of experimental setup will be described in each chapter.

2.2 References

- [1] H. M. Smith and A. F. Turner Appl. Opt. **4**, 147 (1965).
- [2] D. B. Chrisey and G. K. Hubler Pulsed Laser Deposition of Thin Films (John Wiley & Sons, Inc., (1994))
- [3] S. Jin et al. Science **264**, 413 (1994)
- [4] G. Q. Gong, A. Gupta, Gang Xiao, P. Lecoeur and T. R. McGuire, Phys. Rev. B **54**, R3742 (1996).
- [5] M. Yoshimoto, H. Nagata, S. Gonda, J. P. Gong, H. Ohkubo and H. Koinuma, Physica C, **190** (1991) 43.
- [6] H. Tabata, H. Tanaka and T. Kawai, Appl. Phys. Lett. **65**, 1970 (1994).
- [7] H. -M. Christen, L. A. Boatner, J. D. Budai, M.F. Chisholm, L. A. Gea, P. J. Marrero, and D. P. Norton Appl. Phys. Lett. **68**, 1488 (1996).

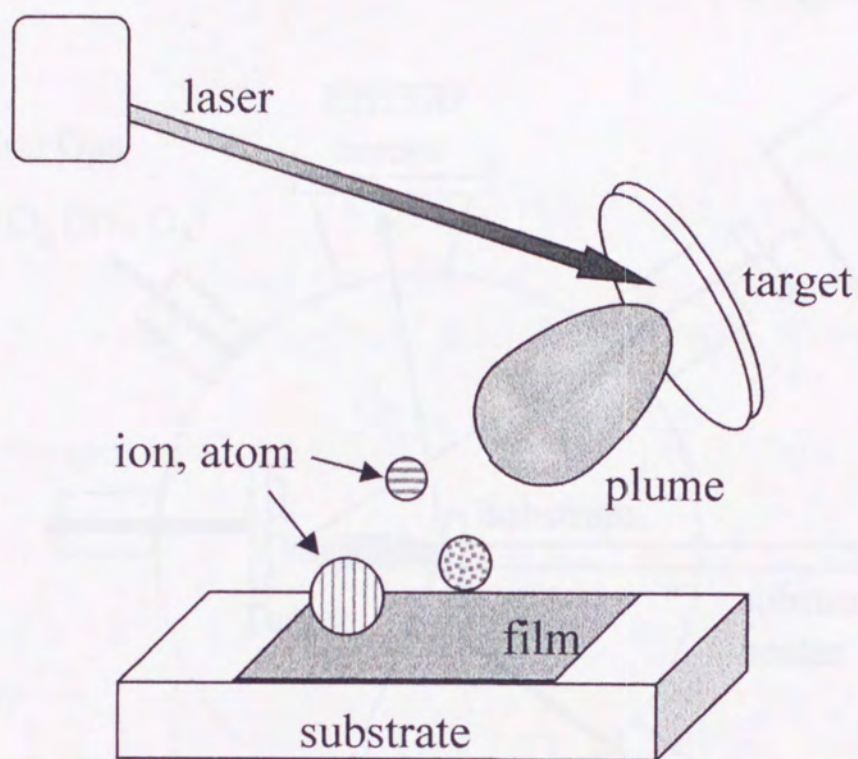


Figure 2-1 Schematic diagram of laser ablation phenomena

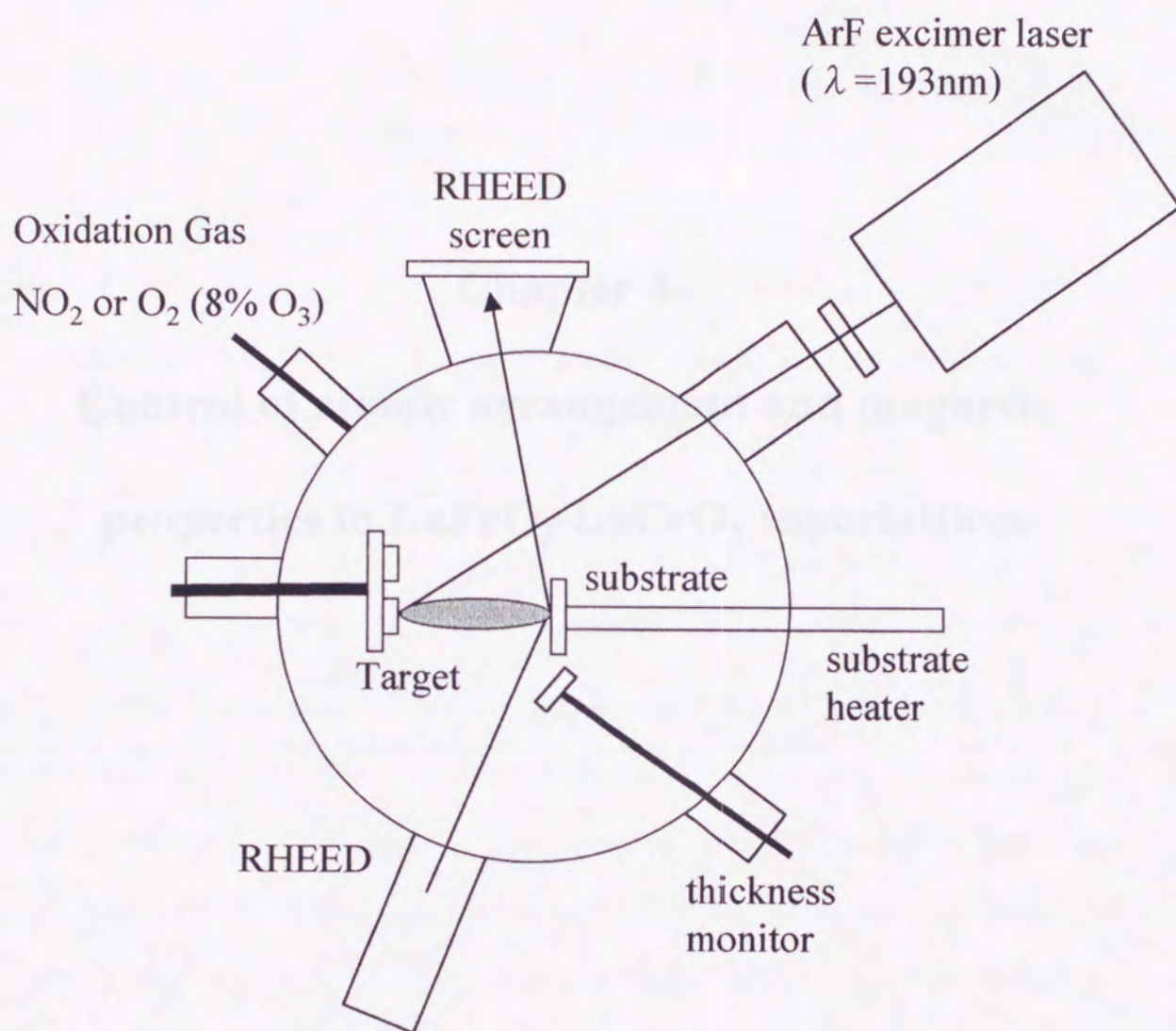


Figure 2-2 Schematic diagram of experimental apparatus for pulsed laser deposition method.

3.1. Crystal structure of $\text{LaFeO}_3\text{-LaCrO}_3$ superlattices

3.2. Crystal structure of $\text{LaFeO}_3\text{-LaCrO}_3$ superlattices

Figure 3.1 shows the crystal structure of the $\text{LaFeO}_3\text{-LaCrO}_3$ superlattice. The structure is based on the perovskite structure of LaFeO_3 and LaCrO_3 . The lattice parameters are $a = b = c = 3.85 \text{ \AA}$. The structure is shown in Figure 3.1.

Chapter 3

Control of atomic arrangement and magnetic properties in $\text{LaFeO}_3\text{-LaCrO}_3$ superlattices

3.1. Introduction

The crystal structure of the $\text{LaFeO}_3\text{-LaCrO}_3$ superlattice was first proposed by Kikkawa [1] and was synthesized by Ishizuka [2]. Later, the crystal structure of the superlattice was studied by Gotoh et al. [3] and Kikkawa [4]. It is well known that the crystal structure of the superlattice is strongly affected by the growth conditions. In this study, we will report the crystal structure of the superlattice synthesized by the solid solution method. The crystal structure of the superlattice was studied by X-ray diffraction (XRD) and electron diffraction (ED). The XRD pattern of the superlattice is shown in Figure 3.2. The XRD pattern shows a sharp peak at $2\theta = 20^\circ$, which corresponds to the (111) reflection of the superlattice. The ED pattern of the superlattice is shown in Figure 3.3. The ED pattern shows a square lattice of spots, which is characteristic of the perovskite structure. The lattice parameters of the superlattice are $a = b = c = 3.85 \text{ \AA}$. It is expected that the Fe^{3+} and Cr^{3+} ions are arranged alternately in the B site of perovskite-type structure.

3.1 Ferromagnetism in LaCrO₃-LaFeO₃ superlattices

Ferromagnetic spin order has been realized in the LaCrO₃-LaFeO₃ superlattices. Ferromagnetic coupling between Fe³⁺ and Cr³⁺ through oxygen has long been expected on the basis of Anderson, Goodenough, and Kanamori rules. Despite many studies have been made on Fe-O-Cr based compounds, random positioning of Fe³⁺ and Cr³⁺ ions has frustrated the observation of ferromagnetic properties. By creating artificial superlattice of Fe³⁺ and Cr³⁺ layer along [111] direction, ferromagnetic ordering has been achieved.

3.1-1 Introduction

A magnetic interaction between two magnetic ions through a nonmagnetic ion (such as oxygen) was first proposed by Kramers [1] and was systematized by Anderson [2]. Later, this so-called superexchange interaction, was refined by Goodenough [3] and Kanamori [4] at a level so that this theory can be applied to various magnetic materials. According to their rules, we can estimate and predict whether a magnetic interaction thorough superexchange interaction between two spins has a ferromagnetic (FM) or antiferromagnetic (AF) character. Many researchers have used this idea as a starting point for synthesizing ferromagnets. On the basis of these rules, the 180° superexchange interaction in a metal dimer bridged via oxygen that has a d³-d⁵ electron state ($\angle M-O-M=180^\circ$, M=Fe³⁺, Cr³⁺ etc) is predicted to have FM order [4]. The most typical and still unachieved combination is Fe-O-Cr systems [5]. It is expected that if Fe³⁺ and Cr³⁺ ions are introduced alternately in the B site of perovskite-type transition

metal oxides (ABO_3), the synthesis of FM materials can be achieved. Although some attempts to synthesize such materials have been made by sintering methods, the atomic order of Fe-O-Cr has not been achieved because such materials phase separate into Fe-oxide and Cr-oxide phases [6]. As a result a FM ordered phase has not been obtained, and the materials shown to have an AF character [7, 8].

The single phase $LaCrO_3$ and $LaFeO_3$ have AF structures with both inter- and intralayer antiparallel spin alignments and Neel temperatures (T_N) of 280K and 750K, respectively [9-11]. If an artificial superlattice of $LaCrO_3$ - $LaFeO_3$ is synthesized by depositing alternating layers of $LaCrO_3$ and $LaFeO_3$ along the [111] direction, it may be possible to form films that have various magnetic properties by controlling the stacking periodicity. Ferromagnetism can occur especially in the case of one layer by one layer stacking on the (111) surface because Fe^{3+} and Cr^{3+} ions are bridged by oxygen ions alternately in the film (Fig. 3.1-1).

We have synthesized a FM artificial superlattice by alternately stacking one unit layer of $LaCrO_3$ and $LaFeO_3$ on a $SrTiO_3$ (111) single crystal using a laser molecular beam epitaxy (MBE) (Fig. 3.1-1). Such materials cannot be obtained in the conventional bulk phase because they are thermodynamically unstable [6-8]. Furthermore, even if phase separation is avoided so that Fe^{3+} and Cr^{3+} ions mix randomly, AF interactions are dominant in the material because Fe^{3+} -O- Cr^{3+} ordered phase could not be achieved statistically. An artificial superlattice is a powerful tool for synthesizing these new materials [12].

3.1-2 Experimental

The magnetic superlattices were constructed as follows. The $LaCrO_3$ and $LaFeO_3$

layers were stacked by multi target pulsed laser deposition (PLD) (Fig. 3.1-1) Targets of LaCrO_3 and LaFeO_3 were synthesized by mixing La_2O_3 with Cr_2O_3 , and La_2O_3 with $\alpha\text{-Fe}_2\text{O}_3$, respectively at a mole ratio of 1:1 and sintering them at 1000 – 1200 °C.

An ArF excimer laser pulse is focused on the targets to induce ablation, and the ablated atoms and ions are deposited on the SrTiO_3 (111) substrate. Atomic-scale control of the crystal growth could be achieved by combining the PLD method with reflection-high-energy electron diffraction (RHEED) observations [12, 13]. The distance between the Fe and Cr layers was varied from 2.3 Å (1 unit layer) to 16.1 Å (7 unit layers), and the total thickness of the superlattices was 600~1100 Å. The films were formed at 580 – 600 °C in an oxygen/ozone (8%) ambient pressure of 1mTorr. The deposition rate was 10 – 15 Å/min. All magnetic measurements were performed using a SQUID magnetometer (Quantum design MPMS-5S).

3.1-3 Results and Discussion

X-ray diffraction measurements of $\text{LaCrO}_3\text{-LaFeO}_3$ superlattices in each stacking periodicity exhibit characteristics of artificial structures (Fig. 3.1-2). The distance of periodic layers (corresponding to the distance of Fe and Cr layer) is 2.29 Å, and the Full Width of Half Maximum is 0.28~0.20°, which indicates that our sample is well constructed as desired. The RHEED measurements of the $\text{LaCrO}_3\text{-LaFeO}_3$ artificial superlattices on $\text{SrTiO}_3(111)$ substrate showed streaked patterns, indicating that the films were formed epitaxially and highly crystallized up to the topmost surface.

The temperature dependence of magnetization for the $\text{LaCrO}_3\text{-LaFeO}_3$ artificial superlattices with a stacking periodicity of 1/1 layer on SrTiO_3 (111) is shown in Fig.

3.1-3. In this case, a magnetic field of 0.1 T was applied parallel to the surface of the substrate. FM transition is apparent at 375K. The magnetization of the LaCrO₃-LaFeO₃ superlattices increases with decreasing temperature. And, the saturation magnetization comes to ~ 60 emu/g (which corresponds to about 3 Bohr magnetons (μ_B) at one site). From the theoretical estimation, the magnetization value of $4 \mu_B$ /one-site would be expected due to the atomic order of Fe³⁺(d⁵)-O-Cr³⁺(d³) high spin state. Our experimental results are slightly less than the calculated one because of imperfections in the crystallinity and the atomic stacking sequence of the superlattices. The magnetization-temperature curve can be fitted with a relation of

$$M / M_0 = \alpha \left(\frac{T_c - T}{T_c} \right)^\beta$$

where M_0 is the saturated magnetization at $T=0$ and T_c is the Curie temperature, respectively. In the case of $\alpha=1.09$ and $\beta=0.33$, the curve is well reproduced. The value of $\beta=0.33$ is similar to that for a standard Heisenberg-type spin-spin coupling.

In the case of artificial superlattice with larger (>1unit layer) stacking periodicity, the FM interactions are introduced in the interface between Fe and Cr layer. Indeed, for the 7/7 layer superlattice, FM character was also observed, and showed magnetization of about $1 \mu_B$ per site. The magnetic moment per site is obtained by assuming that the ferromagnetism comes from the interfacial layers and that other inner layers that are not directly in contact with it do not contribute a spontaneous magnetization. This is further evidence of FM character of our superlattices.

As a reference, the M-T curve of the La(Fe_{0.5}Cr_{0.5})O₃ solid solution film in 0.1-T field

(Fig. 3.1-3) differs from that of the $\text{LaCrO}_3\text{-LaFeO}_3$ (1/1) superlattice. A cusp shape is observed at 320K, which is a typical feature of antiferromagnetism. A ferrimagnetism might also explain for the M-T character of the $\text{LaCrO}_3\text{-LaFeO}_3$ (1/1) superlattice. However, the magnetization value of $3 \mu_B$ per site is too large to attribute to a ferrimagnetic order. The dependence of magnetization on the magnetic field (hysteresis curve) of $\text{LaCrO}_3\text{-LaFeO}_3$ artificial superlattice (1/1 sequence) on substrate (111) is shown in Fig. 3.1-4. Hysteresis was observed in the M-H curves in the temperature region from 6 to 350 K. The magnetization is saturated under the applied field above 5kOe (Fig. 3.1-4B). In the enlarged hysteresis curve (Fig. 3.1-4A), the remnant magnetization of the superlattices decreases with increasing temperature up to 375K. Above a T_C of 375K, it shows a paramagnetic character. These features are typical of FM materials. Our results provide further evidence that the FM spin order is realized in the artificial lattice with a one by one layer stacking combination.

3.1-4 Conclusions

Ferromagnetic spin order has been realized in the $\text{LaCrO}_3\text{-LaFeO}_3$ superlattices formed on SrTiO_3 (111) substrates with 1/1 sequences. By creating artificial superlattice of Fe^{3+} and Cr^{3+} layer along [111] direction, ferromagnetic ordering has been achieved for the first time according to the basis of Anderson, Goodenough, and Kanamori superexchange theories.

3.1-5 References

- [1] H. A. Kramers *Physica* **1**, 182 (1934).
- [2] P. W. Anderson *Phys. Rev.* **79**, 350 (1950).
- [3] J. B. Goodenough *Phys. Rev.* **100**, 564 (1955).
- [4] J. Kanamori *J. Phys. Chem. Solids*, **10**, 87 (1959).
- [5] In the case of Ni^{2+} and Mn^{4+} or Co^{2+} and Mn^{4+} , FM ordering was reported in the bulk sample [G. Blasse, *J. Phys. Chem. Solids* **26**, 1969 (1965).]
- [6] A. Wold and W. Croft *J. Phys. Chem.* **63**, 447 (1959).
- [7] A. Belayachi, M. Nogues, J. -L. Dormann, and M. Taibi *Eur. J. Solid. State. Inorg. Chem.* **t.33**, 1039 (1996).
- [8] K. P. Belov, M. A. Belyanchikova, A. M. Kadomtseva, T. M. Ledneva, M. M. Lykina, T. L. Ovchinnikova and L. P. Shlyakhina *Sov. Phys. - Solid State* **14**, 813 (1972)
- [9] R. Aleorard, R. Pauthenet, J. P. Rebouillat and C. Veyret *J. Appl. Phys.* **39**, 379 (1968).
- [10] W. C. Koehler, E. O. Wollan and M. K. Wilkinson *Phys. Rev.* **118**, 58 (1960).
- [11] D. Treves *J. Appl. Phys.* **36**, 1033 (1965).
- [12] T. Kawai, M. Kanai and H. Tabata *Mater. Sci. Eng.* **B41**, 123 (1996).
- [13] H. Tabata, T. Kawai and S. Kawai *Phys. Rev. Lett.* **70**, 2633 (1993).

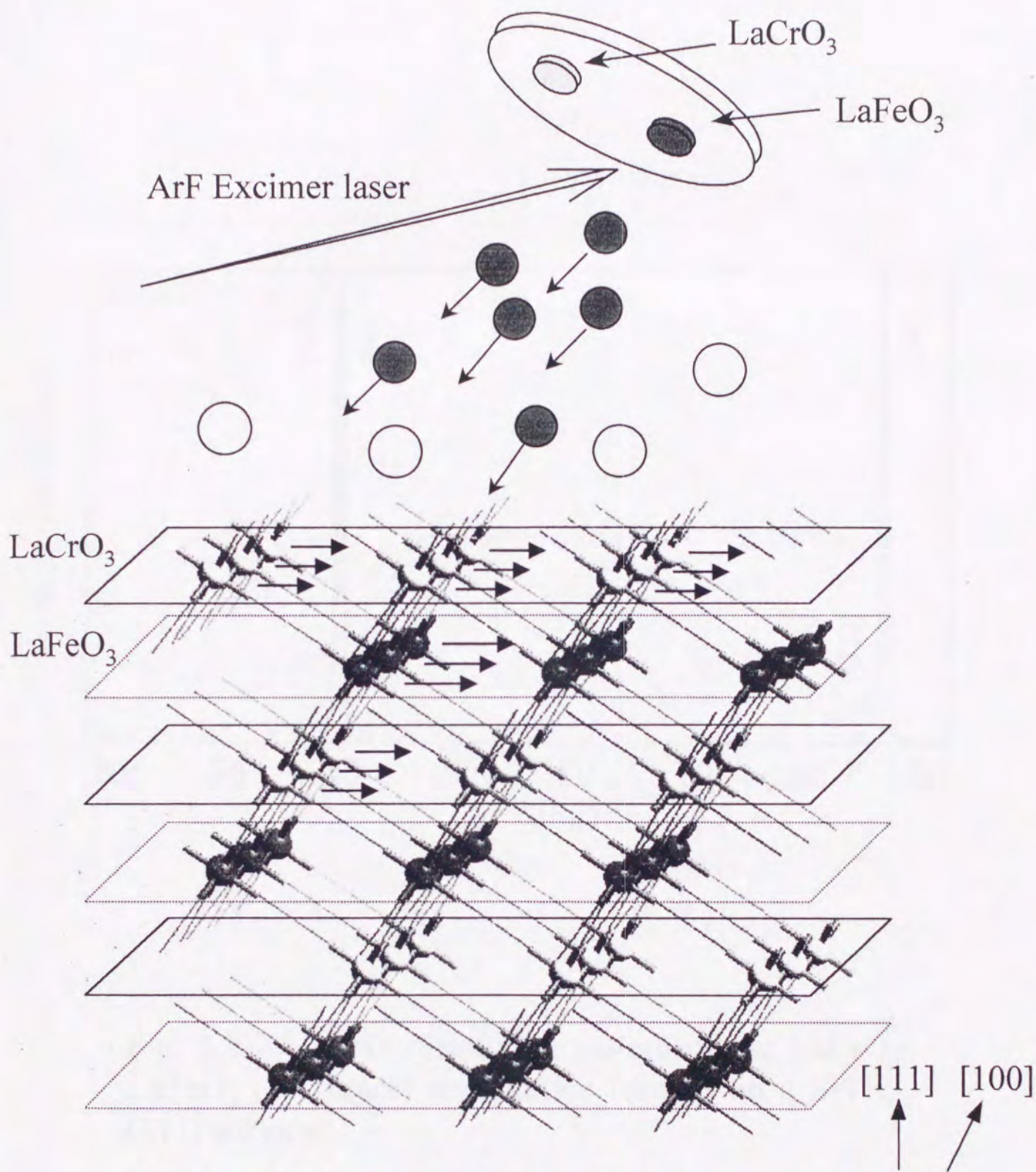


Fig. 3.1-1 : A schematic diagram for the construction of the LaCrO₃-LaFeO₃ superlattice along the [111] direction by the laser molecular beam epitaxy. The Cr layer and Fe layer are stacked alternately. For clarity, the atoms of oxygen and lanthanum have been omitted.

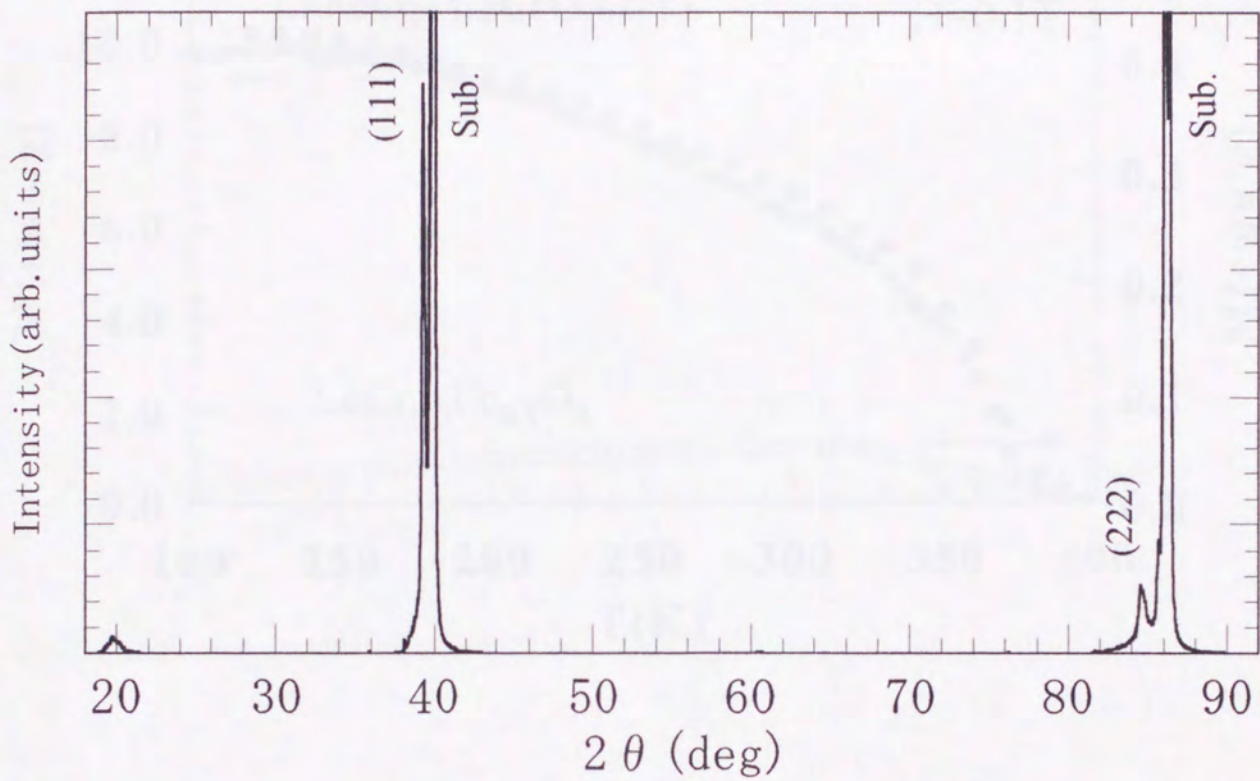


Fig. 3.2-2 : X-ray diffraction pattern of the LaCrO_3 - LaFeO_3 (1/1 layer) superlattice formed on a SrTiO_3 (111) substrate.

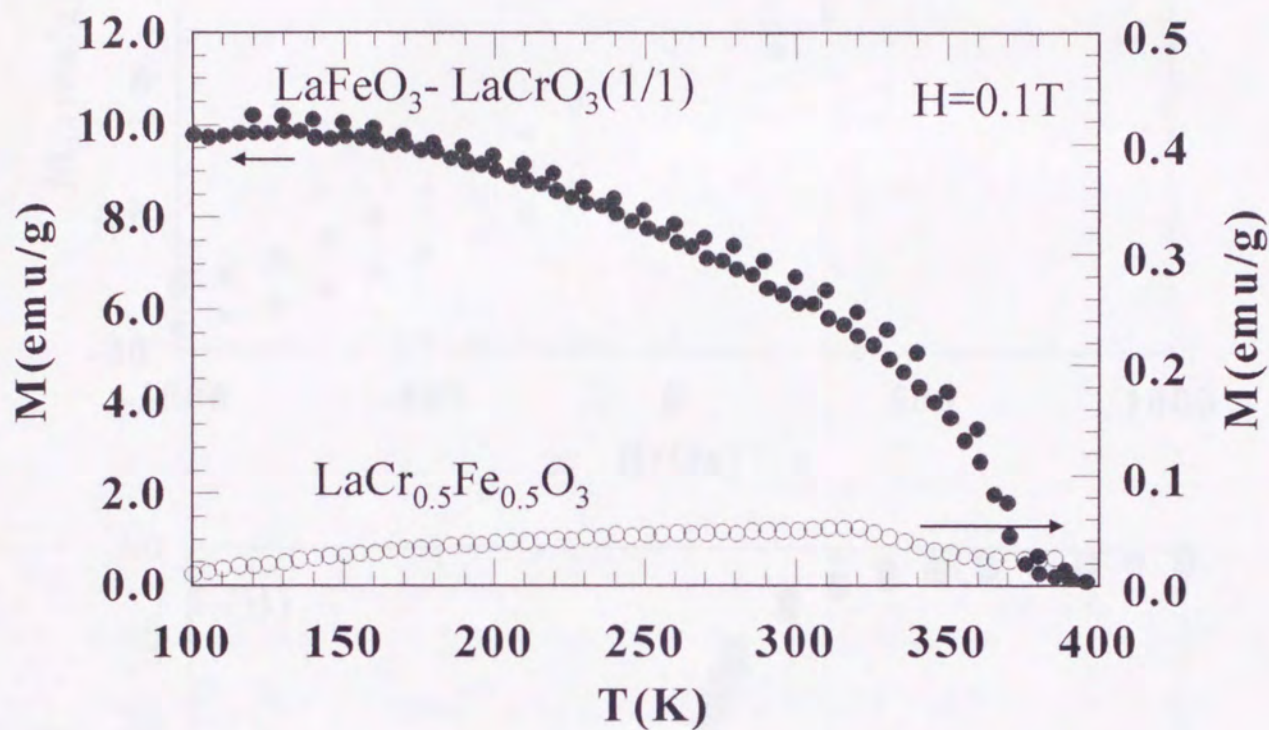


Fig. 3.2-3 : Temperature dependence of magnetization of $\text{LaCrO}_3\text{-LaFeO}_3$ superlattice on $\text{SrTiO}_3(111)$ (\bullet) and that of $\text{LaCr}_{0.5}\text{Fe}_{0.5}\text{O}_3$ solid solution film (\circ) measured in a 0.1-T magnetic field applied parallel to the surface of the substrate.

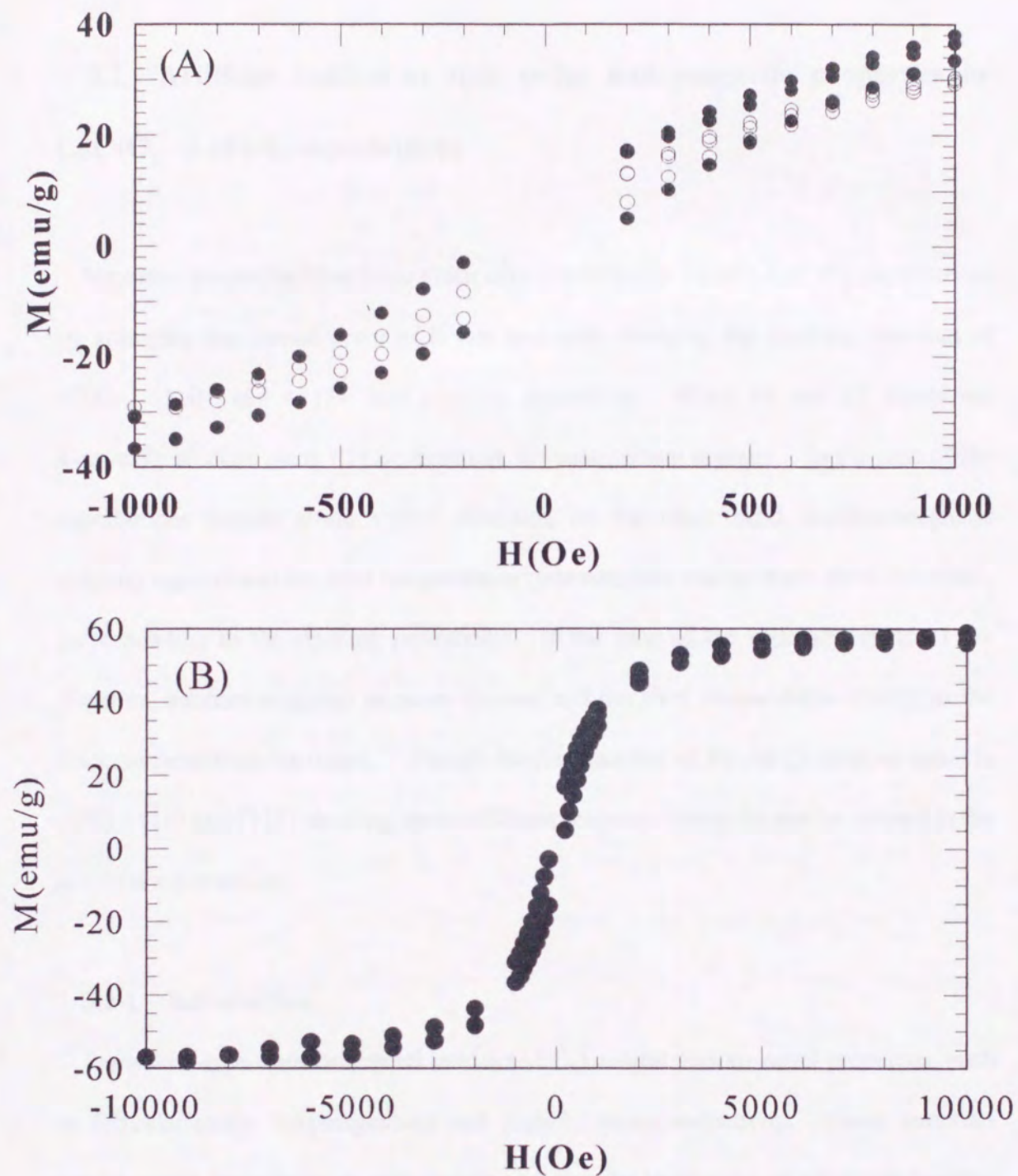


Fig. 3.2-4 : (A) Hysteresis curves for $\text{LaCrO}_3\text{-LaFeO}_3$ on $\text{SrTiO}_3(111)$ in the field range of ± 2000 Oe at 6K (●) and 350K (○). (B) Hysteresis curve at 6 K in the field range of ± 10 kOe. The magnetic field applied parallel to the film plane.

3.2 Artificial control of spin order and magnetic properties in LaCrO_3 - LaFeO_3 superlattices

Magnetic properties have been artificially controlled in LaFeO_3 - LaCrO_3 superlattices by arranging the atomic order of B site ions with changing the stacking direction of $\langle 100 \rangle$, $\langle 110 \rangle$ and $\langle 111 \rangle$ and stacking periodicity. When Fe and Cr layers are atomically stacked along $\langle 111 \rangle$ direction, ferromagnetism appears. In the case of the superlattices formed along $\langle 100 \rangle$ direction, on the other hand, antiferromagnetic property appears and the Neel temperatures systematically change from 250K to $>400\text{K}$, corresponding to the stacking periodicity. In the case of the superlattices of $\langle 110 \rangle$ direction, antiferromagnetic property appears and the Neel temperatures change as the stacking periodicity increases. Though the total number of Fe and Cr ions are same in (100), (110) and (111) stacking, quite different magnetic character can be created in the artificial superlattices.

3.2-1 Introduction

Perovskite-type transition metal oxides (ABO_3) exhibit various novel properties, such as ferroelectricity, ferromagnetism and high- T_c superconductivity. These materials can be grown layer-by-layer with atomic or molecular layer scale on substrates because they have similar lattice constants. Materials with unique properties are constructed by creating artificial superlattices through the combination of different perovskite-type transition metal oxides. Previously, we demonstrated the creation of new materials that have larger dielectric constants than $(\text{Ba}, \text{Sr})\text{TiO}_3$ film by introducing lattice strain

at the interface in artificial superlattice made of ferroelectric BaTiO₃ and dielectric SrTiO₃ layers [1].

It is possible to apply the method of creating artificial superlattices to form new magnetic materials with various magnetic structures by combining different magnetic layers. As is demonstrated in this study, materials with various spin structures can be constructed by the method of artificial superlattice with different orientations, making it possible to develop artificially controlled magnetism.

We have chosen LaCrO₃ and LaFeO₃ as starting materials. Both LaCrO₃ and LaFeO₃ have G-type magnetic structures (inter- and intralayer spin coupling are antiparallel), and their Neel temperatures (T_N) are 280K and 750K, respectively (Fig. 3.2-1) [2-4]. If an artificial superlattice is synthesized by depositing one layer each of LaCrO₃ and LaFeO₃ alternately on (111) substrate, it is possible to form a three-dimensionally ordered structure of Fe³⁺ and Cr³⁺ ions at the B-site. Theoretically, the synthesis of ferromagnetic materials is predicted to be possible when Fe³⁺ and Cr³⁺ ions are introduced alternately in the B site of perovskite-type transition metal oxides [5-6]. Not only the conventional superexchange mechanism but also our ab-initio molecular orbital (MO) calculations support these predictions, as will be described in this paper. Ferromagnetism was observed in the artificial superlattice with one-layer by one-layer sequence (1/1) on the (111) plane for the first time [7].

On the other hand, when the artificial superlattice of LaCrO₃ - LaFeO₃ is synthesized on the (100) plane with a 1/1 sequence, the ferromagnetic spin-ordered structure of Fe³⁺-O-Cr³⁺ is expected to form perpendicular to the substrate surface (along the direction of the c-axis). In contrast, in-plane (a-b plane) spins are ordered antiferromagnetically. The total magnetic structure of the superlattice should become C-type antiferromagnet

(interlayer spin coupling--parallel, intralayer spin coupling--antiparallel). The larger the stacking periodicity, the higher the T_N is expected due to the increment in the antiferromagnetic correlation. Therefore, the lowest Neel temperature is expected to be obtained in the 1/1 sequence superlattice on this (100) substrate.

In the case of (110) superlattice with 1/1 sequence, materials with A-type magnetic structure (interlayer spin coupling--antiparallel, intralayer spin coupling--parallel) can be obtained because the ferromagnetic spin-ordered structure of $\text{Fe}^{3+}\text{-O-Cr}^{3+}$ is expected to form only in a-b plane and same ions are aligned ($\text{Fe}^{3+}\text{-O-Fe}^{3+}$ or $\text{Cr}^{3+}\text{-O-Cr}^{3+}$) along the c-axis.

Based on this strategy, we control the spin order by arranging the atomic order in perovskite superlattices.

3.2-2 Experimental

Magnetic artificial superlattices were constructed as follows. The LaCrO_3 and LaFeO_3 layers were stacked using multi target pulsed-laser deposition (PLD) technique. An ArF excimer laser pulse was focused on the targets to induce ablation, and the ablated atoms and ions were deposited on the substrates (SrTiO_3 (100), (110) and (111), and LaAlO_3 (100)). The PLD technique is an excellent method that spatial and time conditions can be controlled. An atomic scale control of crystal growth is possible with the PLD method combined with reflection high energy electron diffraction (RHEED) observations [1, 8-9]. Targets of LaCrO_3 and LaFeO_3 were synthesized by mixing La_2O_3 with Cr_2O_3 , and La_2O_3 with $\alpha\text{-Fe}_2\text{O}_3$, respectively, at a molar ratio of 1:1 and sintering them at 1200 °C with intermediate grindings. Solid solution $\text{LaCr}_{0.5}\text{Fe}_{0.5}\text{O}_3$ films were also formed as reference samples. All the films were formed

at 580 - 600°C and an oxygen/ozone (8%) pressure of 1×10^{-3} Torr. The deposition rate was 10 - 20 Å/min. The total thickness of the film is 700 - 1000 Å. Magnetic measurements were performed using a superconducting quantum interference devices (SQUID) magnetometer (Quantum design MPMS-5S) with the magnetic field applied parallel to the film plane. Surface morphology was observed by atomic force microscopy (AFM ; Digital Instruments - Nanoscope III). Molecular orbital (MO) calculations were performed using the Gaussian 94 program.

3.2-3 Results and Discussion

The calculated results for the effective exchange integral (J_{ab}) of perovskite-type $M_2O_{11}(M=Fe^{3+}, Cr^{3+})$ clusters are shown in Fig. 3.2-2. When the J_{ab} is positive, the magnetic interaction has ferromagnetic character, and when it is negative, the magnetic interaction appears to be antiferromagnetic. In our calculation, the distance between metal and oxygen is fixed as 2.00 Å. The unrestricted Hartree-Fock (UHF) and density functional (B3LYP) method was employed to estimate the J_{ab} value. The basis sets used were Huzinaga's [10] supplemented by the 4p atomic orbital (AO) with the same exponent as that for 4s AO. The J_{ab} values were calculated according to Yamaguchi et al.'s treatment [11].

From our calculation, the interaction of $Fe^{3+}-O-Cr^{3+}$ is estimated to be ferromagnetic ($J>0$) within the bond angle range ($\angle M-O-M$) from 150° to 180° [Fig. 3.2-2 (a)]. This range is reasonable for perovskite-type crystal structures. In the case of the $Fe^{3+}-O-Fe^{3+}$ calculation, on the other hand, J_{ab} has a negative value in the same bond angle range [Fig. 3.2-2 (b)]. These results are consistent with the theoretical predictions by

Kanamori [5] and Goodenough [6]. In both cases, however, the absolute value of J_{ab} increases with increase in the bond angle (from 150° to 180°) because the bandwidth of one electron is expected to increase as the bond angle is increased toward 180° . Therefore, the superexchange coupling increases due to this tendency, which is in good agreement with the experimental results for the Mn-O-Mn system reported by Hwang et al. [12].

The crystal structures of the LaCrO_3 - LaFeO_3 superlattices have been confirmed by X-ray diffraction (XRD). All the superlattices on the (100) substrate have a single phase c-axis orientation. Typical features of superlattices are observed in our superlattices. In the case of the 1/1 superlattice, small peaks are observed at $2\theta = 11.8^\circ$ and 36° due to the long periodic feature [Fig. 3.2-3 (a)]. The intensity and diffraction angle are explained by the small differences in the scattering factor (several percent) between the Fe and Cr ions. The XRD patterns of the 1/1 superlattice agree well with our calculated patterns [Fig. 3.2-3 (b)]. In the XRD patterns of superlattices with 13/13 sequences, superstructures were also observed as the combination of main peaks with satellite peaks [Fig. 3.2-3 (c), (d)]. The satellites prove the periodic structure and/or chemical modulation, with a modulation length of 90 - 100 Å which well agree with the designed value (13/13 sequence ~ 102 Å). The absence of higher order satellites indicates the existence of fluctuation of thickness of LaCrO_3 and LaFeO_3 layers.

The superlattice formed on (111) plane with 1/1 sequence has a single phase and [111] orientation, and small peaks are observed at $2\theta = 19.4^\circ$ and 60.8° due to the long periodic feature (Fig. 3.2-4).

In the case of superlattice formed on the (110) plane with 6/6 stacking periodicity,

superstructures are also observed as the combination of main peaks with satellite peaks [Fig. 3.2-5(a)]. And specially, the peak due to the long periodic features observed at $\theta = 2.2^\circ$, that well agree with our designed stacking sequence ($6/6 \rightleftharpoons 34 \text{ \AA}$). Our experimental XRD patterns of the superlattice agree well with our calculated patterns [Fig. 3.2-5(b)].

The RHEED patterns show streaks indicating that the superlattices are epitaxially formed on the (100), (110) and (111) substrates up to the topmost surface [Fig. 3.2-6(b), 7, 8].

AFM surface image are taken for $\text{LaCrO}_3\text{-LaFeO}_3$ superlattices on LaAlO_3 (100) (Fig. 3.2-9) and SrTiO_3 (111) with a 5/5 stacking periodicity (Fig. 3.2-10). The root-mean-square roughness (RMS : $1 \mu\text{m} \times 1 \mu\text{m}$) perpendicular to the surface and average roughness is 2.0 \AA for the (100) superlattice and 1.3 \AA for the (111) superlattice (< 1 unit layer), respectively. Surface morphology is very well and it is considered that multilayered systems are constructed by good quality layers.

These results of X-ray diffraction, RHEED patterns and AFM images indicate that the $\text{LaCrO}_3\text{-LaFeO}_3$ superstructures are well constructed as desired.

The temperature dependence of magnetization for $\text{LaCrO}_3\text{-LaFeO}_3$ artificial superlattices (1/1 ~ 13/13 unit) and $\text{LaCr}_{0.5}\text{Fe}_{0.5}\text{O}_3$ films on LaAlO_3 (100) is shown in Fig. 3.2-11(a). The cusp which corresponds to T_N appeared at 250 K for the 1/1 superlattice, around 400 K for the 2/2 superlattice, > 400 K for the 5/5 superlattice (T_N cannot be observed due to the limitations of the instrument.) and 330 K for the 13/13 superlattice. In the cases of 1/1 ~ 5/5 sequence, T_N is lowered as the stacking periodicity is decreased. In the superlattice with a 1/1 sequence, the Neel temperature

appears to be at the lowest temperature compared with those of other superlattices because one-third of the interactions are replaced with ferromagnetic interactions [see Fig. 3.2-11 (b)]. In the 2/2 sequence, 1/7 of antiferromagnetic interactions are replaced [Fig. 3.2-11 (c)], and in the 4/4 sequence, 1/15 are replaced. After all, the Neel temperature (T_N) is lowered as the stacking periodicity is decreased, that is, as the volume of ferromagnetic interaction increases. After all, the Neel temperature (T_N) is lowered as the stacking periodicity is shortened, that is, as the volume of ferromagnetic interaction increases. The relation between the total magnetic interactions (J_{total}) and the stacking periodicity can be generally expressed as follows,

$$J_{total} = \frac{\alpha \cdot (2s - 1) \cdot (J_{Fe-Fe} + J_{Cr-Cr}) + \beta \cdot J_{Fe-Cr}}{4s - 1} \quad (1)$$

where S indicates the stacking periodicity of artificial superlattices, and J_{Fe-Fe} , J_{Cr-Cr} and J_{Fe-Cr} represent the magnetic interactions between Fe^{3+} - Fe^{3+} , Cr^{3+} - Cr^{3+} and Fe^{3+} - Cr^{3+} ions, respectively. The variable α and β is the parameter for the effect of interfacial mixing and roughness and/or some other effects. The considerations of the interfacial imperfection effect are very important for thinking of the physical properties of artificial superlattices. The effect of weakening the magnetic interactions at the interface for the interfacial roughness and mixing is introduced in quotation (1) by this operation.

In the 13/13 sequence, T_N appears at 330 K. The tendency of this film is different from that of other films that have shorter periodicities because the properties of $LaCrO_3$ and $LaFeO_3$ appear independently in the superlattice with longer periodicity. However, the T_N of these films appears at a temperature different from that of the original $LaCrO_3$ phase ($T_N=280$ K). Since the thickness of one layer in the 13/13 sequence is less than

the Bloch wall, the magnetic interactions do not behave in the same manner as that in the original LaCrO_3 .

One T_N originating from the nature of the superlattice is observed when the stacking periodicity is short (1/1-5/5). On the other hand, two T_N 's originating from each single phase (LaCrO_3 and LaFeO_3) may exist when the stacking periodicity is large (13/13). (We can only observe one T_N which originates from the LaCrO_3 phase. T_N that originated from LaFeO_3 is not confirmed due to the limitations of our instrument because T_N of LaFeO_3 is much higher than the measurable temperature (bulk T_N : 750 K).) These behaviors agree with the results of CoO/NiO superlattices reported by Abara et al. [13] and of $\text{FeF}_2/\text{CoF}_2$ superlattices by Ramos et al. [14].

In contrast, the temperature dependence of the magnetization and hysteresis curve (M-H curve) of the LaCrO_3 - LaFeO_3 artificial superlattice (1/1 sequence) grown on the (111) substrate exhibits characteristic of ferromagnetic (or ferrimagnetic) materials [Fig. 3.2-12]. The saturation magnetization (M_s) is estimated to be 60 emu/g ($\approx 2.5 \mu_B/\text{site}$) from the hysteresis curve measured at 6 K. It is considered that the material is ferromagnetic because the value of M_s is too large to attribute to ferrimagnetic order (theoretical estimation : $1 \mu_B/\text{site}$ for Fe^{3+} -O- Cr^{3+} ferrimagnetic interaction). The decrease of our M_s from the theoretical estimation ($4 \mu_B/\text{site}$ for Fe^{3+} -O- Cr^{3+} ferromagnetic interaction) is considered to be due to the imperfection at the interface.

In the case of superlattices constructed on (110) planes, all the superlattices (1/1, 2/2, 6/6) show antiferromagnetic behaviors (Fig. 3.2-12). The cusp which correspond to the Neel temperature appeared at 320 K (1/1), 320 K (2/2) and 340 K (6/6), respectively. The cusp changed systematically as stacking periodicity increases.

These results suggest that the control of the growth direction of the superlattices actually govern the magnetic properties as proposed in Fig. 1.

3.2-4 Conclusion

In summary, we demonstrated that artificial control of magnetic properties is possible by changing the stacking periodicity and direction in $\text{LaCrO}_3\text{-LaFeO}_3$ superlattices. Antiferromagnetic behaviors are observed in all the films deposited on (100) and (110) substrates. And, the T_N changed systematically as the stacking periodicity changed. On the other hand, the film with 1/1 periodicity on a (111) substrate exhibits ferromagnetic character. Though the total number of Fe and Cr ions are same in (100), (110) and (111) superlattices, quite different magnetic character can be created in the artificial superlattices.

3.2-5 References

- [1] H. Tabata, H. Tanaka and T. Kawai, *Appl. Phys. Lett.* **65**, 1970 (1994)
- [2] R. Aleorard, R. Pauthenet, J. P. Rebouillat and C. Veyret, *J. Appl. Phys.* **39**, 379 (1968).
- [3] W. C. Koehler, E. O. Wollan and M. K. Wilkinson, *Phys. Rev.* **118**, 58 (1960).
- [4] D. Treves, *J. Appl. Phys.* **36**, 1033 (1965).
- [5] J. Kanamori, *J. Phys. Chem. Solids* **10**, 87 (1959).
- [6] J. B. Goodenough, *Phys. Rev.* **100**, 564 (1955).
- [7] K. Ueda, H. Tabata and T. Kawai, *Science* **280** (1998) 1064.
- [8] T. Kawai, M. Kanai and H. Tabata, *Mater. Sci. Eng.* **B41**, 123 (1996).
- [9] M. Kanai, T. Kawai and S. Kawai, *Appl. Phys. Lett.* **58** 771 (1991).
- [10] S. Huzinaga, J. Andzelm, M. Klobukowshi, E. Radzio-Andzelm, Y. Sakai and H. Tatewaki ; 'Gaussean Basis Sets for Molecular Calculations', Elsevier (1984).
- [11] K. Yamaguchi, T. Tsunekawa, Y. Toyoda, and T. Fueno, *Chem. Phys. Lett.* **143**, 371 (1988)
- [12] H. W. Hwang, T. T. M. Palstra, S-W. Cheong and B. Batlogg, *Phys. Rev.* **B52**, 15046 (1995).
- [13] E. N. Abarra, K. Takano, F. Hellman, and A. E. Berkowitz, *Phys. Rev. Lett.* **77**, 3451 (1996).
- [14] C. A. Ramos, D. Lederman, A. R. King, and V. Jaccarino, *Phys. Rev. Lett.* **65**, 2913 (1990).

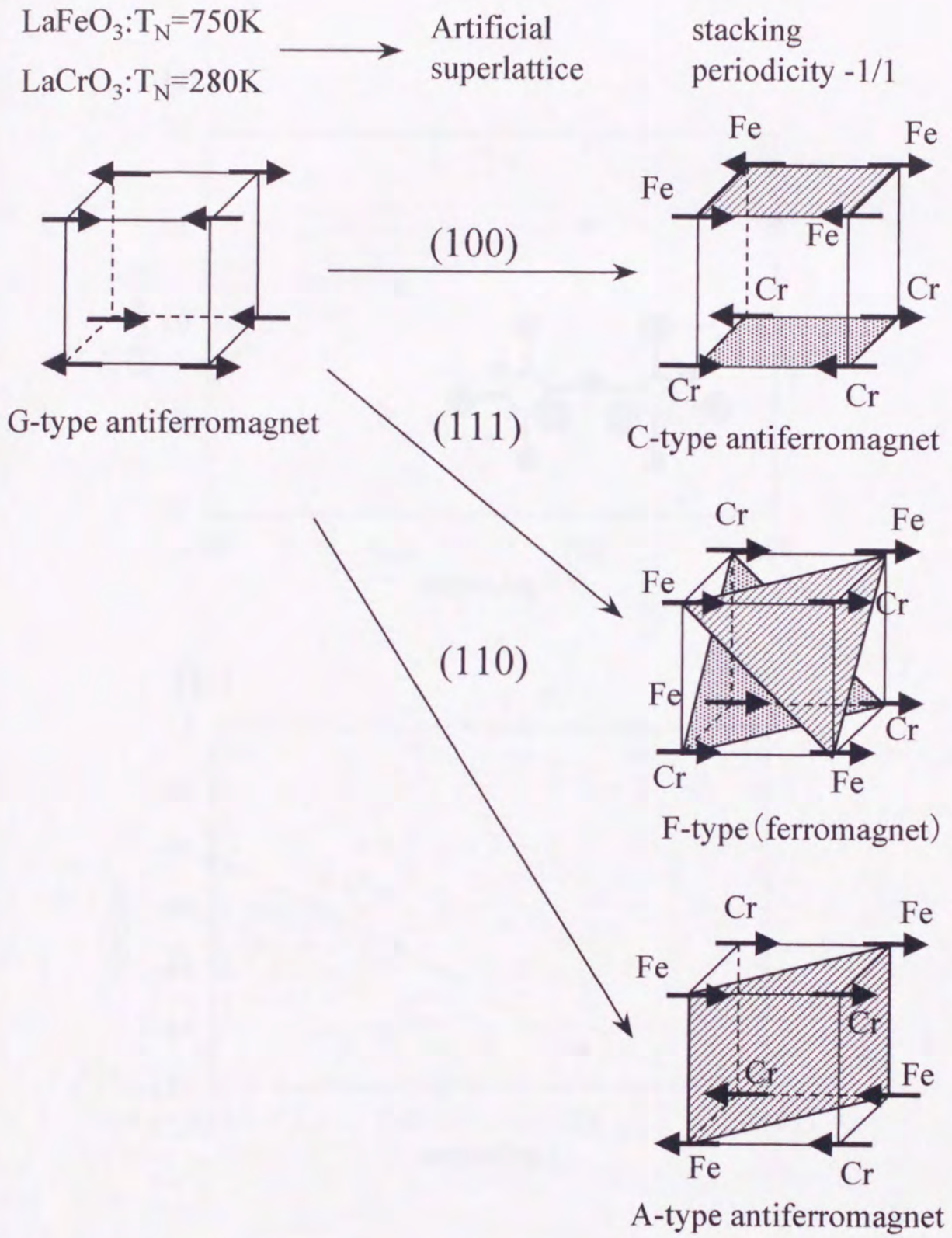


Fig. 3.2-1 : Schematic models of spin structures in the $\text{LaCrO}_3\text{-LaFeO}_3$ artificial superlattices grown on (100), (110) and (111) surfaces.

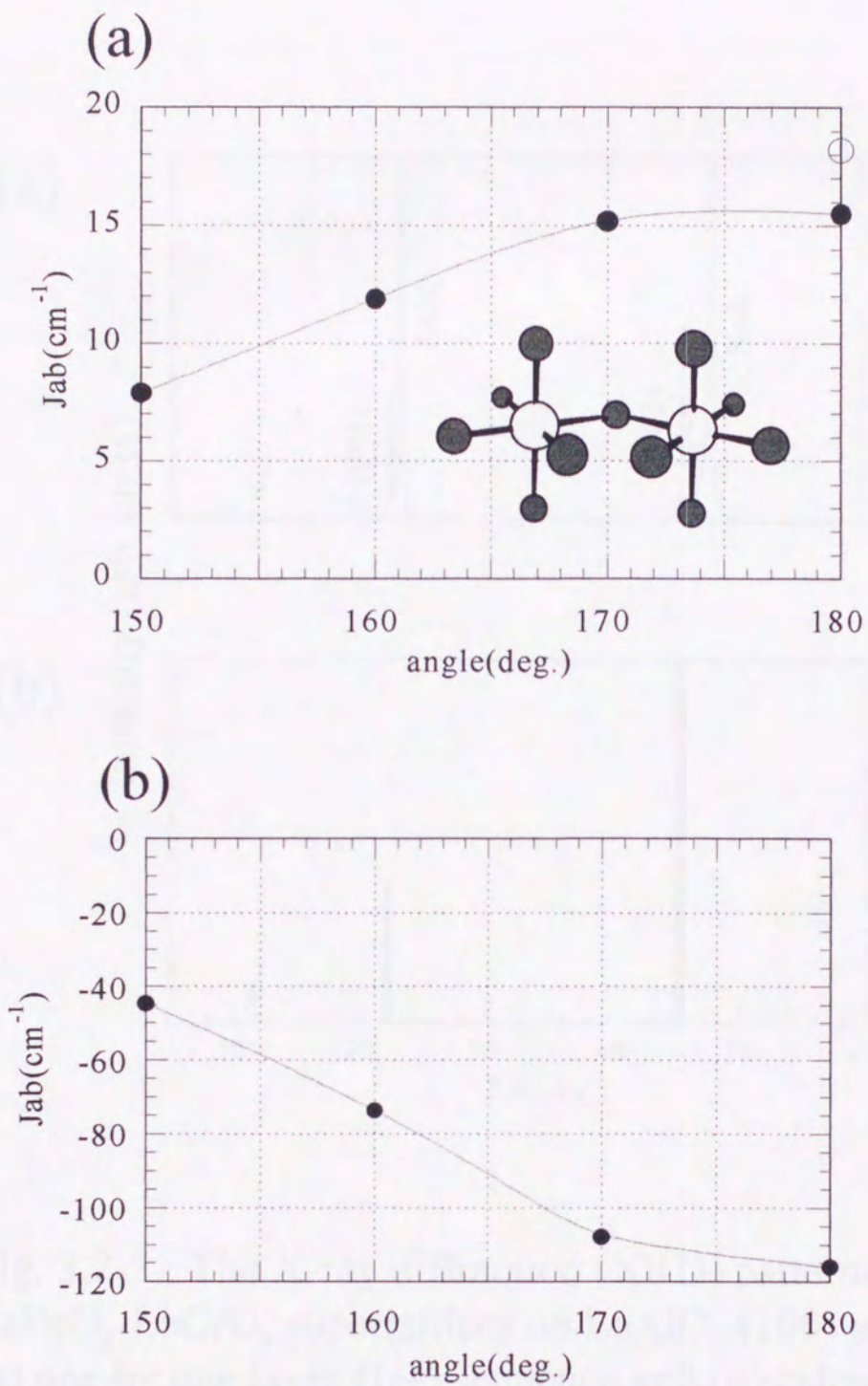


Fig. 3.2-2 : Calculations of effective exchange integral (J_{ab}) of (a) FeCrO_{11} and (b) Fe_2O_{11} cluster derived by an ab-initio MO method (UHF – filled circle and B3LYP – open circle : see text).

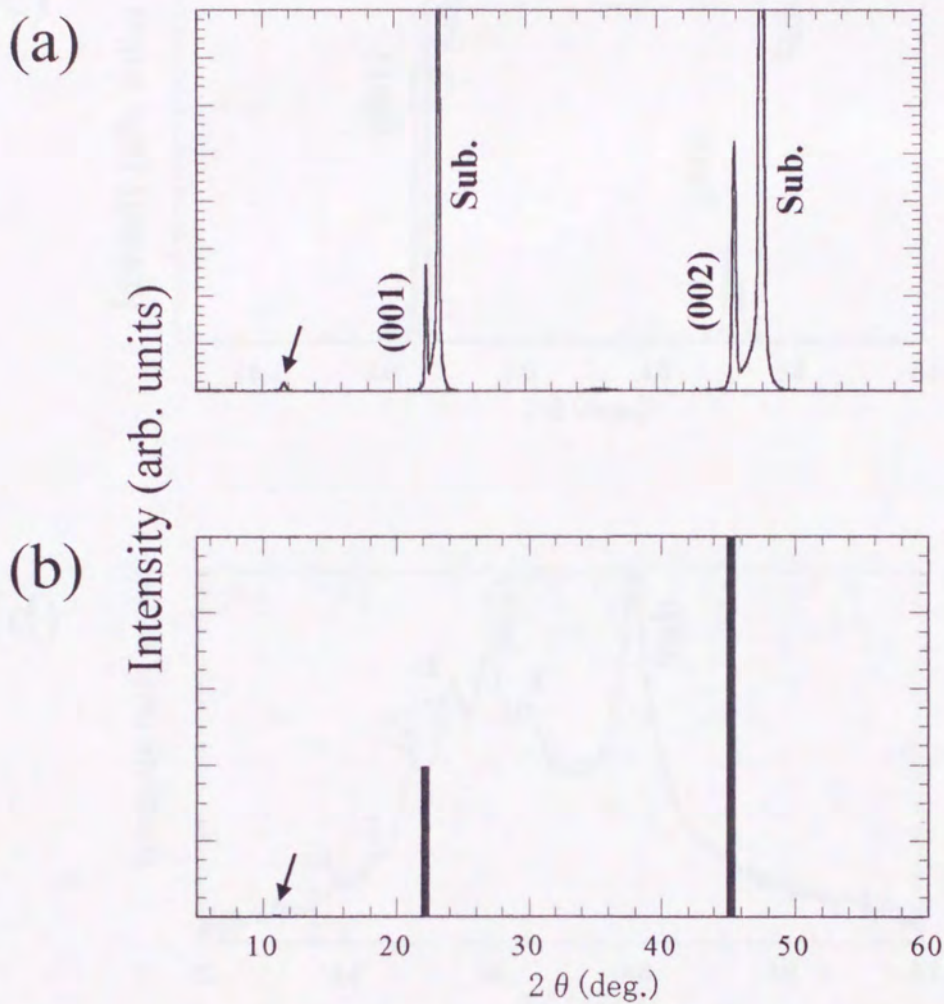


Fig. 3.2-3 : The X-ray diffraction (XRD) patterns of $\text{LaFeO}_3\text{-LaCrO}_3$ superlattices on LaAlO_3 (100) plane with (a) one by one layer (1/1) sequence and (b) calculated XRD patterns of 1/1 superlattice with ideal crystal structure.

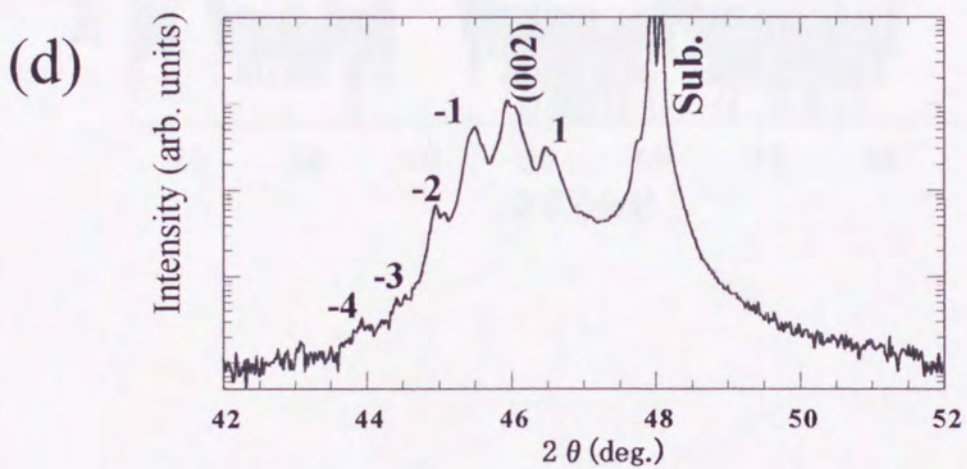
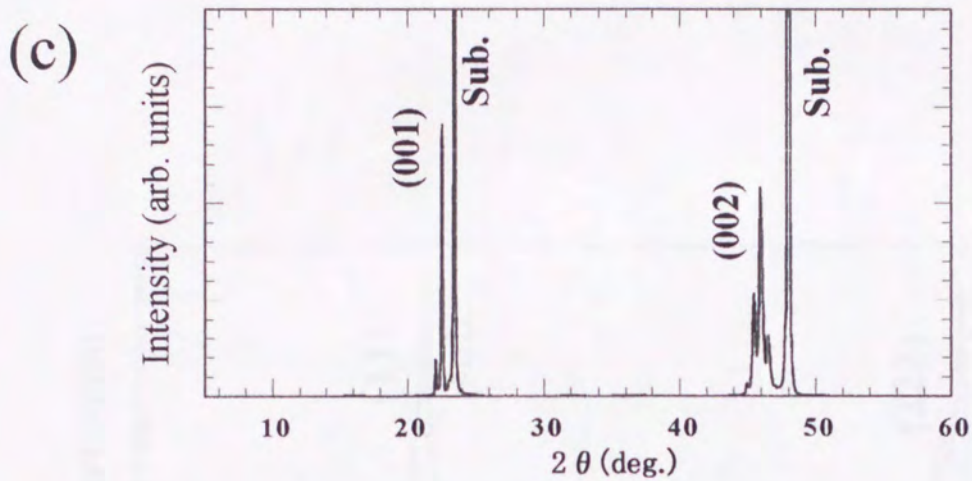


Fig. 3.2-3 : The XRD patterns of $\text{LaFeO}_3\text{-LaCrO}_3$ on LaAlO_3 (100) with (c) 13/13 sequence. (d) The high angle XRD pattern for 13/13 superlattices. Indices in the figures show the position of the l th satellite peak around the fundamental (002) peak.

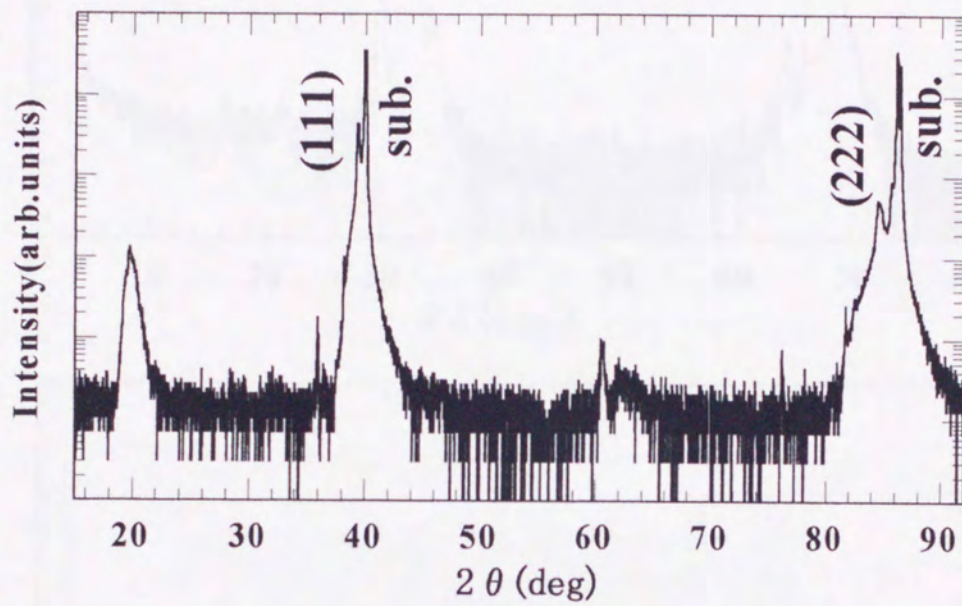
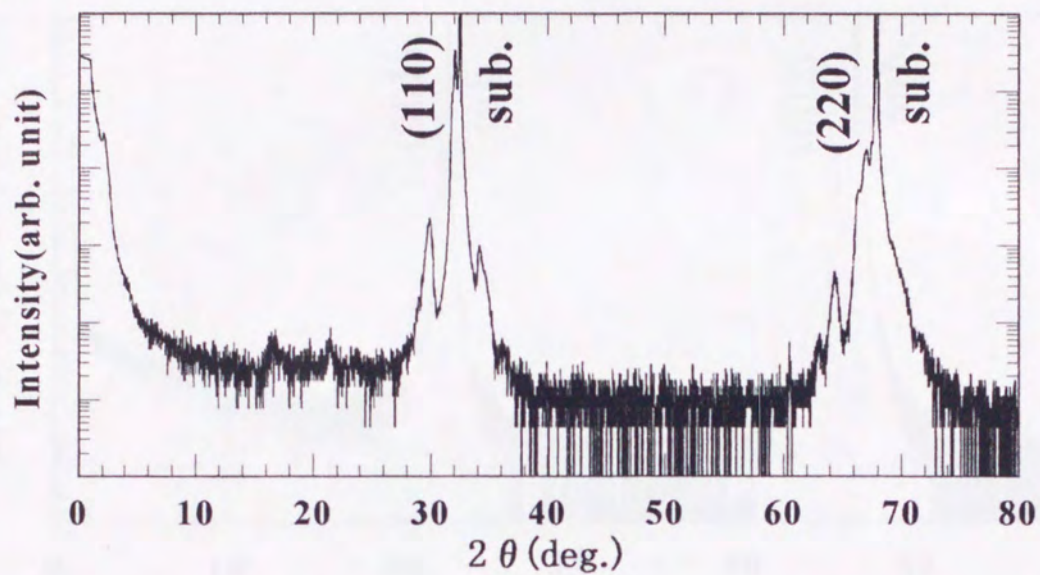


Fig. 3.2-4 : The X-ray diffraction (XRD) patterns of superlattices on the (111) plane with 1/1 sequence.

(a)



(b)

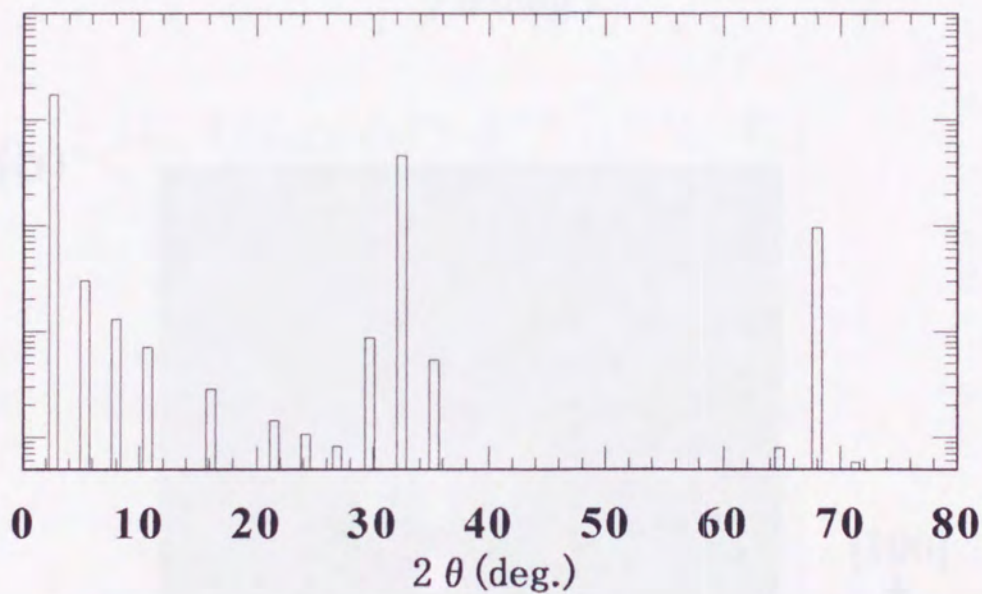


Fig. 3.2-5 : The (a) experimental and (b) simulated X-ray diffraction (XRD) patterns of superlattices on the (110) plane with 6/6 sequences.

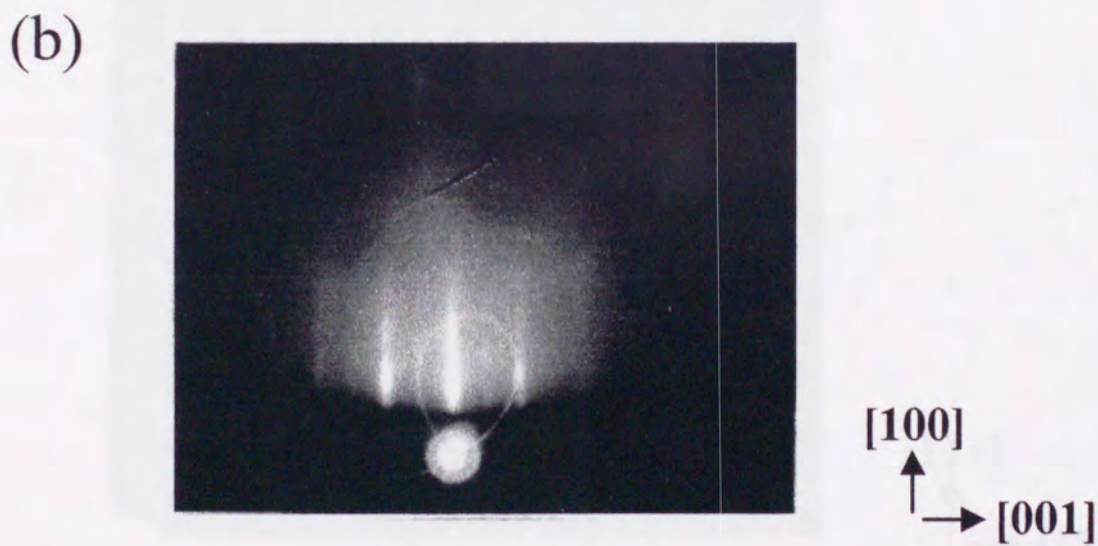
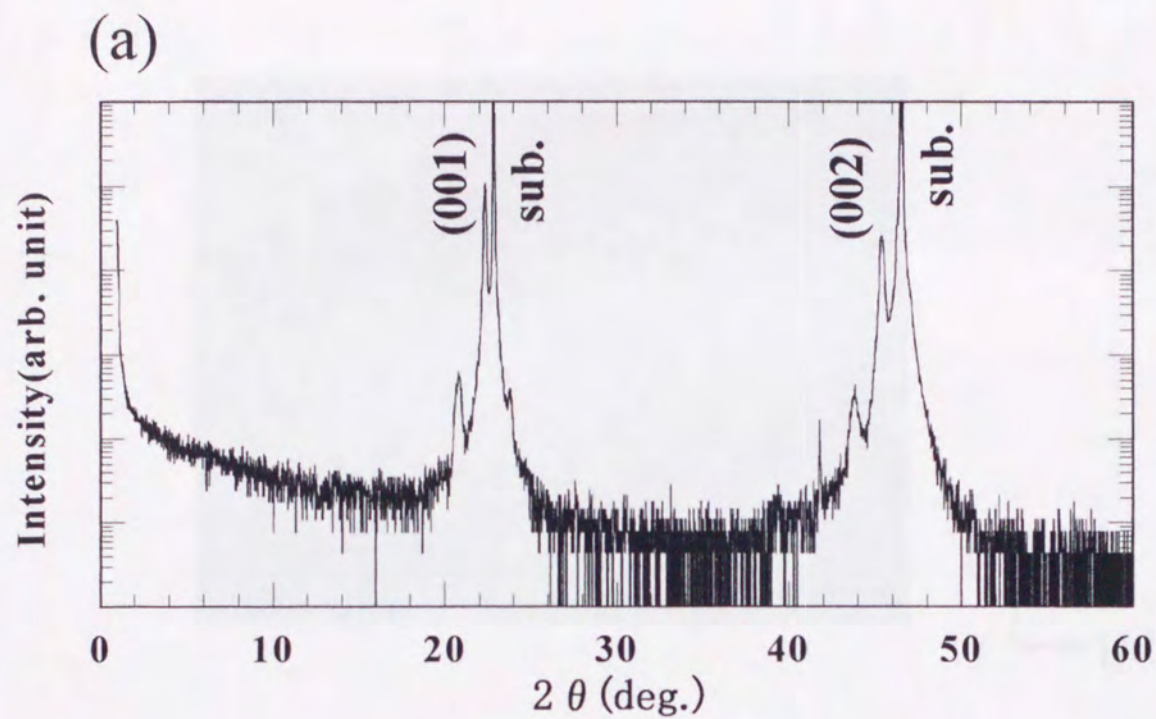
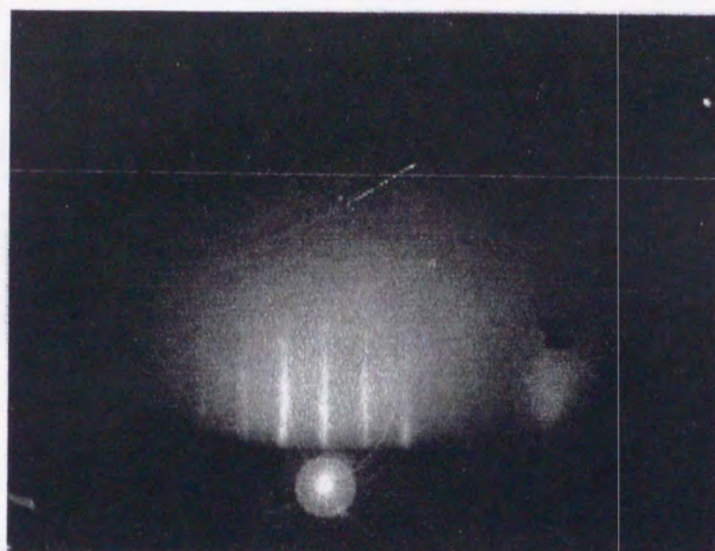
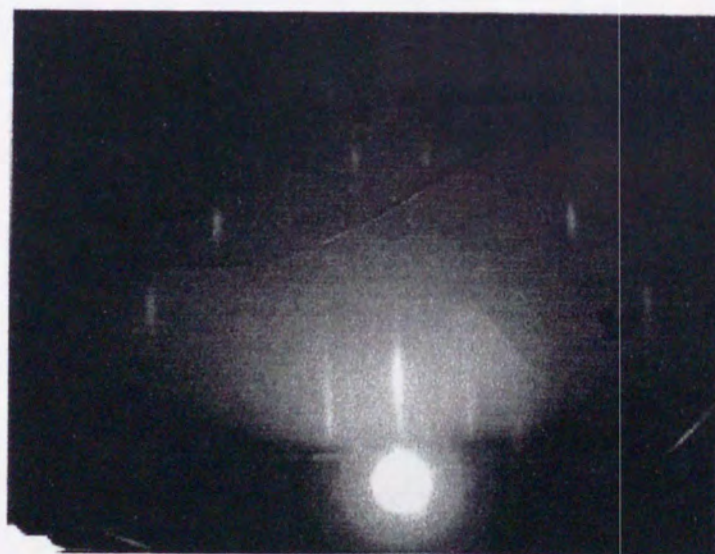


Fig. 3.2-6 : The (a) XRD and (b) reflection high energy electron diffraction (RHEED) patterns of superlattices formed on the SrTiO_3 (100) plane with 8/8 sequence.



$[111]$
↑
→ $[\bar{1}10]$



$[111]$
↑
→ $[11\bar{2}]$

Fig. 3.2-7 : The reflection high energy electron diffraction (RHEED) patterns of superlattices on the SrTiO_3 (111) plane with 5/5 sequence.



[110]
 \uparrow
 \rightarrow [001]



[110]
 \uparrow
 \rightarrow [1 $\bar{1}$ 0]

Fig. 3.2-8 : The reflection high energy electron diffraction (RHEED) patterns of superlattices on the SrTiO_3 (110) plane with 6/6 sequence.

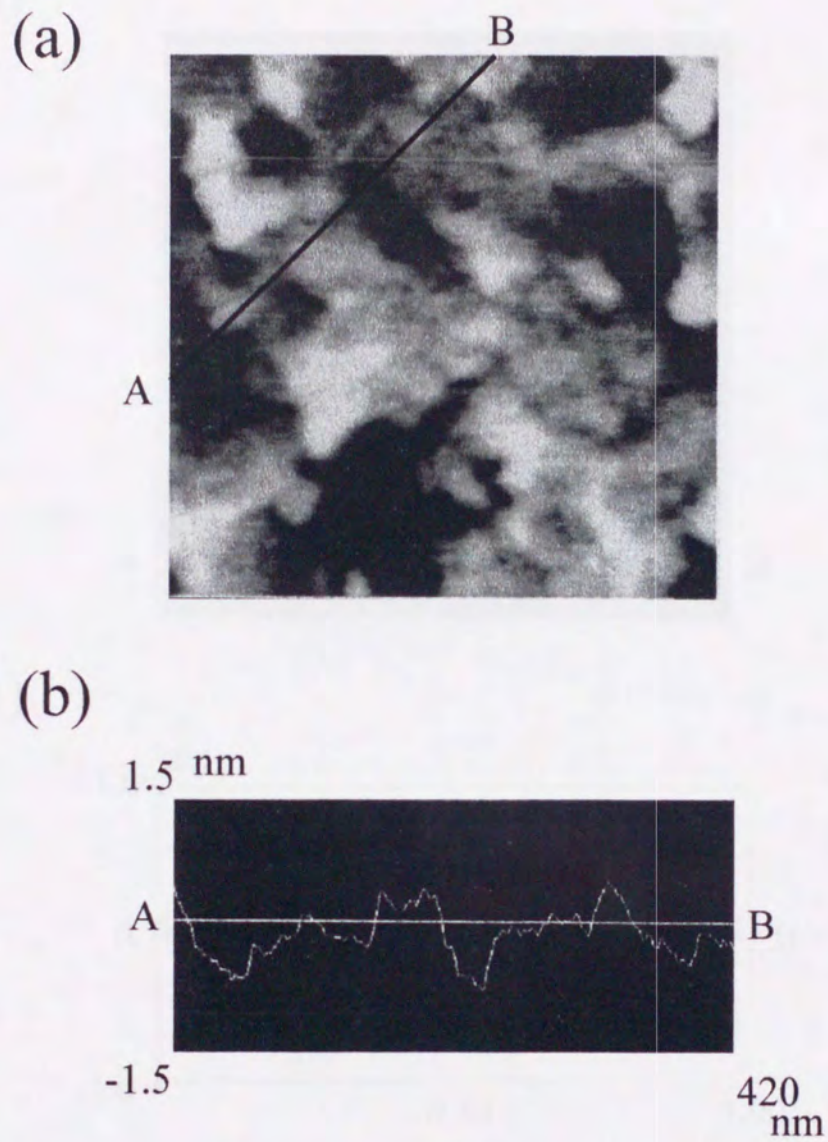
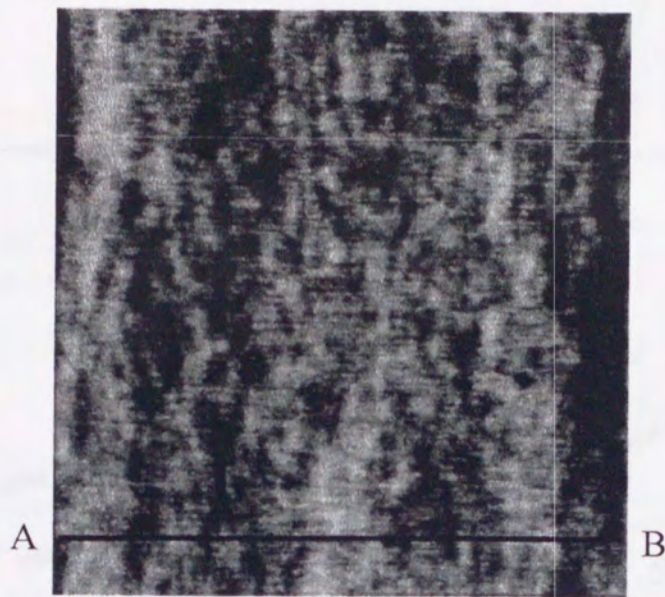


Fig. 3.2-9 : The (a) AFM surface image (scanning area, $0.5 \times 0.5 \mu\text{m}$) and (b) cross-sectional image for $\text{LaCrO}_3\text{-LaFeO}_3$ superlattices on LaAlO_3 (100) substrate with 5/5 sequence.

(a)



(b)

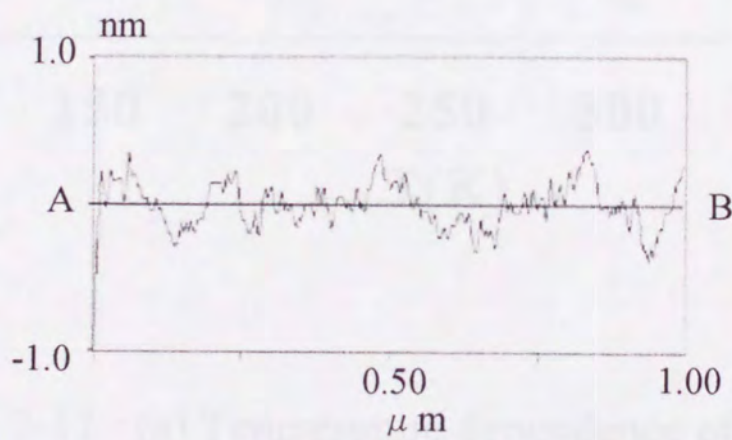


Fig. 3.2-10 : The (a) AFM surface image (scanning area, $1 \times 1 \mu\text{m}$) and (b) cross-sectional images for SrTiO_3 (111) substrate with 5/5 stacking periodicity.

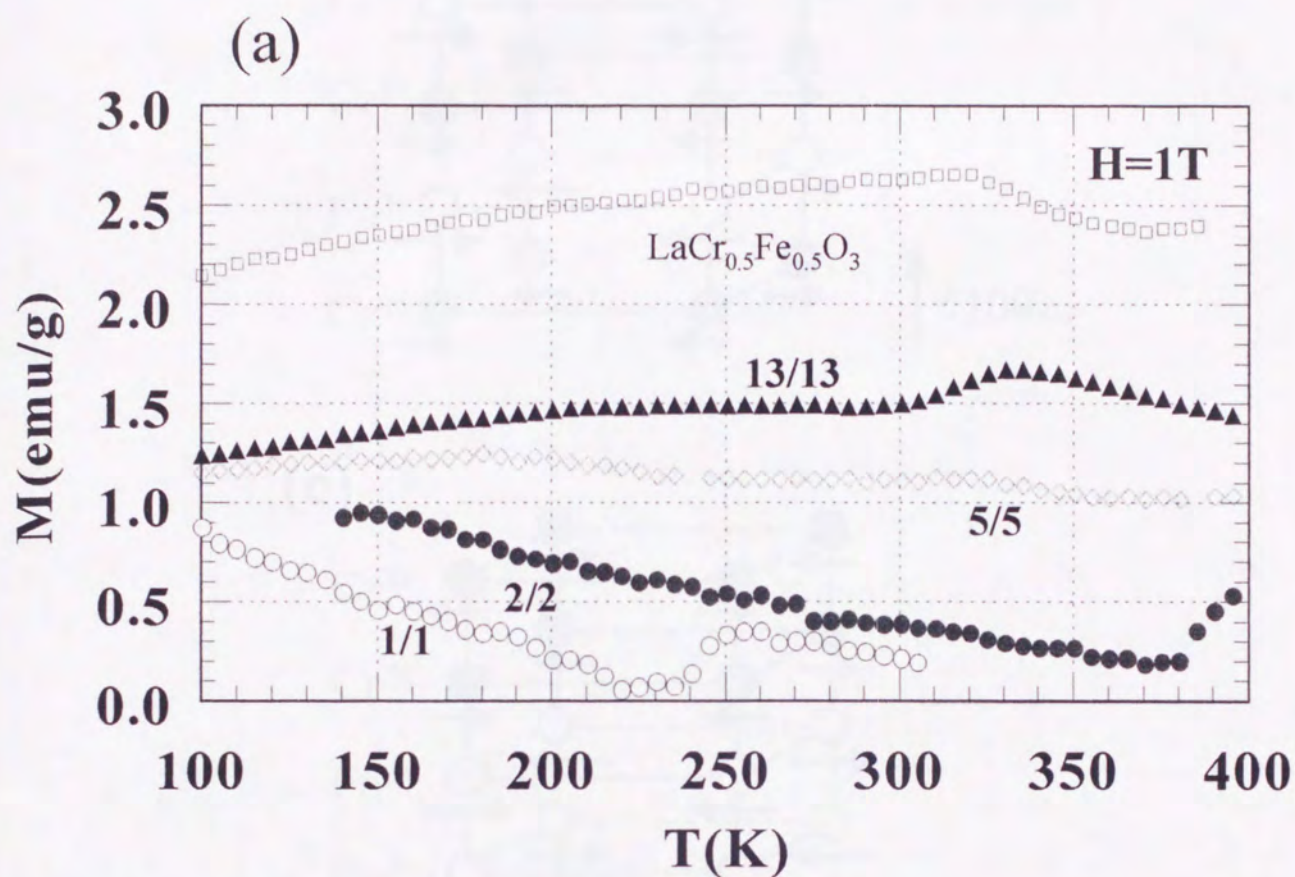


Fig. 3.2-11 : (a) Temperature dependence of Magnetization for the LaCrO_3 - LaFeO_3 superlattices formed on LaAlO_3 (100) with various stacking periodicity (1/1, 2/2, 5/5, 13/13 unit) and $\text{LaCr}_{0.5}\text{Fe}_{0.5}\text{O}_3$ solid solution film in the magnetic field of 1T.

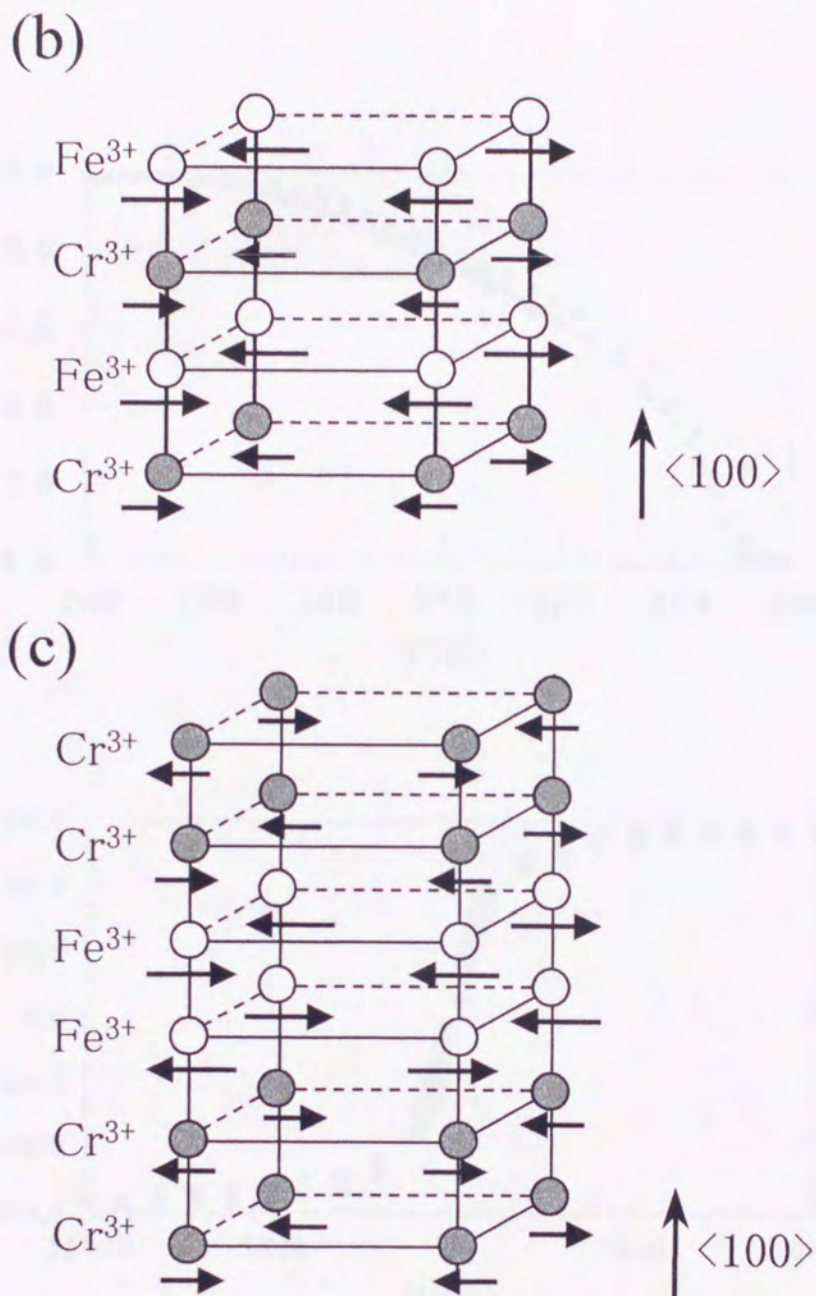


Fig. 3.2-11 : Schematic spin structures of $\text{LaCrO}_3\text{-LaFeO}_3$ superlattice with (b) 1/1 sequence and (c) 2/2 sequence on (100) plane. Arrow size corresponds to an ideal high-spin structure of $S=5/2$ (d^5) and $S=3/2$ (d^3) in Fe^{3+} and Cr^{3+} , respectively. Oxygen ions are deleted for simplicity.

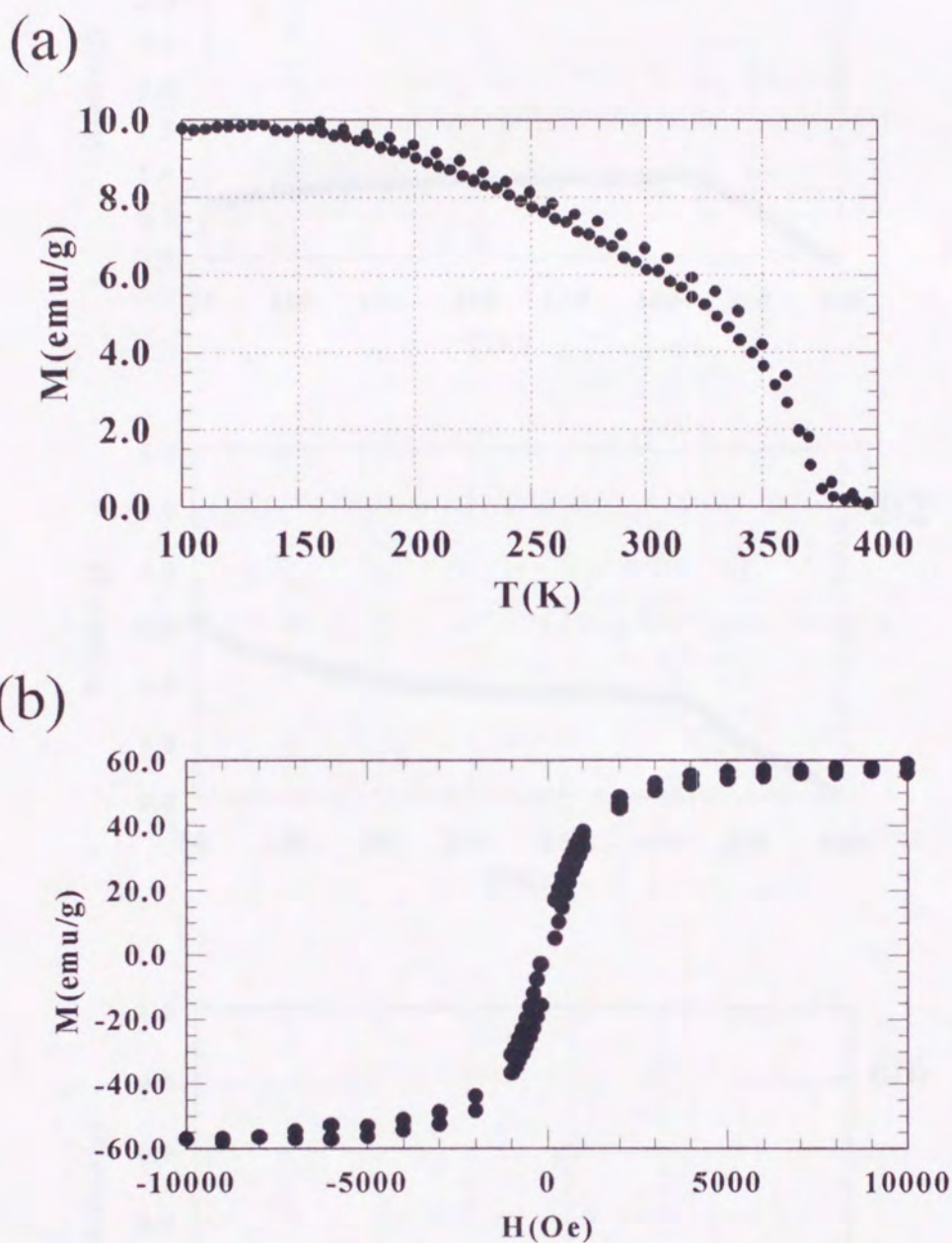


Fig. 3.2-12 : (a) Temperature dependence of Magnetization for the $\text{LaCrO}_3\text{-LaFeO}_3$ superlattices formed on SrTiO_3 (111) with 1/1 sequence in the magnetic field of 0.1T and (b) the hysteresis curve measured at 6K in the magnetic field of $-1\text{T} \sim 1\text{T}$.

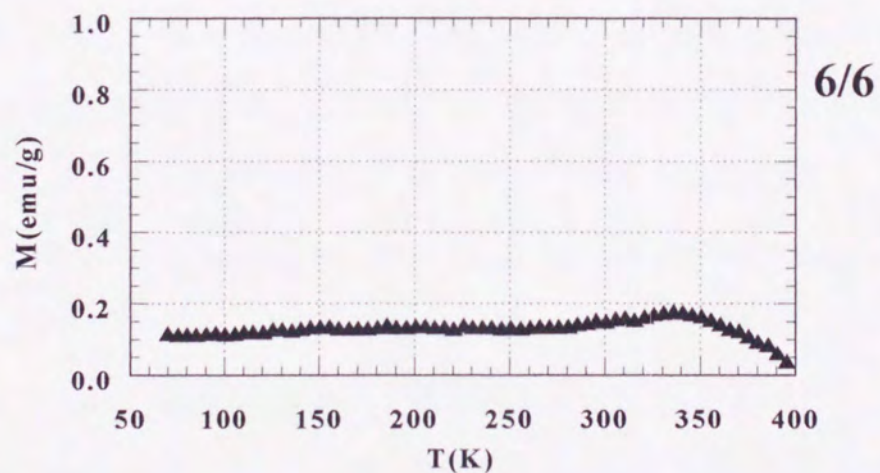
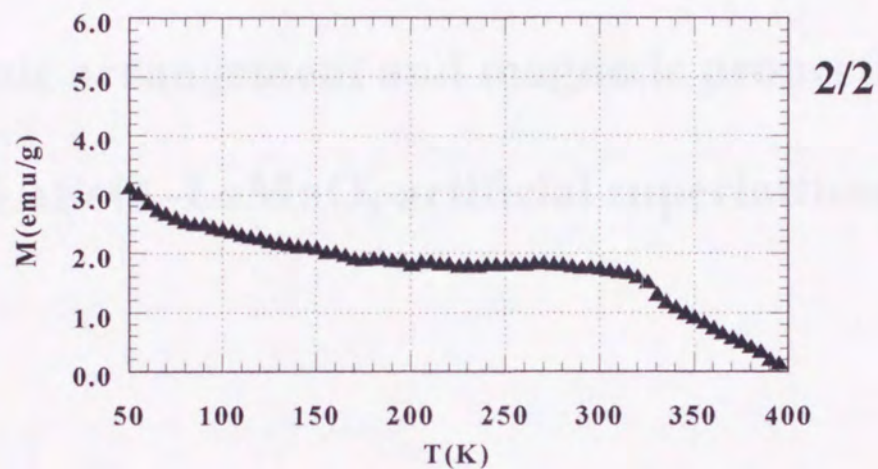
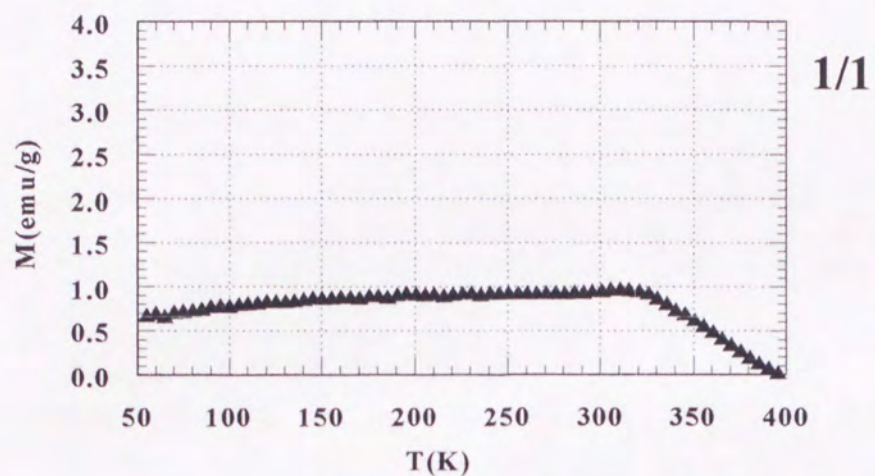


Fig. 3.2-13 : Temperature dependence of Magnetization for the $\text{LaCrO}_3\text{-LaFeO}_3$ superlattices formed on SrTiO_3 (110) with various stacking periodicity (1/1, 2/2, 6/6) in the magnetic field of 1T.

Chapter 4
**Atomic arrangement and magnetic properties of
LaFeO₃-LaMnO₃ artificial superlattices**

Artificial superlattices of LaFeO_3 - LaMnO_3 were formed on SrTiO_3 (111), (100) and (110) substrates with various stacking periodicity using a pulsed laser deposition technique, and their magnetic properties were controlled by altering the ordering of magnetic ions (Fe or Mn). For superlattices constructed on the (111) plane, all the superlattices showed ferromagnetic (or ferrimagnetic) behaviors and the same Curie temperatures (T_C) at 230 K. The magnetization was reduced as the stacking periodicity of the superlattices decreased. On the other hand, in the case of superlattices formed on (110) and (100) substrates, the increase of the spin frustration effect at the LaFeO_3 - LaMnO_3 interface with decreasing the stacking periodicity caused a reduction of T_C and magnetization. In particular, spin glass like behavior was observed in superlattices of less than $3/3$ stacking periodicity.

4-1 Introduction

Materials that do not exist in nature can be created artificially using the method of depositing superlattices with the layering of different materials on an atomic or molecular scale. The method can be applied to a wide range of fields such as the fabrication of new superconductors, magnetic and ferroelectric materials, etc.. New materials with unique physical properties are constantly being created [1-3]. However, the atomic order can only be controlled in the direction parallel to the film plane (i.e., one-dimensional control), and current techniques do not support three-dimensional control of the atomic order.

In an earlier study, we demonstrated that the control of the arrangement of magnetic ions, i.e., the spin order could be controlled by constructing artificial superlattices with

various stacking directions and periodicity [4-5]. Pseudo three-dimensional control of the atomic order was achieved by the method.

In this chapter, LaMnO_3 - LaFeO_3 artificial superlattices were formed on SrTiO_3 (111), (100) and (110) planes with various stacking periodicity, and their magnetic properties were controlled by managing the ordering of the Mn and Fe ions. LaFeO_3 is antiferromagnetic (Fe^{3+} -O- Fe^{3+} superexchange interaction) and has a G-type magnetic structure (inter- and intralayer spin coupling are antiparallel) [6-7]. On the other hand, LaMnO_3 films exhibit ferromagnetic behavior with a Curie temperature of 130 K for La deficiency ($\text{La}_{1-\delta}\text{MnO}_3$) [8]. In this chapter, the ferromagnetic $\text{La}_{1-\delta}\text{MnO}_3$ is noted as LaMnO_3 .

For artificial superlattices constructed on the (111) plane, ferromagnetic interactions should be introduced at the Mn-Fe interface because the Fe^{3+} -O- Mn^{3+} superexchange interaction is considered to be ferromagnetic according to the theory of Goodenough-Kanamori [9-10]. As a result, ferromagnetism should appear in the superlattice with one-layer by one-layer (1/1) stacking periodicity (see Fig. 4-1).

On the other hand, for superlattices constructed on (100) and (110) planes a spin frustration effect occurs at the LaMnO_3 - LaFeO_3 interface because the LaMnO_3 film is ferromagnetic [8] and LaFeO_3 is antiferromagnetic with a G-type spin structure [6-7] (Fig. 4-1). The spin frustration effect increases as the stacking periodicity decreases. The spin frustration effect of (110) superlattices becomes larger than that of (100) superlattices in terms of their spin structure. This method even allows a spin frustration effect to be introduced artificially into the system. The LaMnO_3 - LaFeO_3 artificial superlattices were formed according to these concepts.

4-2 Experimental

Magnetic artificial superlattices were constructed by stacking LaMnO_3 and LaFeO_3 layers on (111), (100) and (110) SrTiO_3 substrates using a multi-target pulsed laser deposition (PLD) technique [4-5]. LaMnO_3 and LaFeO_3 targets were prepared using standard ceramic techniques. All the films were formed at 590 – 600 °C in an oxygen/ozone (8 %) ambient pressure of 1×10^{-3} Torr with an energy density of 0.5 - 1 mJ/cm^2 . The deposition rate was 10 - 20 Å/min. The total thickness of the films was 800 – 1000 Å. The thickness of individual layers were controlled by the number of laser pulses (The deposition rate from LaFeO_3 and LaMnO_3 targets were calibrated against the number of laser pulses). The structure of the lattices was characterized by X-ray diffraction ($2\theta - \theta$ scan) using a Cu-K_α source (Rigaku : RINT 2000). Surface morphology was observed by atomic force microscopy (AFM : Digital Instruments-Nanoscope III). Magnetic measurements were performed using a commercial superconducting quantum interference device (SQUID) magnetometer (Quantum design MPMS-5S) with the magnetic field applied parallel to the film plane.

4-3 Results and Discussion

The crystal structures of the LaMnO_3 - LaFeO_3 superlattices on SrTiO_3 (111), (100) and (110) were studied using X-ray diffraction. All the films showed a single phase and had a preferred orientation normal to the surface of the substrate. Typical features of superlattices were observed. In particular, for a superlattice formed on a (111) substrate with one-layer by one-layer (1/1) stacking periodicity, small peaks were observed at $2\theta = 19.8^\circ$ and 61.6° due to the double perovskite features (Fig. 4-2).

The RHEED patterns show streaks which also indicate that the superlattices are epitaxially formed on the (111), (100) and (110) surfaces. The results of the X-ray diffraction and reflection high-energy electron diffraction (RHEED) measurements indicate that the LaMnO_3 - LaFeO_3 superstructures were sufficiently well formed.

In addition, the morphology of the superlattice on the (111) substrate was observed using an AFM. The average roughness (R_a) and mean square roughness (R_{MS}) of the film surface (area: $1 \mu\text{m} \times 1 \mu\text{m}$) were found to be 1.7 and 2.2 Å (i.e., less than one layer), respectively, indicating that the artificial superlattice was well formed at the atomic level (Fig. 4-3).

Magnetization versus temperature curves (M-T curves) of LaMnO_3 - LaFeO_3 artificial superlattices (1/1-30/30 sequence) on SrTiO_3 (111) are shown in Fig. 4-4 (a). A magnetic field of 0.1 T was applied parallel to the film surface. The magnetic property of the 30/30 superlattice resembles that of the original LaMnO_3 film. The properties of LaMnO_3 and LaFeO_3 can be observed independently in superlattices with stacking periodicity greater than a 30/30 sequence, and the property of LaMnO_3 was strongly apparent in the temperature 5 - 400 K because the magnetization of LaMnO_3 is much larger than that of LaFeO_3 .

For the 1/1 - 9/9 sequences, the magnetization increases as the stacking periodicity decreases. It must be noted that all the superlattices show the same Curie temperatures (T_C) of 230K. The change of magnetization and the same T_C value may be explained as follows. Fig. 4-4 (b) shows that the ratio of spins which contribute to the magnitude of magnetization increases as the stacking periodicity decreases, i.e., an increase of the number of Fe-Mn interfaces, because the spins of the magnetic ions (Fe^{3+} or Mn^{3+}) on each (111) planes are aligned in the same direction. As a result, the magnetization

increases when the stacking periodicity is reduced. Ferromagnetic (or ferrimagnetic) behavior in particular is observed in the 1/1 superlattice. The saturation magnetization (M_s) of the superlattice was measured to be about 30 emu/g ($\approx 1.3 \mu_B/\text{site}$) from the hysteresis curve measured at 6 K (Fig. 4-5 (a)). However, the value of M_s is estimated to be 103 emu/g ($= 4.5 \mu_B/\text{site}$) for the $\text{Mn}^{3+}(\text{d}^4)\text{-O-Fe}^{3+}(\text{d}^5)$ state theoretically. The measured value, therefore, is relatively small compared with the above estimation. We suppose that the reduction of M_s is caused by the complex effect arising from the partial displacement between Fe and Mn ions, charge separation between Fe and Mn as seen in $\text{LaMn}_{0.5}\text{Co}_{0.5}\text{O}_3$ (or $\text{LaMn}_{0.5}\text{Ni}_{0.5}\text{O}_3$) ordered perovskites [11-12] and the deviation from stoichiometry due to La and/or oxygen deficiency. In the first case, a 10% displacement of Fe by Mn ions causes the value of M_s to be 80% of the theoretical value. When charge separation between Fe and Mn ions ($\text{Fe}^{3+} + \text{Mn}^{3+} \rightarrow \text{Fe}^{2+} + \text{Mn}^{4+}$) occurs, as described in the second case, M_s becomes 80 emu/g ($= 3.5 \mu_B/\text{site}$). Annealing of the 1/1 superlattice was performed at 500°C (less than deposition temperature) with O_2 flowing to remove the oxygen deficiency. The magnetic behavior after annealing did not change from that seen before.

The Curie temperature of superlattices with 1/1 - 9/9 sequences is constant (Fig. 4-4 (a)). The fixed T_C of 230 K can be explained based on the fact that T_C is determined by the average of all magnetic interactions. For a superlattice with 3/3 sequence, the total magnetic interaction (J_{total}) is expressed by the following relation because $J_{\text{Fe-Fe}}$, $J_{\text{Mn-Mn}}$ and $J_{\text{Fe-Mn}}$ each accounts for one-third of all the magnetic interactions (see Fig. 4 (b)).

$$3/3 : J_{\text{total}} = [(J_{\text{Fe-Fe}} + J_{\text{Mn-Mn}}) + J_{\text{Fe-Mn}}] / 3$$

where $J_{\text{Fe-Fe}}$, $J_{\text{Mn-Mn}}$ and $J_{\text{Fe-Mn}}$ represent the magnetic interactions between $\text{Fe}^{3+}\text{-Fe}^{3+}$,

Mn³⁺-Mn³⁺ and Fe³⁺-Mn³⁺ ions, respectively. For superlattices with 5/5 and 7/7 stacking periodicity, the total magnetic interactions are given as follows based on the same concept.

$$5/5 : J_{total} = [2(J_{Fe-Fe} + J_{Mn-Mn}) + J_{Fe-Mn}] / 5$$

$$7/7 : J_{total} = [3(J_{Fe-Fe} + J_{Mn-Mn}) + J_{Fe-Mn}] / 7$$

From these results, the total magnetic interactions can be generally expressed as a function of the stacking periodicity as follows :

$$N/N : J_{total} = \frac{[(N-1)(J_{Fe-Fe} + J_{Mn-Mn}) + 2J_{Fe-Mn}]}{2N} \quad (1)$$

where N indicates the stacking periodicity of artificial superlattices.

Factors that weaken superexchange interactions, such as interfacial imperfections characteristic of artificial superlattices [13-15], and oxygen and La deficiency, must be considered in order to calculate the values of the magnetic interaction precisely. The parameters α and β are added to Equation (1) to take these effects into account. Equation (1) is transformed into Equation (2) by the procedure.

$$J_{total} = \frac{[(N-1)\alpha(J_{Fe-Fe} + J_{Mn-Mn}) + 2\beta \cdot J_{Fe-Mn}]}{2N} \quad (2)$$

The experimental J values were applied to this equation. The experimental J values were calculated using mean field approximation (nearest neighbor interactions were only considered). With $\alpha=0.5$ and $\beta=1$, the experimental values were successfully reproduced, suggesting that the interactions between Fe-Fe and Mn-Mn ions are

weakened more significantly than the interactions between Fe-Mn at the interfaces.

Only one T_C is observed when the stacking sequence is short (1/1-9/9), and the T_C originating from the single LaMnO_3 phase is observed when the stacking periodicity is large (30/30). (The T_N originating from LaFeO_3 in the superlattice with larger sequence is not confirmed because of the temperature limitation of our instrument.) The behavior of these superlattices agree well with the results from Abara et al. [16] on CoO/NiO superlattices and those of Ramos et al. [17] on $\text{FeF}_2/\text{CoF}_2$ superlattices.

Furthermore, unusual behaviors was observed in the hysteresis curve with 5/5 stacking periodicity (Fig. 4-5 (b)). Broad hysteresis with a coercive field (H_C) at 0.15 T was observed in a superlattice with 1/1 stacking periodicity (Fig. 4-5 (a)). The hysteresis curve for LaMnO_3 (Fig. 4-5 (c)), on the other hand, shows the slim shape characteristic of soft magnetic materials. The superlattice of 5/5 stacking periodicity exhibits a complex hysteresis curve such as that produced when the properties of a superlattice with 1/1 stacking periodicity and LaMnO_3 are mixed. The hysteresis curve was considered to reflect the properties of both the Fe-Mn interface and LaMnO_3 . The reason for such unique hysteresis is as follows.

Mn layers are pinned by the Fe-O-Mn superexchange interaction at the interface, and the layers become magnetically harder. The effect of the Fe-Mn interaction can reach only the nearest or second-nearest adjacent layers because the magnetic interaction is short range, with the other layers retaining the original LaMnO_3 characteristics.

From these results, the length for conveying the interactions at the interface, i.e., correlation length of the spin, is supposed to be less than two layers.

The magnetization versus temperature curves for $\text{LaMnO}_3\text{-LaFeO}_3$ artificial superlattices (2/2, 3/3, 11/11 sequence) on SrTiO_3 (100) and on LaMnO_3 film (LMO) as

a reference sample are shown in Fig. 4-6 (a). The inset shows the magnetization versus temperature curves of 2/2 superlattices on (100) substrate with different cooling (zero-field cooling (ZFC) and field cooling (FC)) processes and different magnetic fields. For superlattices formed on (100) and (110) substrates, the magnetic properties differed significantly from those of (111) due to the spin frustration effect. For superlattices of larger stacking periodicity, the properties of LaMnO_3 and LaFeO_3 are highly distinct. The properties of LaMnO_3 appear strongly in the temperature range of 5 - 400 K because LaMnO_3 shows a larger magnetization than the antiferromagnetic LaFeO_3 . In contrast to the results from superlattices on SrTiO_3 (111) substrates, the magnetization and T_C of superlattices on (100) substrates decreases as stacking periodicity decreases, and the magnetization becomes unsaturated. The ferromagnetic properties of LaMnO_3 are weakened by the neighboring LaFeO_3 layer because the spin frustration effect occurs at the Mn-Fe interface. To explain this behavior, magnetization versus temperature curves were measured for a 2/2 superlattice at different applied magnetic fields (0.005 and 0.1 T) using different cooling processes (see inset of Fig. 4-6 (a)). The magnetic behavior differs depending on whether the sample is cooled with (FC) or without (ZFC) an applied field. A sharp cusp at about 65 K is observed in the ZFC sample when the applied field is 0.005 T, but this cusp loses its sharpness and becomes a broad maximum, and moves to a lower temperature when the applied field is increased to 0.1 T. This behavior is one of clear evidences for the spin glass state. The increased spin frustration effect caused by the reduced stacking periodicity leads to the formation of a spin-glass-like phase. This is caused by the competition between ferromagnetism in Fe-Mn and Mn-Mn, and antiferromagnetism in Fe-Fe.

The superlattice formed on (110) substrates with $2/2$ stacking periodicity also shows spin-glass-like behavior (Fig. 4-6 (b)). The magnetic field was applied parallel to the [001] direction in the (110) and (100) superlattices to avoid the magnetic anisotropy effects. The magnetization at the glass temperature (T_g) is about $1/3$ that of the (100) superlattice. This is caused by the larger frustration effect than that of (100) superlattices as shown in figure 4-1. The number of bonds where the spin frustration effect occurs in the (110) superlattice is twice as large as that in the (100) superlattice per eight-metal unit cell (Fig. 4-1), which correlates well with the suppression of the magnetization ($1/2 \sim 1/3$). In the case of (110) superlattices, the spin frustration effect is twice as great as that of the (100) superlattice.

($\text{LaFe}_{0.5}\text{Mn}_{0.5}\text{O}_3$ solid solution film)

$\text{LaFe}_{0.5}\text{Mn}_{0.5}\text{O}_3$ solid solution film was formed by PLD method as a reference sample. The XRD patterns for $\text{LaFe}_{0.5}\text{Mn}_{0.5}\text{O}_3$ film formed on SrTiO_3 (111) substrate are shown in Fig. 4-7. The film showed a single phase and had a preferred orientation normal to the surface of the substrate. And, two peaks also observed at 19.7° and 61.5° , respectively. It is considered that it is due to the long periodic features, that is double perovskite features (Fe and Mn ions ordered) of $\text{LaFe}_{0.5}\text{Mn}_{0.5}\text{O}_3$ film. The RHEED patterns also show streaks indicating that the film is epitaxially formed on the substrates up to the topmost surface (Fig. 4-8).

The results of magnetic measurements are shown in Fig. 4-9. The abrupt increase of magnetization, which corresponds to the Curie temperature (T_c), observed in the film at about 380 K and the magnetization increased as temperature decreased (Fig. 4-9 (a)). On the other hand, the bulk material had no clear phase transition in the temperature

range from 50 to 400 K. The clear hysteresis with the coercive field (H_C) of 500 Oe was observed at 6 K (Fig. 4-9 (b)). The saturation magnetization (M_S) from the hysteresis curve was estimated to be about $1.5 \mu_B/\text{site}$ ($\approx 33 \text{ emu/g}$). It is too small if it is due to the ferromagnetic interactions between $\text{Fe}^{3+}\text{-O-Mn}^{3+}$ (theoretical estimation $4.5 \mu_B/\text{site}$) and too large for ferrimagnetic interactions (theoretical estimation $0.5 \mu_B/\text{site}$). It is considered that this is due to the partial ordering of Fe and Mn ions (because there are no signs for phase separation in XRD patterns) and the bulk $\text{LaFe}_{0.5}\text{Mn}_{0.5}\text{O}_3$ has no ordering. The simulation of XRD patterns for ordered $\text{LaFe}_{0.5}\text{Mn}_{0.5}\text{O}_3$ film was performed and the intensity and positions of superlattice peaks were estimated. The simulated intensity of the superlattice peak as compared with the (111) peak ($I_{\text{SL}}/I_{(111)}$) was 0.8 % and our experimental result was 0.33 %. The ratio of ordering of Fe and Mn ions are estimated to be 41.25 %, and M_S is estimated to be $1.86 \mu_B/\text{site}$ ($=4.5 \mu_B/\text{site} * 41.25\%$) from the result. The estimation agree well with the results of magnetization measurements ($M_S \approx 1.5 \mu_B/\text{site}$).

The reasons for ordering of Fe and Mn ions in $\text{LaFe}_{0.5}\text{Mn}_{0.5}\text{O}_3$ film are considered as follows. The reasons for ionic ordering in other well known bulk double perovskite ($\text{AB}'\text{B}''\text{O}_3$ type- $\text{LaMn}_{0.5}\text{Co}_{0.5}\text{O}_3$, $\text{SrFe}_{0.5}\text{Mo}_{0.5}\text{O}_3$ etc. : the order of B' and B'' ions in the (111) direction occurred naturally) are considered as follows. One reason is that large difference of ionic size between B' and B'' ions and that the other is charge separation between B' and B'' ions ($\text{B}'^{3+} + \text{B}''^{3+} \rightarrow \text{B}'^{4+} + \text{B}''^{2+}$ etc.). The first one is omitted because the ionic size of Fe and Mn ions are almost the same. The XPS (X-ray photoemission spectroscopy) measurements of the films were performed to determine the valence number of Fe and Mn ions. The valence number of Mn ions is 3+ and 4+,

and the relative intensity is 2:1 for 3+:4+, respectively. The valence number of Fe ions, is 3+ and 2+, and the relative intensity is 2:1 for 3+:2+, respectively. I think that the Mn⁴⁺ ions appeared for the doping effect for La deficiency [8] and Fe²⁺ ions appeared for the lower oxygen pressure to form the films than those in bulk materials. The Ellingham diagram for Mn and Fe oxides are shown in Fig. 4-10. The mixed valence state of Fe³⁺ and Fe²⁺ are appeared in the conditions around 10⁻³ Torr (PO₂) and 600 °C (conditions to film formation). It is thought that the charge separation between Fe and Mn ions (Fe³⁺+Mn³⁺→Fe²⁺+Mn⁴⁺) cause the partial ordering of Fe and Mn ions. The process of film formation stabilize the metastable state.

The magnetic properties of LaFe_{0.5}Mn_{0.5}O₃ solid solution film and LaFeO₃-LaMnO₃ formed on SrTiO₃ (111) with 1/1 sequence show different behaviors in spite of the similarity of crystal structures. The T_C of the superlattice (1/1) and LaFe_{0.5}Mn_{0.5}O₃ solid solution film was appeared at about 230 K and 380 K, respectively. I think this is because the valence number of Fe ions are quite different in these materials. But, we need detailed measurements (XPS etc.) to compare the valence state of Fe ions in these materials.

4-4 Conclusion

To summarize, LaMnO₃-LaFeO₃ artificial superlattices were constructed on SrTiO₃ (111), (100) and (110) substrates using PLD methods and their magnetic properties were evaluated. The magnetization of superlattices constructed on the (111) plane increased as the stacking periodicity decreased, and the superlattice with 1/1 stacking periodicity exhibited ferromagnetic (or ferrimagnetic) behavior. For (100) and (110) superlattices, on the other hand, the spin frustration effect increased with lower stacking

periodicity and spin-glass-like behaviors was observed in superlattices with a stacking periodicity of less than $3/3$.

[1] H. Fujita, H. Tamura and J. Kaneko, *Appl. Phys. Lett.* **65**, 1070 (1994).

[2] S. G. Samal, A. Gupta, *Chem. Phys. Lett.* **171**, 105 (1989) and *Phys. Rev. B* **44**, 8772 (1991).

[3] M. Yoshizawa, H. Inagaki, S. Okada, T. T. Wang, S. Okajima and H. Kuroki, *Physica C*, **199**, 157 (1995).

[4] K. Oishi, T. Gotoh and T. Kuroki, *Physica C*, **199**, 161 (1995).

[5] H. Tamura, K. Oishi and T. Kuroki, *J. Phys. Chem. B*, **104**, 1011 (2000).

[6] W. C. Yeh, C. H. Yeh and M. H. Wu, *Appl. Phys. Lett.* **78**, 1198 (2001).

[7] D. Byers, *J. Appl. Phys.* **76**, 1774 (1994).

[8] S. Ghosh, T. R. Maloney, P. A. Thirumangalakudi, M. Kato, J. Sun, W. J. Gallagher, and J. H. Park, *Appl. Phys. Lett.* **87**, 1094 (2005).

[9] I. Kozlov, *J. Phys. Chem. Solids* **18**, 27 (1961).

[10] J. B. Goodenough, *Phys. Rev.* **100**, 564 (1951).

[11] G. Blau, *J. Phys. Chem. Solids* **14**, 108 (1960).

[12] J. B. Goodenough, A. Watt, R. J. Auld and H. Morosin, *Phys. Rev.* **124**, 171 (1961).

[13] Eric E. Fullerton, K. T. Regan, C. H. Seaman, and L. D. Bateman, *Phys. Rev. Lett.* **75**, 28 (1995).

[14] Eric E. Fullerton, L. D. Bateman and J. L. Johnson, *Phys. Rev. Lett.* **77**, 2002 (1996).

[15] Z. Q. Qiu, J. Pomonis, A. Brink and S. M. Mansur, *Phys. Rev. Lett.* **64**, 1796 (1990).

[16] E. N. Abarca, K. Takaya, J. Terabe, and A. E. Giblin, *Phys. Rev. Lett.* **77**,

4-5 References

- [1] H. Tabata, H. Tanaka and T. Kawai, Appl. Phys. Lett. **65**, 1970 (1994).
- [2] G. Q. Gong, A. Gupta, Gang Xiao, P. Lecoeur and T. R. McGuire, Phys. Rev. B **54**, R3742 (1996).
- [3] M. Yoshimoto, H. Nagata, S. Gonda, J. P. Gong, H. Ohkubo and H. Koinuma, Physica C, **190** (1991) 43.
- [4] K. Ueda, H. Tabata and T. Kawai, Science **280**, (1998) 1064.
- [5] H. Tabata, K. Ueda and T. Kawai, J. Mat. Sci. & Eng. B **56**, 140 (1998).
- [6] W. C. Koehler, E. O. Wollan and M. K. Wilkinson, Phys. Rev. **118**, 58 (1960).
- [7] D. Treves, J. Appl. Phys. **36**, 1033 (1965).
- [8] A. Gupta, T. R. McGuire, P. R. Duncombe, M. Rupp, J.Z.Sun, W. J. Gallagher, and Gang Xiao, Appl. Phys. Lett. **67**, 3494 (1995).
- [9] J. Kanamori, J. Phys. Chem. Solids **10**, 87 (1959).
- [10] J. B. Goodenough, Phys. Rev. **100**, 564 (1955).
- [11] G. Blasse, J. Phys. Chem. Solids **26**, 1969 (1965).
- [12] J. B. Goodenough, A. Wold, R. J. Arnett and N. Menyuk, Phys. Rev. **124**, 373 (1961).
- [13] Eric E. Fullerton, K. T. Riggs, C. H. Sowers, and S. D. Bader, Phys. Rev. Lett. **75**, 330 (1995).
- [14] Eric E. Fullerton, S. D. Bader and J. L. Robertson, Phys. Rev. Lett. **77**, 1382 (1996).
- [15] Z. Q. Qiu, J. Pearson, A. Berger and S. D. Bader, Phys. Rev. Lett. **68**, 1398 (1992).
- [16] E. N. Abarra, K. Takano, F. Hellman, and A. E. Berkowitz, Phys. Rev. Lett. **77**,

3451 (1996).

[17] C. A. Ramos, D. Lederman, A. R. King, and V. Jaccarino, Phys. Rev. Lett. **65**, 2913 (1990).



Fig. 4-1. Schematic models of spin structures in LaMnO₃-LaFeO₃ artificial superlattices grown on (111), (100) and (110) surfaces. In the figure, AF and FM means antiferromagnetic and ferromagnetic, respectively. For (100) and (110) superlattices, the 'X' signs show the interactions where the spin frustration effect decays.

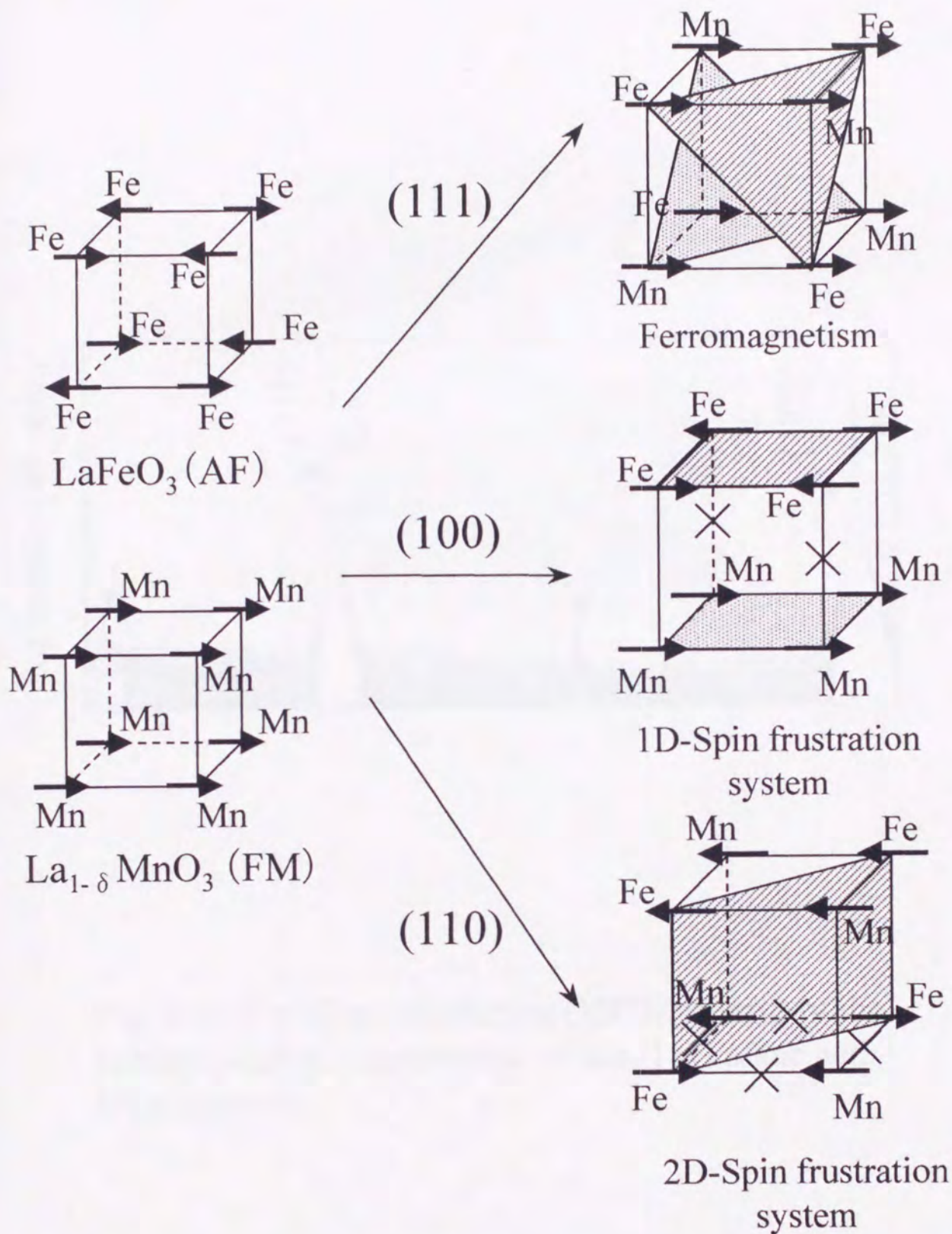


Fig. 4-1 : Schematic models of spin structures in LaMnO_3 - LaFeO_3 artificial superlattices grown on (111), (100) and (110) surfaces. In the figure, AF and FM means antiferromagnetic and ferromagnetic, respectively. For (100) and (110) superlattices, the \times signs show the interactions where the spin frustration effect occurs.

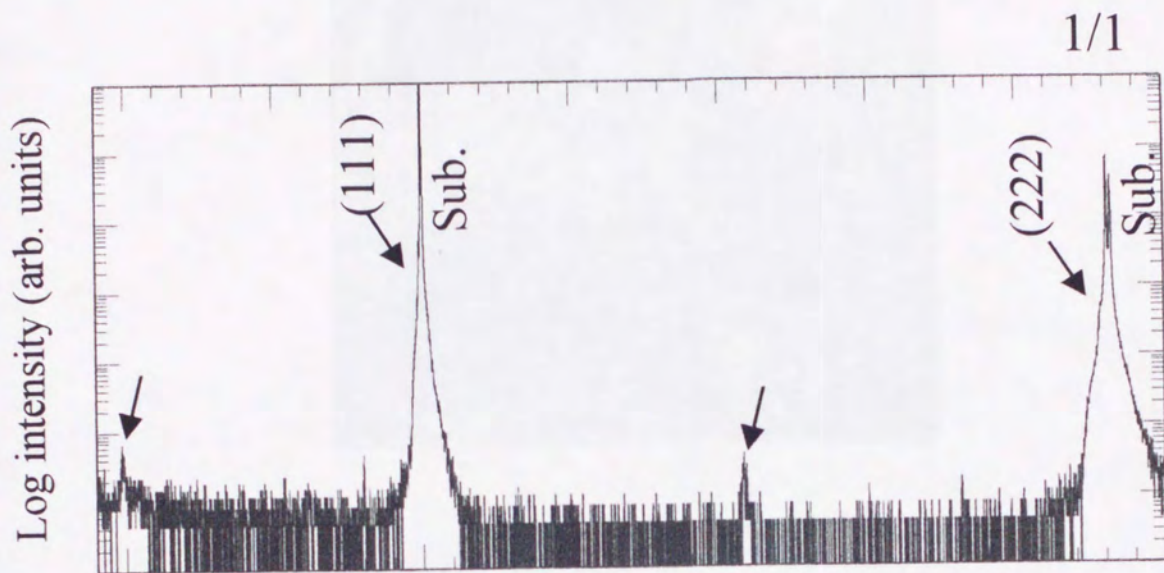
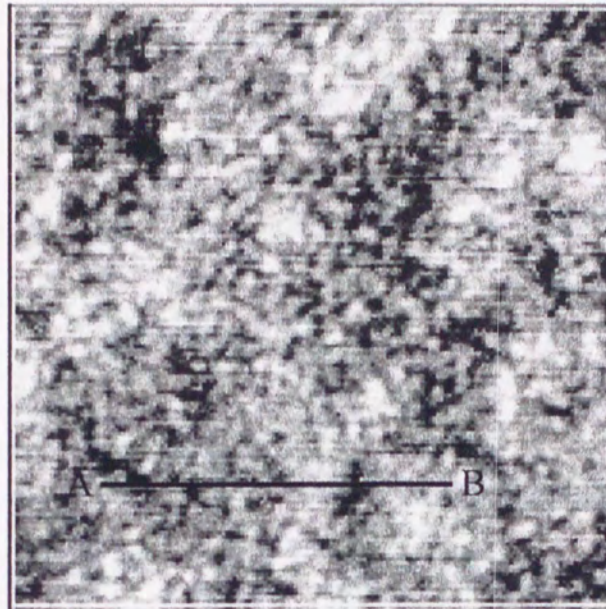


Fig. 4-2 : The X-ray diffraction (XRD) patterns of the $\text{LaMnO}_3\text{-LaFeO}_3$ superlattice on the (111) plane with 1/1 sequences.

(a)



(b)

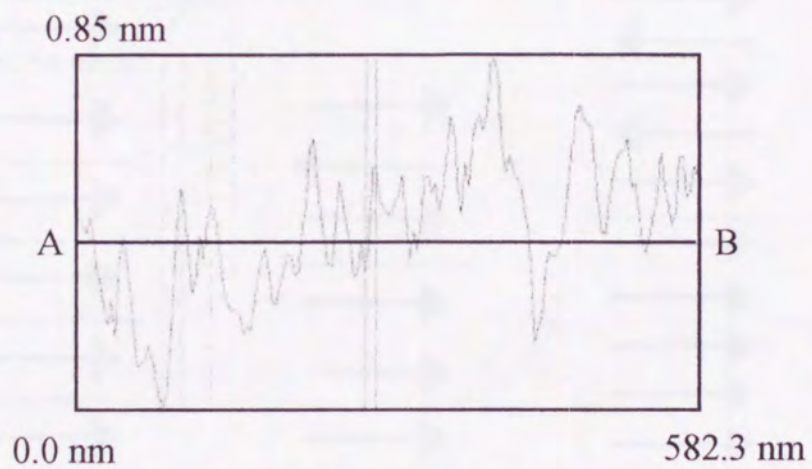


Fig. 4-3 : The (a) AFM image and (b) cross-sectional view of the $\text{LaMnO}_3\text{-LaFeO}_3$ superlattice on the (111) plane with 17/17 sequences.

(111)

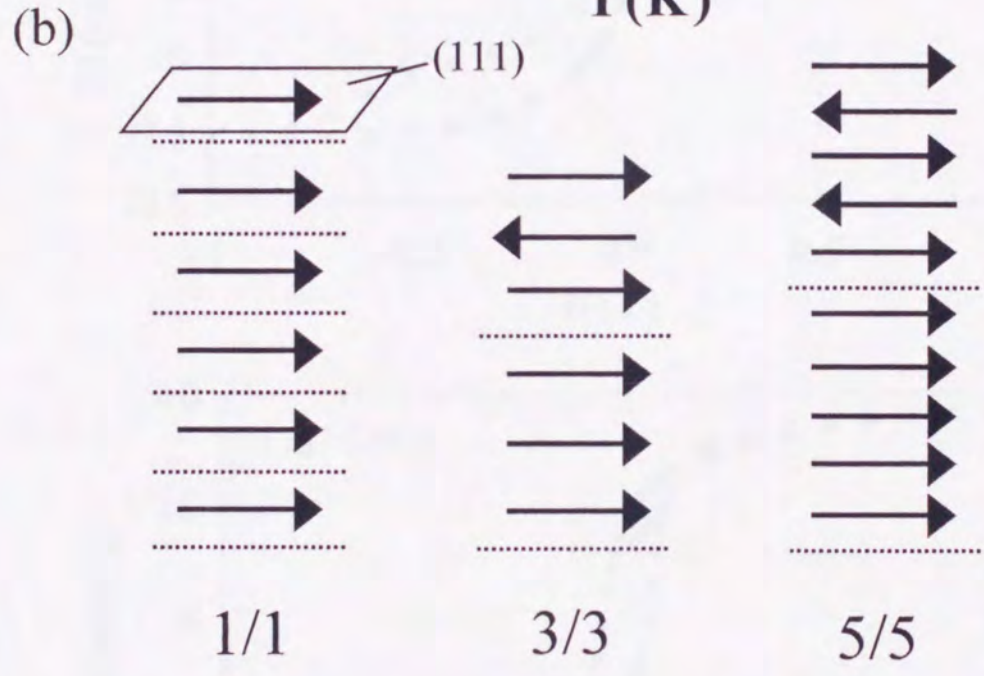
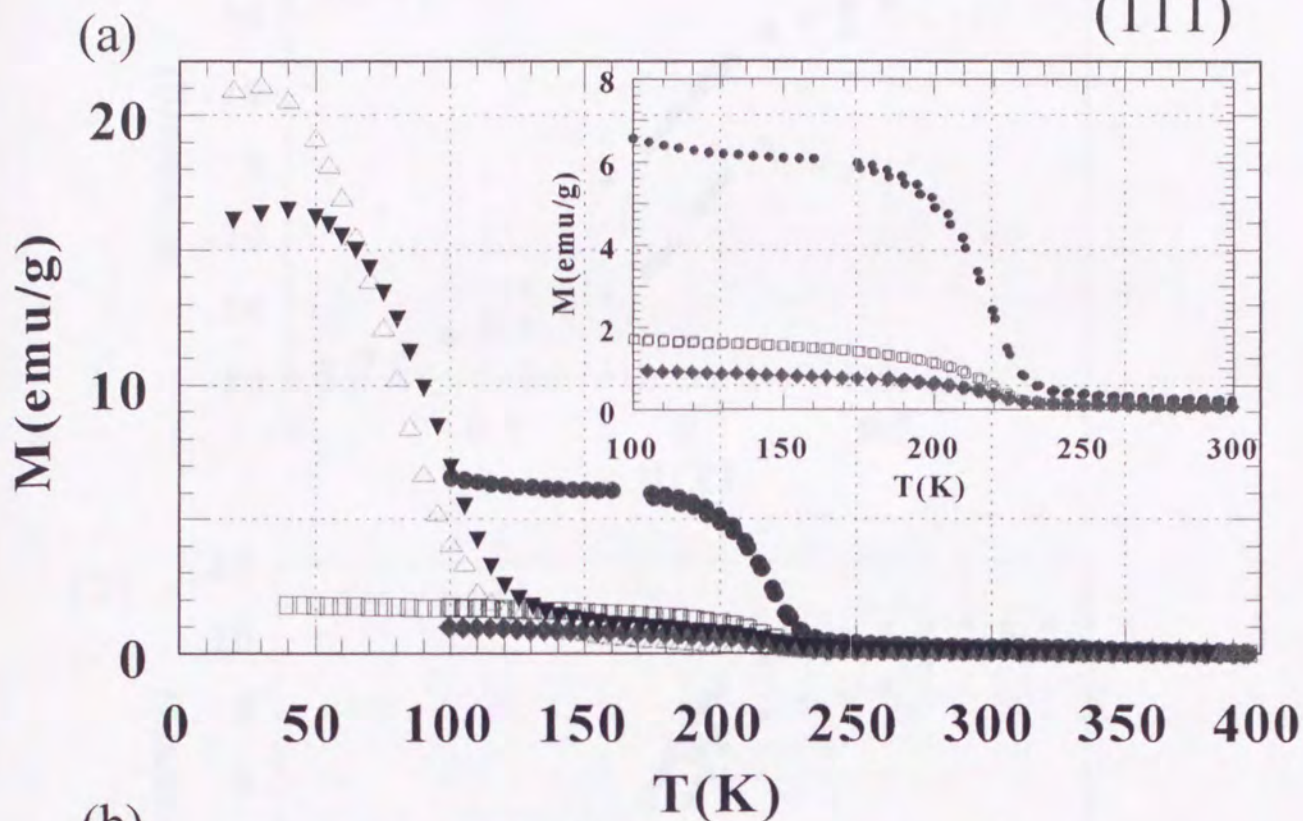


Fig. 4-4 : (a) Temperature dependence of Magnetization for LaMnO_3 - LaFeO_3 superlattices formed on SrTiO_3 (111) with various stacking periodicity (1/1-●, 5/5-□, 9/9-◆, 30/30-▼) and for LaMnO_3 film (Δ) in a magnetic field of 0.1T. The inset shows an enlargement of the M - T curves of (111) superlattices with 1/1, 5/5 and 9/9 sequences. (b) Schematic spin structures of LaMnO_3 - LaFeO_3 superlattice with 1/1, 3/3 and 5/5 sequence on a (111) plane. Each arrow shows the synthesis of the spin moment of magnetic ions in each (111) surface.

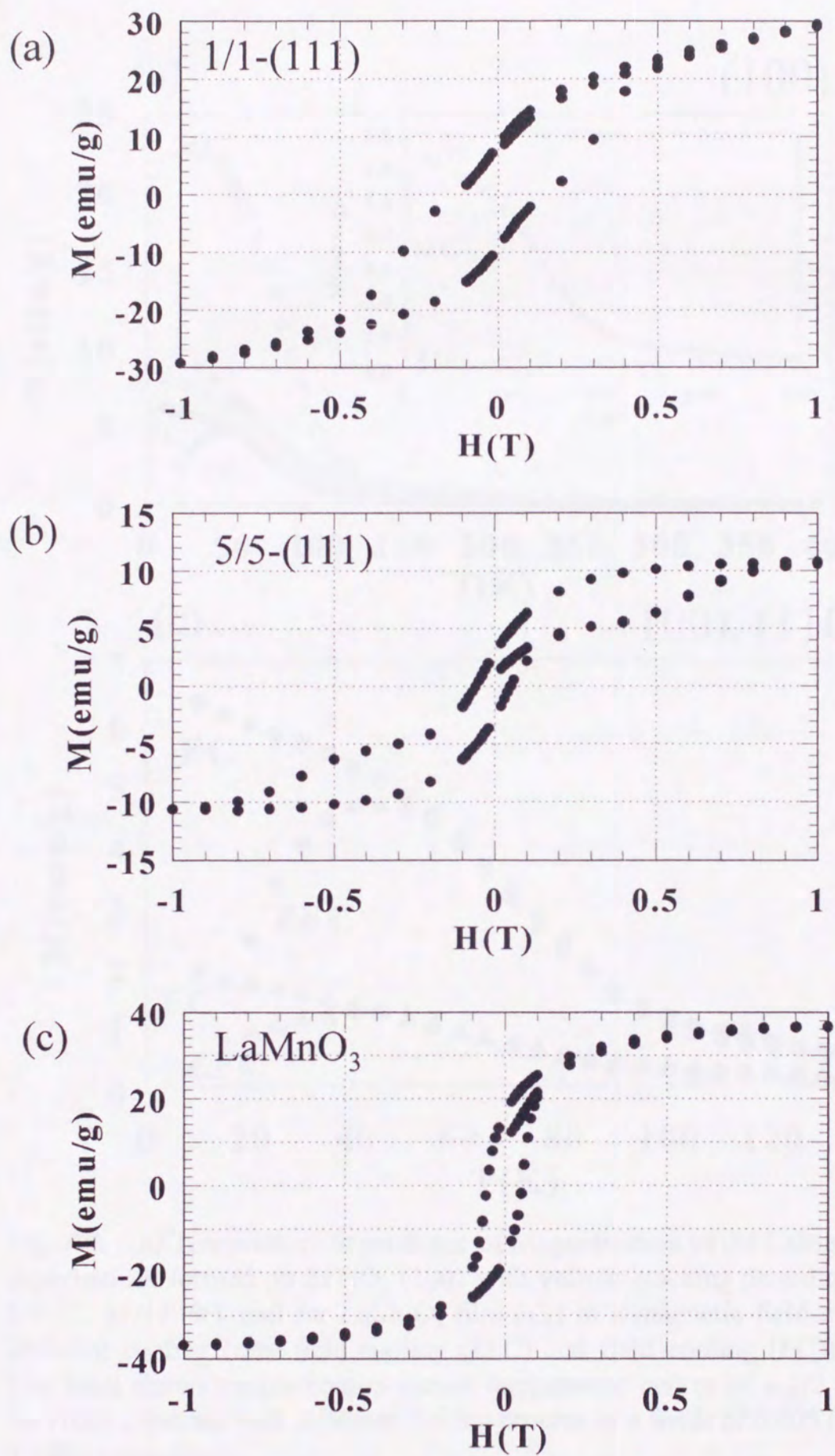


Fig. 4-5 : Hysteresis curves of LaMnO_3 - LaFeO_3 superlattices formed on SrTiO_3 (111) with (a) $1/1$ and (b) $5/5$ stacking periodicity, and (c) that of LaMnO_3 film at 6K.

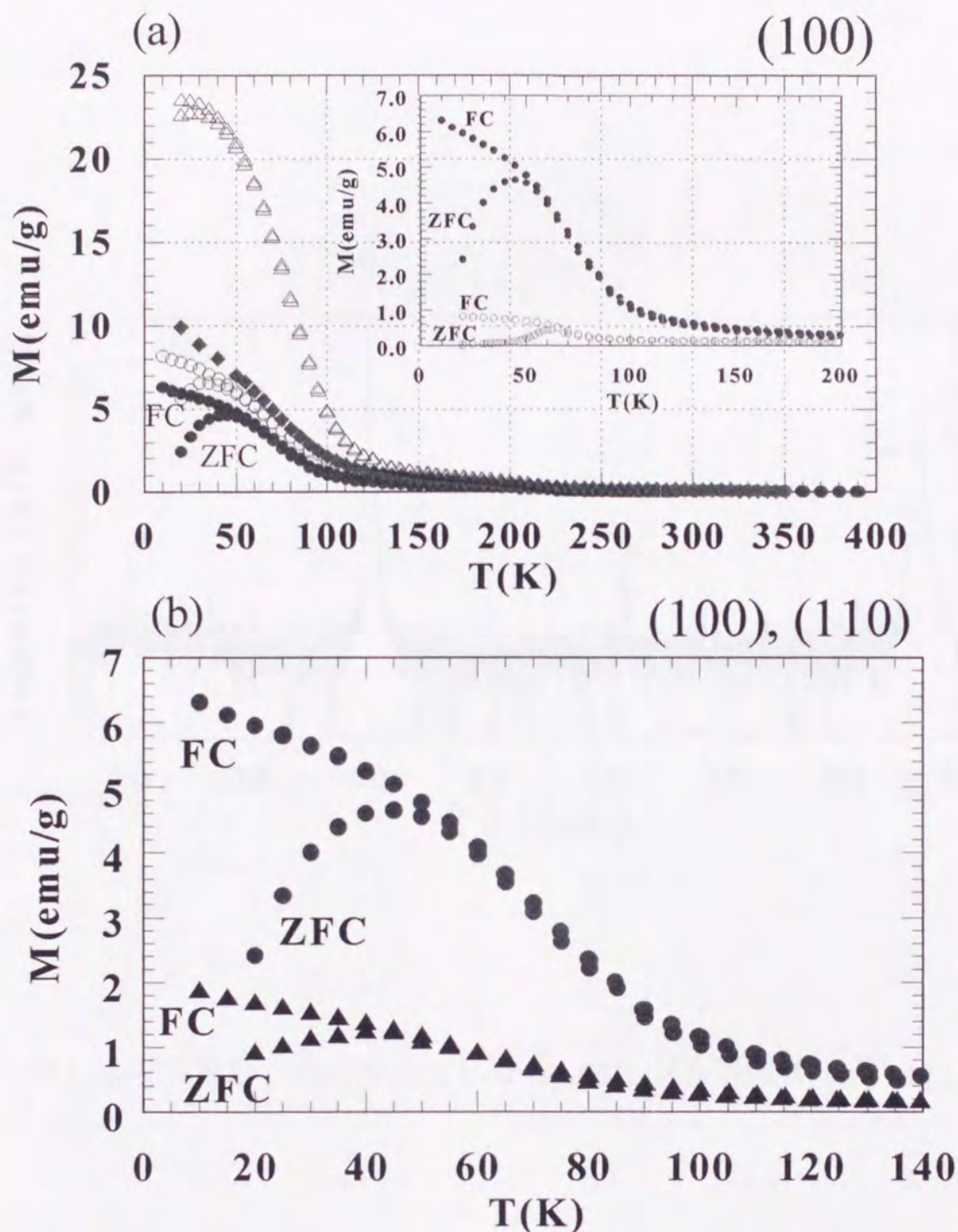


Fig. 4-6 : (a) Temperature dependence of Magnetization of the $\text{LaMnO}_3\text{-LaFeO}_3$ superlattices formed on SrTiO_3 (100) with various stacking periodicity (2/2-●, 3/3-○, 11/11-◆), and for LaMnO_3 film (Δ) in a magnetic field of 0.1T with different cooling (zero-field cooling (ZFC) and field cooling (FC)) processes. The inset shows magnetization versus temperature curves of a 2/2 superlattice on (100) substrate with different cooling process in a fields of 0.005 (○) and 0.1 T (●), respectively.

(b) Magnetization versus temperature curves of 2/2 superlattices on (100) (●) and (110) (▼) substrates with different cooling process.

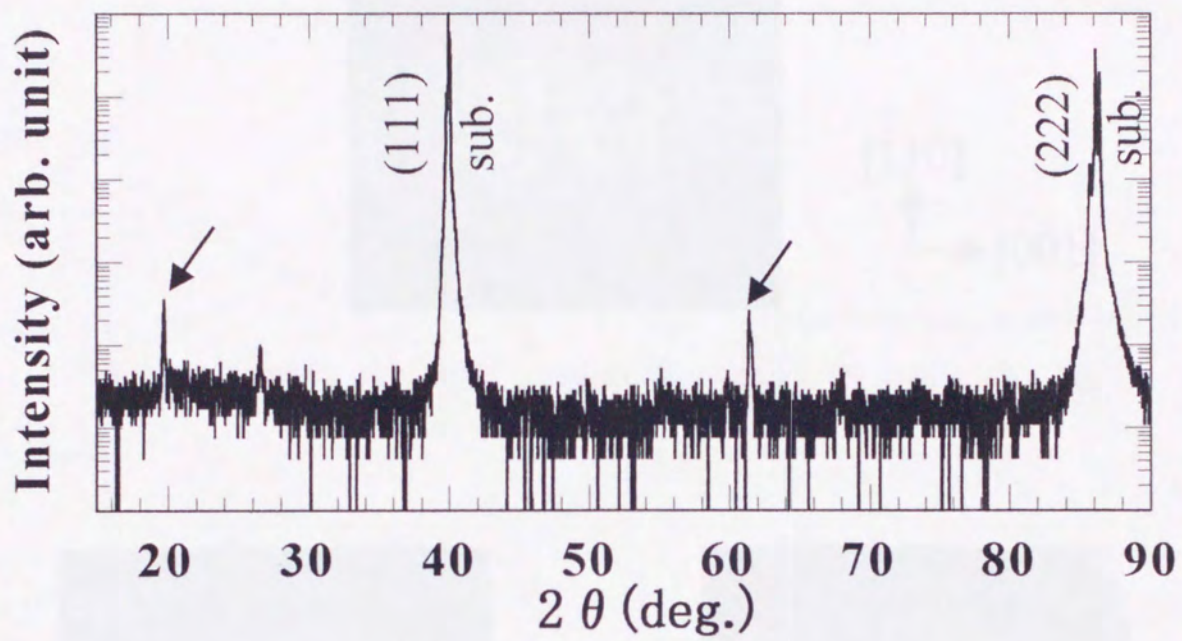


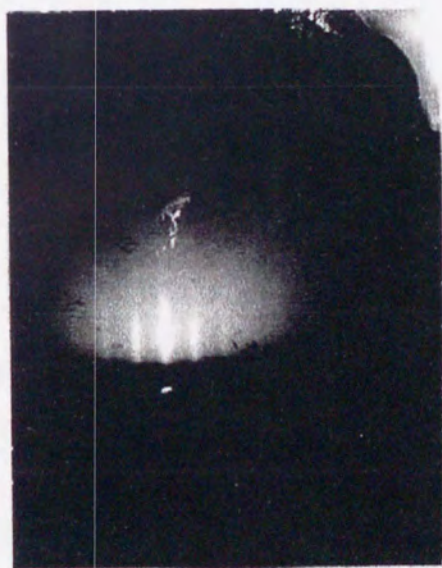
Fig. 4-7 XRD patterns for $\text{LaFe}_{0.5}\text{Mn}_{0.5}\text{O}_3/\text{SrTiO}_3$ (111)



[110]
↑
→ [001]



[110]
↑
→ [102]



[110]
↑
→ [1 $\bar{1}$ 0]

Fig. 4-8 RHEED patterns for $\text{LaFe}_{0.5}\text{Mn}_{0.5}\text{O}_3/\text{SrTiO}_3(110)$

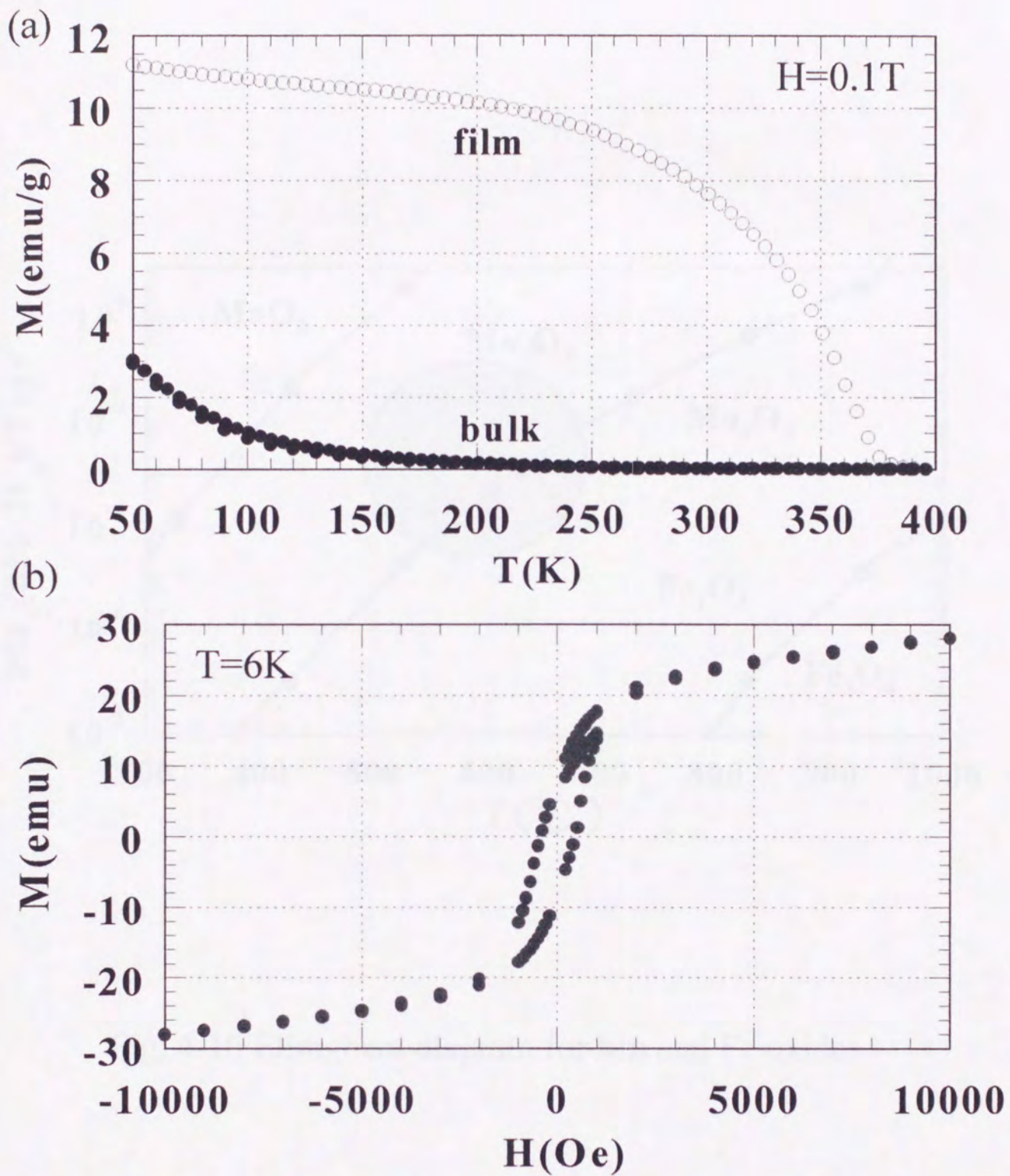


Fig. 4-9 (a) Magnetization vs. temperature curves of $\text{LaFe}_{0.5}\text{Mn}_{0.5}\text{O}_3$ bulk material and film in the magnetic field of 0.1 T and (b) hysteresis curve of $\text{LaFe}_{0.5}\text{Mn}_{0.5}\text{O}_3$ film at 6 K.

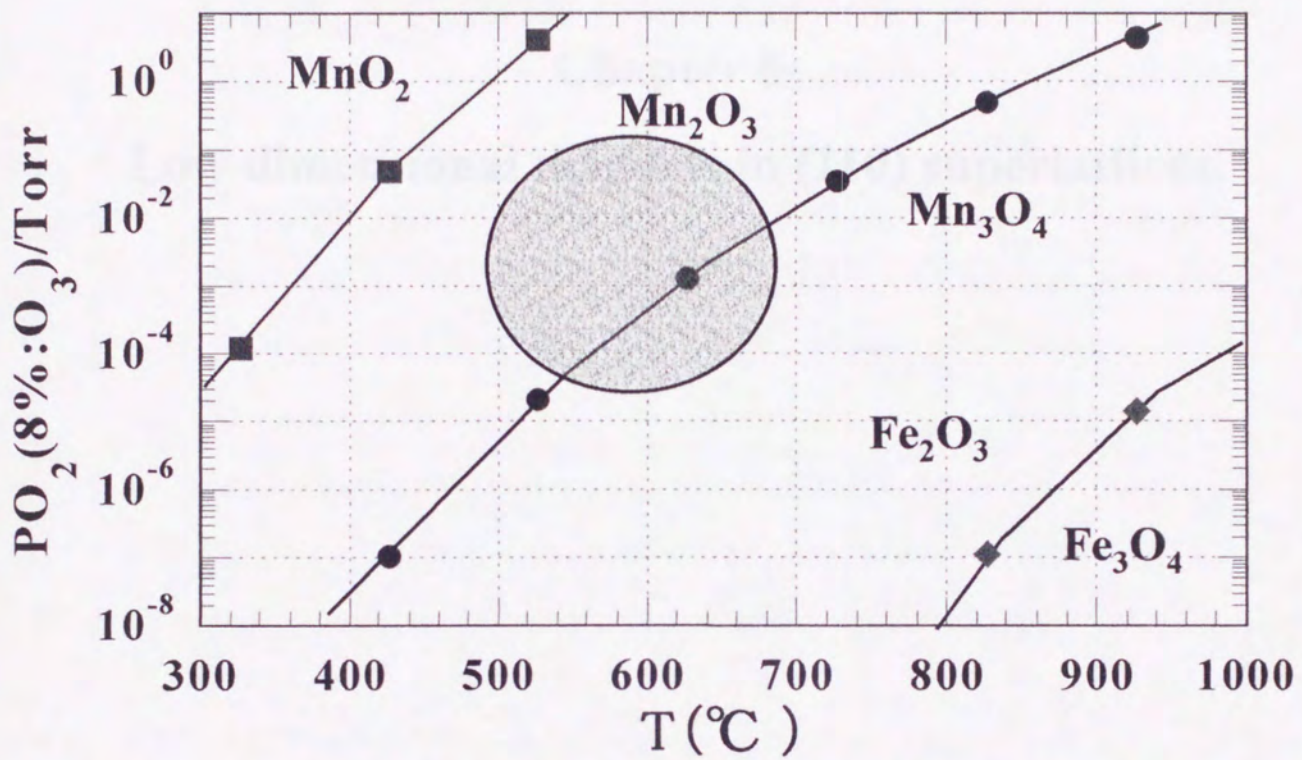


Fig. 4-10 Ellingham diagram for Mn and Fe oxides

5.1 - Control of the magnetic and electric properties of low-dimensional
magnets in (110) superlattices

Chapter 5

Low dimensional magnets in (110) superlattices

The importance of low-dimensional magnets in (110) superlattices is
highlighted by the fact that they are the only system where the
magnetic and electric properties are coupled. This is due to the
presence of the spin-orbit interaction which couples the spin and
orbital degrees of freedom.

5.1.1 Introduction

Low-dimensional magnets have been studied for many years. The
interest in these systems is due to the fact that they exhibit
unique magnetic properties which are not observed in bulk
materials. In particular, the magnetic properties of these
systems are highly sensitive to the dimensionality of the system.
This is due to the fact that the magnetic interactions are
strongly anisotropic in these systems. In particular, the
magnetic interactions are much stronger in the plane of the
system than they are perpendicular to the plane. This leads to
the formation of magnetic layers which are coupled to each other
along the direction of the system.

5.1 Control of the magnetic and electric properties of low dimensional SrRuO₃-BaTiO₃ superlattices

Artificial superlattices of SrRuO₃ and BaTiO₃ were formed on SrTiO₃(110) substrates with various stacking periodicity, and their magnetic and electric properties were examined. The ferromagnetic Curie temperature and magnetization of the superlattices decreased as stacking periodicity decreased. Especially, the antiferromagnetic behaviors and anisotropy of resistivity were observed in the 2/5 superlattice. The low dimensional effects appeared remarkably in the 2/5 superlattice.

5.1-1 Introduction

Many important researches have been performed on the systems in which the magnetic interactions are restricted in one- or two-dimension, that is, the low-dimensional quantum spin system. In the system, many quantum effects such as spin-Peierls transition [1], Haldane-gap [2], etc. appear remarkably, and these effects have attracted many researchers. A lot of studies have been devoted to clarify the physical properties of low dimensional quantum spin system, but there still remain unknown subjects.

Especially, the one-dimensional (1D) system is very interesting because of their quantum properties. There are a few materials which have 1D spin structure naturally because they have peculiar types of crystal structures. They are limited to some metal oxides such as CuGeO_3 [3], NENP [4], NaV_2O_5 [5], etc. and organic materials such as TTF-CuBDT [6], MEM-(TCNQ)₂ [7], etc.. The control of the carrier density, spin number, magnitude of the exchange interaction, etc. are also not easy in these materials.

It is thought that the method that allow us to make low dimensional structures and to control the number of carriers, spin number, etc. of the system freely brings very large impact on the study of low dimensional spin system. The method of the artificial superlattice in perovskite-type oxides (ABO_3) is one of the candidates to satisfy the demand. The materials with various electronic states, that is, various spin states can be formed by the selection of proper A-site and B-site ions in perovskites and the crystal structures remain almost unchanged to the substitution of A-site and B-site ions. The low dimensional magnetic materials with various spin states can be formed by depositing magnetic and nonmagnetic layers alternately with an atomic or molecular scale using the method of the artificial superlattice in perovskite type oxides (Fig. 5-1). The control of the dimensionality is possible by changing the number of layers of the magnetic material, that is, the thickness of the magnetic layer.

Such attempts had been already performed. In these studies, the low dimensional spin structures were constructed by the combination of magnetic and nonmagnetic layers epitaxially formed on SrTiO_3 (100) substrates [8-10]. However, the method allows us to form two-dimensional spin structure at most because the SrTiO_3 (100) surfaces have the isotropic feature (we can not make one-dimensional magnets by the method). The path composed by B-site ions and oxygen (B-O-B-O chain) exist two dimensionally in the (100) surface (Fig. 5-2 (a)). However, it only exists in one direction on the (110) surface (Fig. 5-2 (b)). The two-dimensional feature of (100) surfaces and one-dimensional features of (110) is called isotropic and anisotropic, respectively in this study.

In this study, I paid attention to the anisotropy of perovskite (110) surfaces and tried to form one-dimensional magnetic materials by the magnetic-nonmagnetic artificial superlattices formed on SrTiO_3 (110) substrates.

The SrRuO_3 and BaTiO_3 were selected as starting materials. The SrRuO_3 is one of the ferromagnetic materials with the Curie temperature (T_C) of 140 - 150 K and show metallic behaviors [11-13]. It has a low spin structure ($S=1$) due to its relatively weak correlating interaction. The BaTiO_3 is one of well known ferroelectric material, that is, nonmagnetic insulator [14]. It used as the spacer layer of SrRuO_3 . The reduction of

the dimensionality of SrRuO₃ layer by the formation of magnetic-nonmagnetic superlattice is expected to affect both electric and magnetic properties.

These are the concepts of the material design to make one-dimensional magnetic materials. Artificial superlattices with various stacking sequences were also formed to determine the region where the low dimensional effects appeared, and their physical properties are examined simultaneously.

5.1-2 Experimental

Artificial superlattices were formed on SrTiO₃ (110) substrate by stacking SrRuO₃ and BaTiO₃ layers using a multi-target pulsed laser deposition (PLD) technique [15-16]. The SrRuO₃ and BaTiO₃ targets were prepared by standard ceramic techniques. All the films were formed at 720 - 750 °C in an oxygen/ozone (8%) ambient pressure of 1×10^{-3} Torr with an energy density of 1 - 2 J/cm². The deposition rate was 10 - 20 Å /min. The total thickness of the films was 800 - 1000 Å. The thickness of individual layers were controlled by the number of laser pulses (The deposition rate were calibrated against the number of laser pulses combined with reflection high energy electron diffraction (RHEED) measurements). The structure of the lattice was characterized by X-ray diffraction ($2\theta - \theta$ scan) using a Cu-K_α source (Rigaku :

RINT 2000). Surface morphology was observed by atomic force microscopy (AFM : Digital Instruments-Nanoscope III). Magnetic measurements were performed using a commercial superconducting quantum interference device (SQUID) magnetometer (Quantum design MPMS-5S) with the magnetic field applied parallel to the film plane. Resistivity measurements were carried out using the standard four probe technique.

5.1-3 Results and Discussion

The crystal structures of the SrRuO₃ and BaTiO₃ on SrTiO₃ (110) substrates were studied using $2\theta - \theta$ X-ray diffraction (XRD) (Fig. 5-3). All the films showed a single phase and had a preferred orientation normal to the surface of the substrate (<110> direction).

The results of magnetic and electric measurements of SrRuO₃ single phase film formed on SrTiO₃ (110) are shown in Fig. 5-4. The abrupt increase in magnetization vs. temperature (M-T) curve and the cusp in resistivity vs. temperature (R-T) curve appeared at about 140 K, which considered to be the Curie temperature (T_C). The T_C of 140 K is almost the same with that of bulk SrRuO₃ [11-12].

The superlattices of SrRuO₃ and BaTiO₃ were formed on SrTiO₃ (110) substrates with various stacking periodicity (5/5 : five-layers by five-layers, 11/11, 25/25). The crystal

structures of the superlattices were examined by XRD measurements (Fig. 5-5). Typical features of the superlattice were observed in the superlattices. Satellite peaks can be observed adjacent to the main (110) and (220) peaks, indicating the chemical modulation and/or strained interfacial profile of the superlattice structures. From the position of the peaks, the modulation wave length of the superlattices was estimated to be 32, 60 and 138 Å for 5/5, 11/11 and 25/25 superlattices, respectively, which agree well with our designed sequence (5/5 for 28 Å, 11/11 for 62 Å, 25/25 for 140 Å). The absence of higher order satellites indicates the existence of thickness variation of SrRuO₃ and BaTiO₃ layers.

The reflection high energy electron diffraction (RHEED) measurements show streaked patterns indicating that the superlattices are formed epitaxially on the substrates up to the topmost surface (Fig. 5-6). These results of X-ray diffraction and RHEED patterns indicate that the SrRuO₃-BaTiO₃ superlattices are well constructed as desired.

The AFM surface image and cross-sectional view is taken for SrRuO₃-BaTiO₃ superlattices with a 5/5 stacking periodicity (Fig. 5-7). The root-mean-square roughness perpendicular to the surface (scanning area : 1 μm × 1 μm) and the average roughness is 0.7 and 0.5 Å (less than 1 unit layer), respectively. Surface

morphology is very good and it is considered that multilayered systems are constructed by good quality layers.

The M-T curves of the superlattices with various stacking periodicity (two-layer of SrRuO₃ and five-layer of BaTiO₃-2/5, 5/5, 11/11, 25/25 and 45/45) are shown in Fig. 5-8. The magnetic field of 0.2 T were applied in <001> direction for the 5/5, 11/11, 25/25 and 45/45 superlattices and 1 T for the 2/5 superlattice. The magnetization and the T_C (140 - 150K) of 45/45 and 25/25 superlattices, which have larger stacking periodicity, was almost the same with those of the SrRuO₃ single phase film. In the case of 5/5 and 11/11 superlattices, which have smaller stacking periodicity, the magnetization and the T_C decreased as stacking periodicity decreased. Especially, in the M-T curve of the 2/5 superlattice, the cusp feature appeared at around 250 K, which is considered to be antiferromagnetic Neel temperature (T_N) (Fig5-8 inset). These results are due to the reduction of dimensionality of the magnetic SrRuO₃ layers. These antiferromagnetic behaviors of the 2/5 superlattice agree well with those of Sr₂RuO₄ and Sr₃Ru₂O₇ (layered perovskite-type oxides) which have natural low dimensional perovskite structure [17].

The R-T curves of the superlattices (5/5, 11/11, 25/25 and 45/45) are shown in Fig. 5-9 (a), and the enlargement of the R-T curve of 11/11 superlattice is shown in Fig. 5-9 (b). In 45/45 and 25/25 superlattices, the metallic features were observed and the anomaly

appeared at around 150 K. These behaviors resemble with those of SrRuO₃ single phase film (Fig. 5-4 (b)). The ferromagnetic and metallic features remains almost perfectly in 45/45 and 25/25 superlattice. On the other hand, the 5/5 superlattice shows semiconductive behaviors, and the 11/11 superlattice shows behaviors from metallic to semiconductive at around 150 K. These results of magnetic and electric measurements show that the ferromagnetic and metallic properties of SrRuO₃ begins to collapse from around the 11 layers, that is, the thickness of around 30 Å because of the reduction of dimensionality of the magnetic layer.

The R-T curves of 2/5, 5/5 and 45/45 superlattice along <001> and <110> directions are compared (Fig. 5-10). In the case of the 5/5 and 45/45 superlattice, the R-T curves along <001> and <110> directions were almost overlapped. This means that the conductivity are almost isotropic. The anisotropy of conductivity appeared in the 2/5 superlattice. The resistivity along <110> direction is one order larger than that along <001> direction. The anisotropy is caused by the reduction of dimensionality of the SrRuO₃ layer and appeared remarkably in the 2/5 superlattice.

The effects of lattice strain were also considered because the lattice mismatch between SrRuO₃ and BaTiO₃ is relatively large ($\approx 1.5\%$). The lattice constants and T_c against the number of SrRuO₃ layers of the superlattices are plotted in Fig. 5-11. It

seems that the behaviors of lattice constants and T_C well correlated and that the sudden decrease of T_C around 11 layers is caused by the increase of lattice constants, that is, lattice strain effects.

These results were compared with those of the layered perovskite [17] and SrRuO_3 - SrTiO_3 superlattices formed on SrTiO_3 (100) [8-9] which has little lattice mismatch ($\approx 0.6\%$). In these studies, the ferromagnetism of SrRuO_3 collapsed from 3 - 4 unit cell layers, that is the film thickness of 12 - 15 Å. In our system, the ferromagnetism collapsed from 11 layers, that is the film thickness of about 30 Å. I consider this early breakdown of ferromagnetism is mainly due to the lattice strain effects. The formation of SrRuO_3 - SrTiO_3 superlattices on SrTiO_3 (110) is needed to clarify the effects of the lattice strain.

5.1-4 Conclusions

The artificial superlattices of SrRuO_3 and BaTiO_3 were formed on SrTiO_3 (110) substrates with various stacking periodicity and their magnetic and electric properties were examined. The ferromagnetic and metallic features of SrRuO_3 began to collapse from 11 layers. Especially, the antiferromagnetic behaviors and anisotropy effects of resistivity were observed in the 2/5 superlattice. It is thought that these behaviors are

due to both the reduction of dimensionality of the SrRuO_3 layer and lattice strain between the interfaces of SrRuO_3 and BaTiO_3 .

[1] J. H. Park and J. C. Lagarias, *Phys. Rev. Lett.* **74**, 1077 (1995).

[2] T. M. Rice, *Phys. Rev. Lett.* **20**, 1175 (1968).

[3] M. Imada, J. Terakura, and E. Ohno, *Phys. Rev. Lett.* **79**, 3671 (1997).

[4] G. Z. Brown, M. Verdaguer, C. F. Majumdar, W. H. Li, *Phys. Rev. Lett.* **79**, 3671 (1997).

[5] J. Lagarias, *Phys. Rev. Lett.* **79**, 3671 (1997).

[6] M. Imada and E. Ohno, *J. Phys. Soc. Jpn.* **68**, 1175 (1999).

[7] T. H. Kim, H. W. Han, K. J. Yoon, J. S. Kim, J. B. Seok, G. D. Park, A. H. Wu, and J. C. Lagarias, *Phys. Rev. Lett.* **85**, 1111 (2000).

[8] J. H. Park and J. C. Lagarias, *Phys. Rev. Lett.* **85**, 1111 (2000).

[9] S. Maiti, J. Terakura, D. A. Swanson, R. F. Smith, K. Terakura, W. J. M. de Jong, and J. Rhee, *Phys. Rev. Lett.* **85**, 4321 (2000).

[10] M. Imada, K. Nakamura, and E. Ohno, *J. Phys. Soc. Jpn.* **67**, 661 (1998).

[11] M. Imada, K. Nakamura, E. Ohno, T. Yamada, and J. Terakura, *Solid State Comm.* **106**, 111 (1998).

[12] H. Terakura, H. Watanabe, K. Terakura, *Phys. Rev. Lett.* **74**, 385 (1995).

[13] J. M. Longo, M. Katoch, and J. B. Goodenough, *J. Appl. Phys.* **39**, 1377 (1967).

[14] A. Kanamori, *J. Phys. Soc. Jpn.* **41**, 1876 (1976).

5.1-5 References

- [1] J. W. Bray, H. R. Hart, Jr., L. V. Interrante, I. S. Jacobs, J. S. Kasper, G. D. Watkins, S. H. Wei and J. C. Bonner, *Phys. Rev. Lett* **35**, 744 (1975).
- [2] F. D. M. Haldane, *Phys. Rev. Lett.* **50**, 1153 (1983).
- [3] M. Hase, I. Terasaki and K. Uchinokura, *Phys. Rev. Lett.* **70**, 3651 (1993).
- [4] J. P. Renard, M. Verdaguer, L. P. Regnault, W. A. C. Erkelens, J. Rossat-Mignod and W. G. Stirling, *Europhys. Lett.* **3**, 945 (1987).
- [5] M. Isobe and Y. Ueda, *J. Phys. Soc. Jpn.* **65**, 1178 (1996).
- [6] J. W. Bray, H. R. Hart, Jr., L. V. Interrante, I. S. Jacobs, J. S. Kasper, G. D. Watkins, S. H. Wei and J. C. Bonner, *Phys. Rev. Lett.* **35**, 744 (1975).
- [7] S. Huizinga, J. Kommandeur, G. A. Sawatzky, B. T. Thole, K. Kopinga, W. J. M. de Jonge and J. Roos, *Phys. Rev. B* **19**, 4723 (1979).
- [8] M. Izumi, K. Nakazawa, and Y. Bando, *J. Phys. Soc. Jpn.* **67**, 651 (1998).
- [9] M. Izumi, K. Nakazawa, Y. Bando, Y. Yoneda and H. Terauchi, *Solid State Ionics* **108**, 227 (1998).
- [10] H. Tanaka, H. Tabata, M. Kanai and T. Kawai, *Physica B* **245**, 301 (1998).
- [11] J. M. Longo, P. M. Raccach and J. B. Goodenough, *J. Appl. Phys.* **39**, 1327 (1968).
- [12] A. Kanbayasi, *J. Phys. Soc. Jpn.* **41**, 1876 (1976).

- [13] C. L. Chen, Y. Cao, Z. J. Huang, Q. D. Jiang, Z. Zhang, Y. Y. Sun, W. N. Kang, L. M. Dezeneti, W. K. Chu, and C. W. Chu, *Appl. Phys. Lett.* **71**, 1047 (1997).
- [14] R. A. McKee, F. J. Walker, J. R. Conner, E. D. Specht and D. E. Zelmon, *Appl. Phys. Lett.* **59**, 782 (1991).
- [15] H. Tabata, H. Tanaka and T. Kawai, *Appl. Phys. Lett.* **65**, 1970 (1994).
- [16] K. Ueda, H. Tabata and T. Kawai, *Phys. Rev. B* **60**, R12561 (1999).
- [17] M. Itoh, M. Shikano and T. Shimura, *Phys. Rev. B* **51**, 16432 (1995).

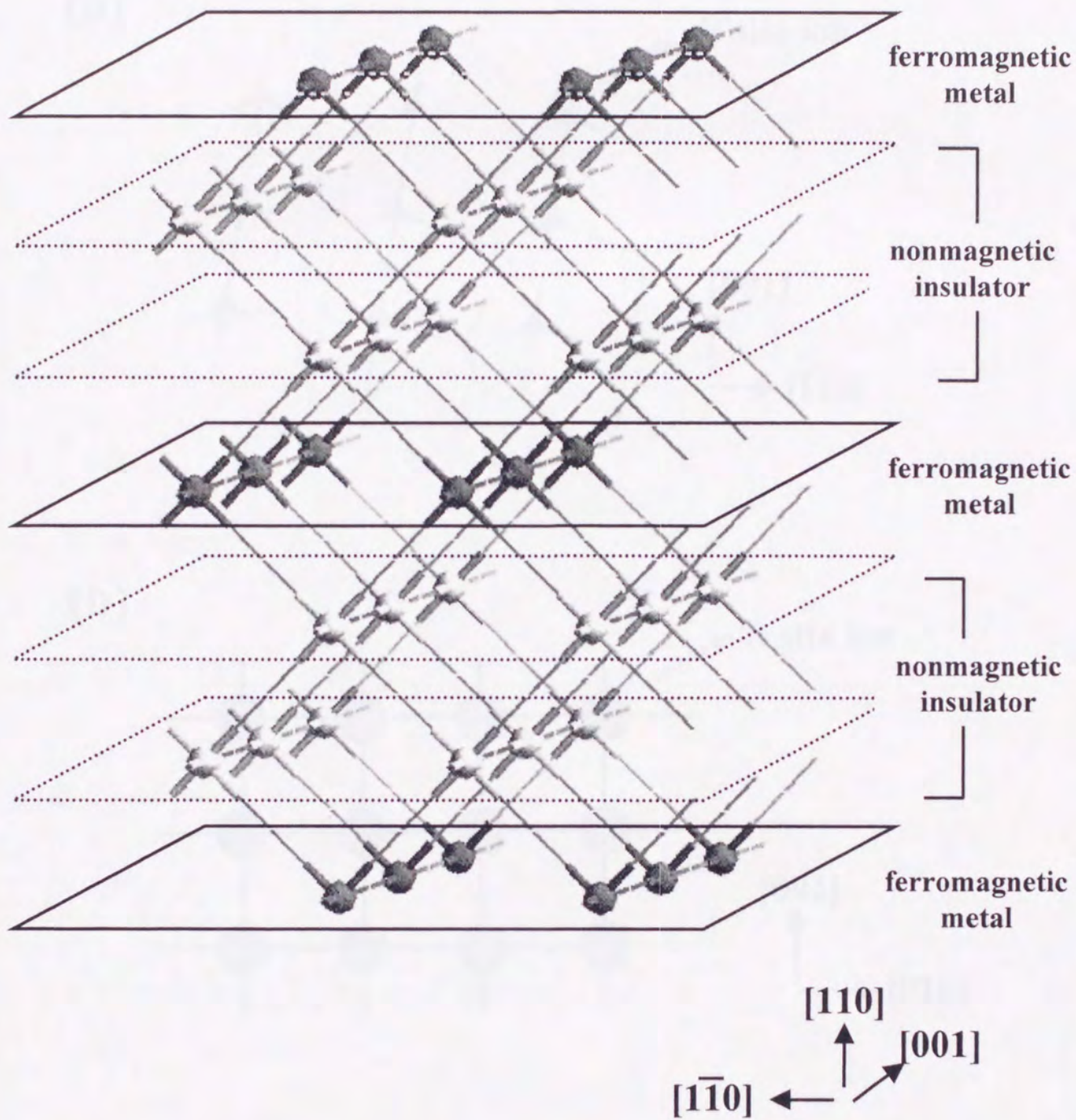
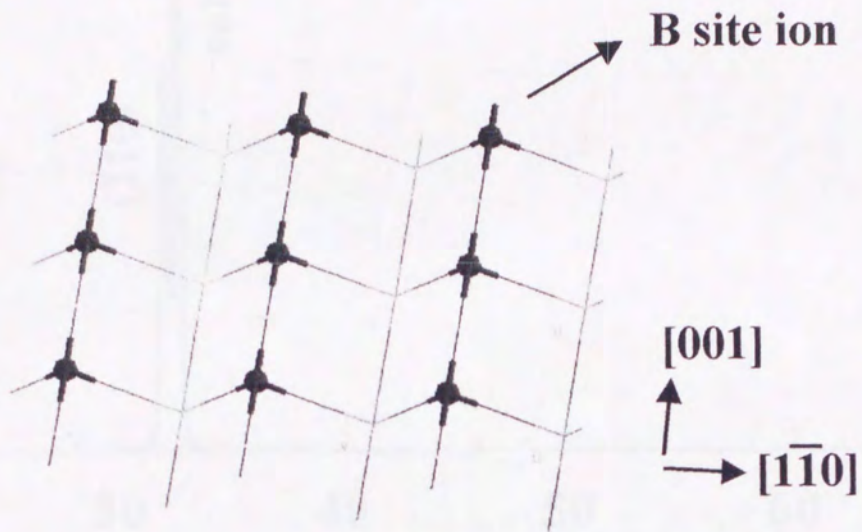


Fig. 5-1 : Schematic illustration for the construction of the perovskite type one dimensional magnet in the artificial superlattice formed on the (110) substrate.

(a)



(b)

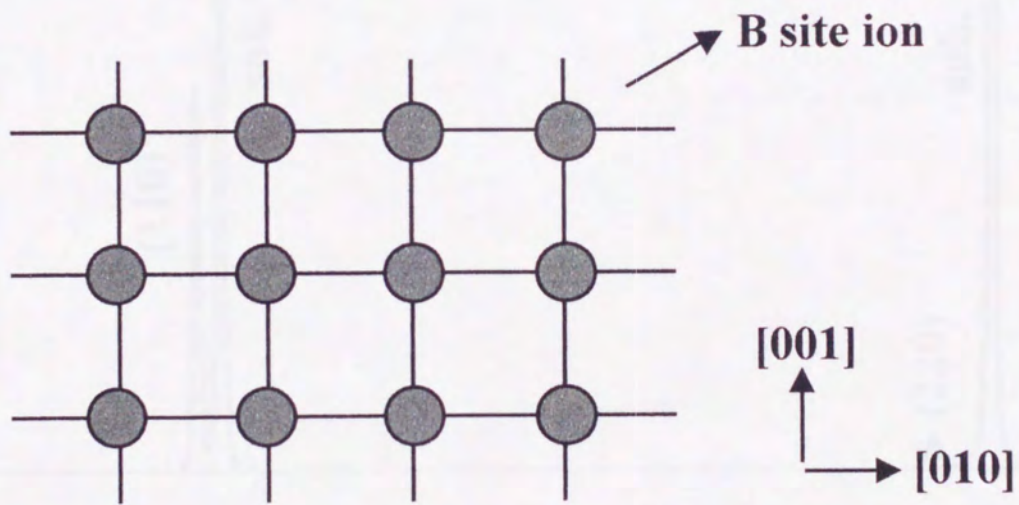


Fig. 5-2 : The structure of (a) (110) and (b) (100) surfaces of the perovskite-type oxides.

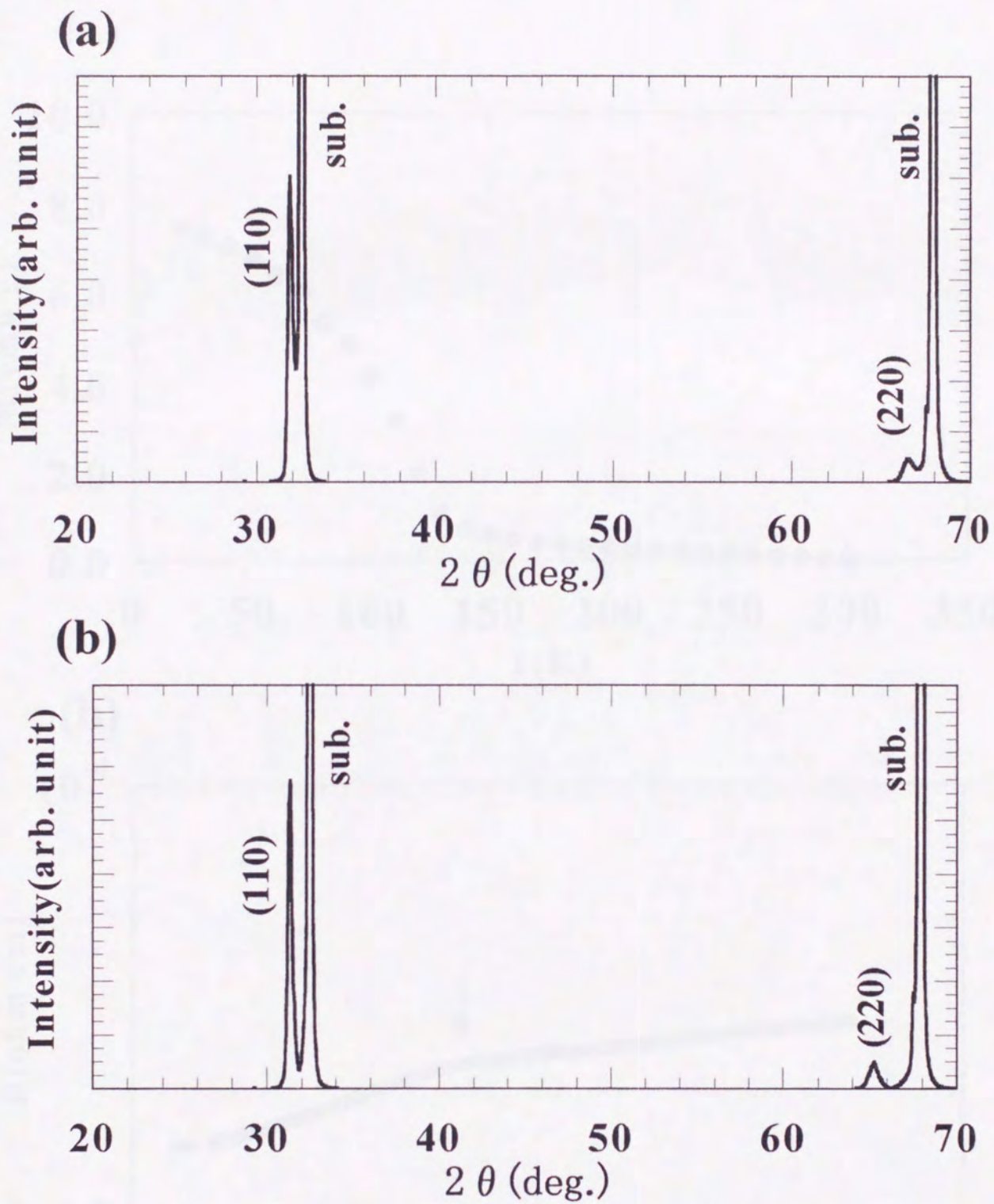


Fig. 5-3 : The XRD-patterns of (a) SrRuO₃ and (b) BaTiO₃ single phase film on the SrTiO₃ (110) substrate.

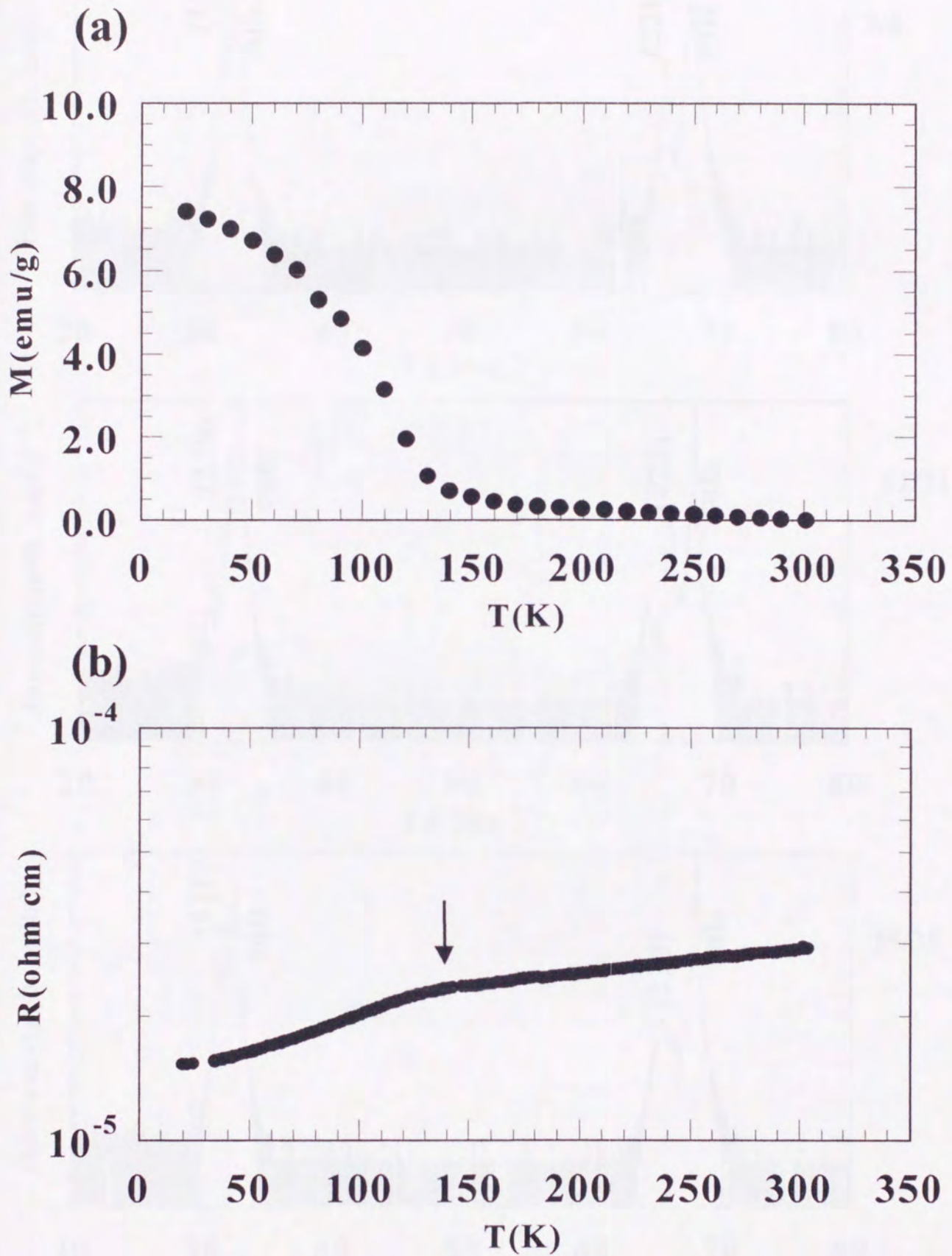


Fig. 5-4 : The (a) magnetization vs. temperature curve and (b) resistivity vs. temperature curve of SrRuO₃ film on the SrTiO₃ (110) substrate.

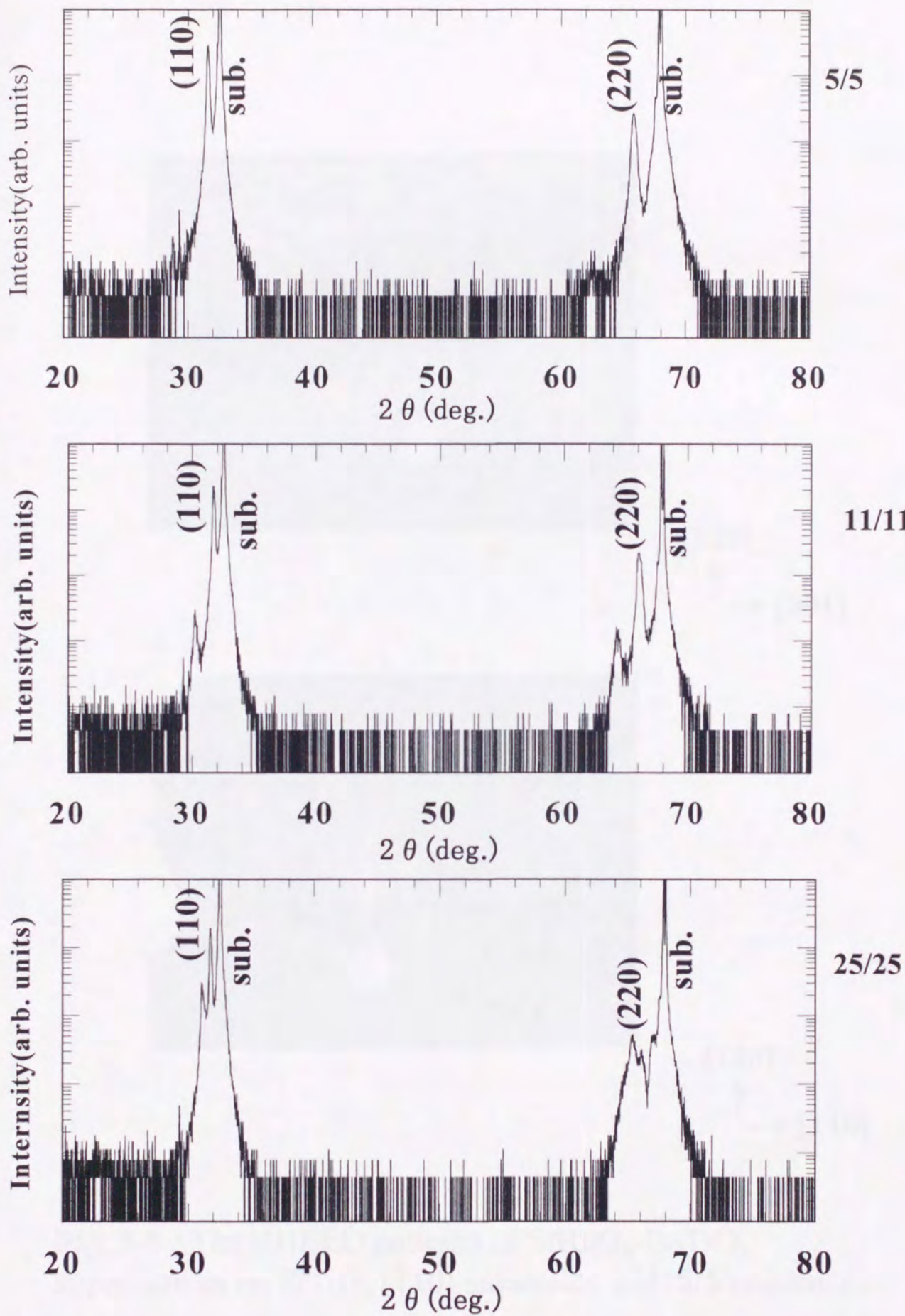
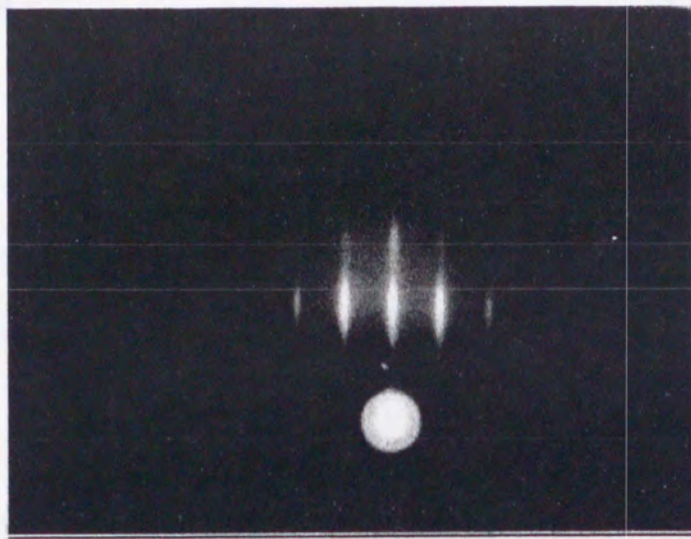
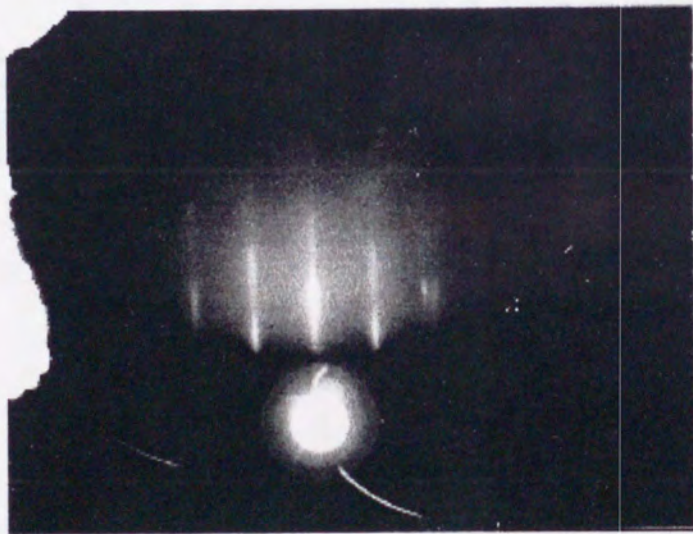


Fig. 5-5 : The XRD patterns of SrRuO₃-BaTiO₃ superlattices on SrTiO₃ (110) substrates with (a) 5/5, (b) 11/11 and (c) 25/25 sequences.



[110]
 ↑
 → [001]



[110]
 ↑
 → [11̄0]

Fig. 5-6 : The RHEED patterns of SrRuO₃-BaTiO₃ superlattices on SrTiO₃ (110) substrates with 5/5 sequences.

(a)

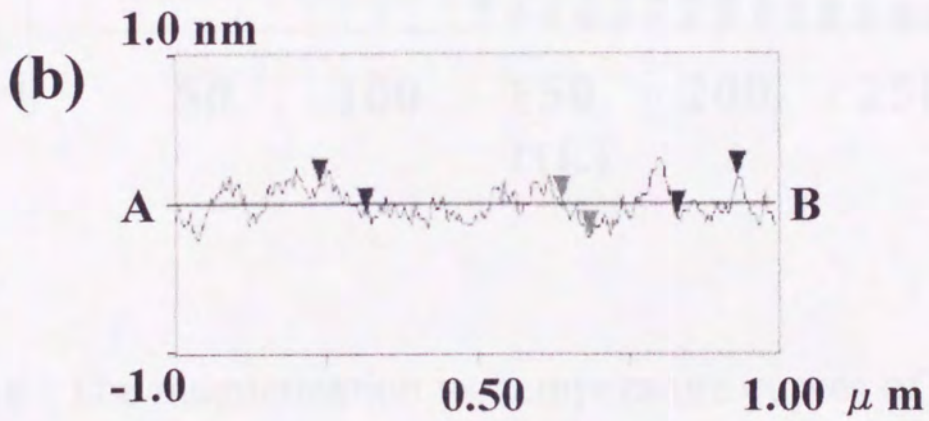
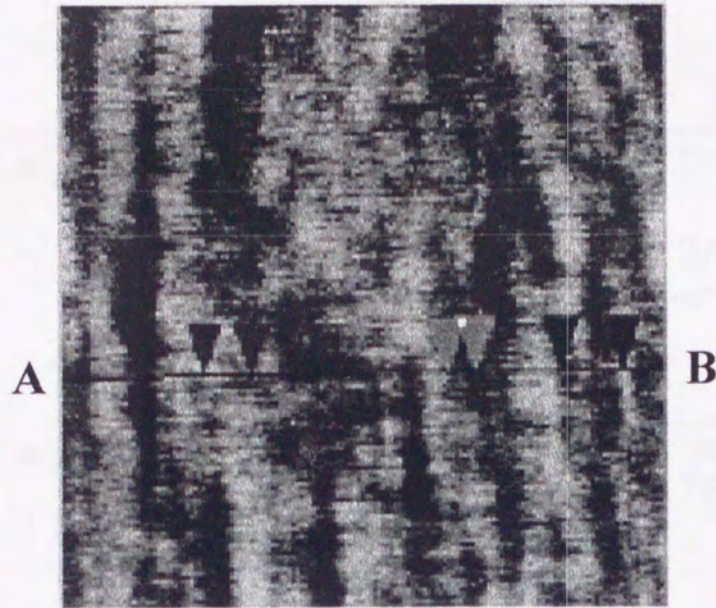


Fig. 5-7 : The (a) AFM image and (b) cross-sectional view of $\text{SrRuO}_3\text{-BaTiO}_3$ superlattices on SrTiO_3 (110) substrates with 5/5 sequences (scanning area : $1 \mu\text{m} \times 1 \mu\text{m}$).

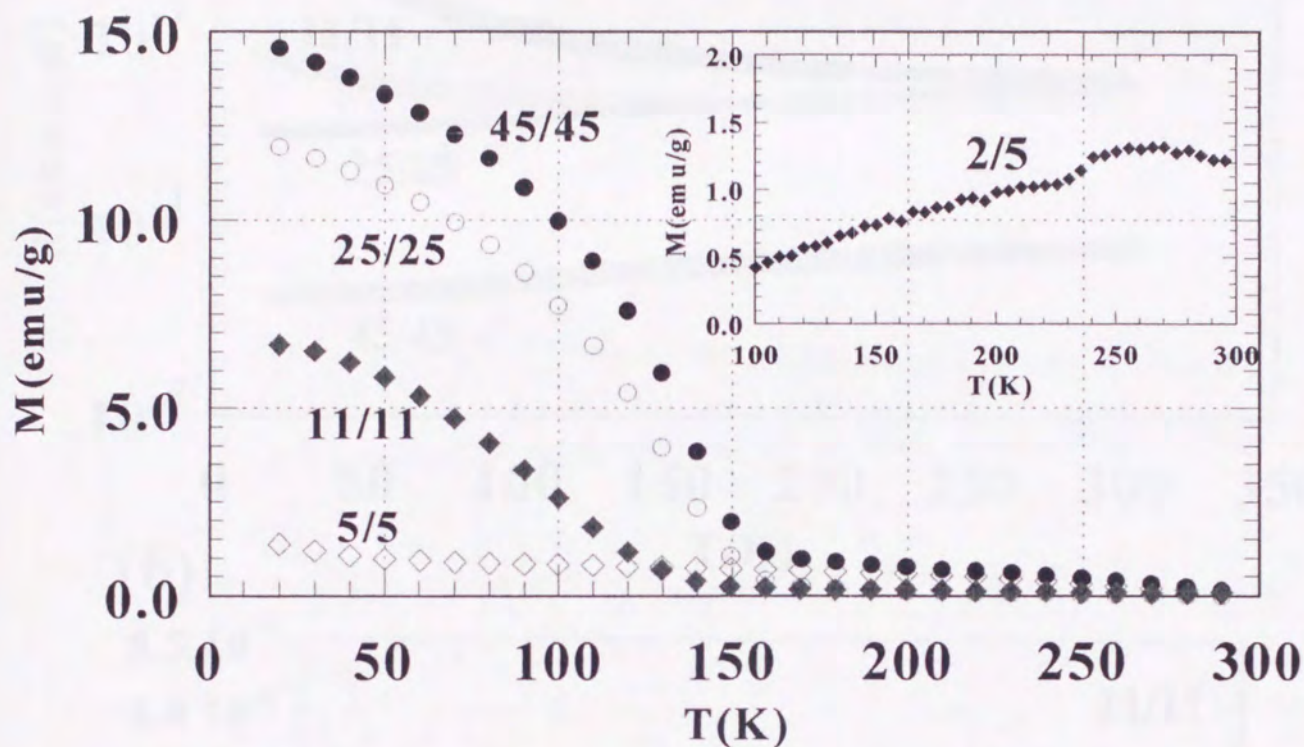


Fig. 5-8 : The magnetization vs. temperature curves of SrRuO_3 - BaTiO_3 superlattices formed on SrTiO_3 (110) substrates with various stacking sequences (5/5, 11/11, 25/25, 45/45). The magnetic field of 0.2 T was applied parallel to the film ($\langle 001 \rangle$ direction). The inset shows the M-T curve of the 2/5 superlattice in the field of 1 T.

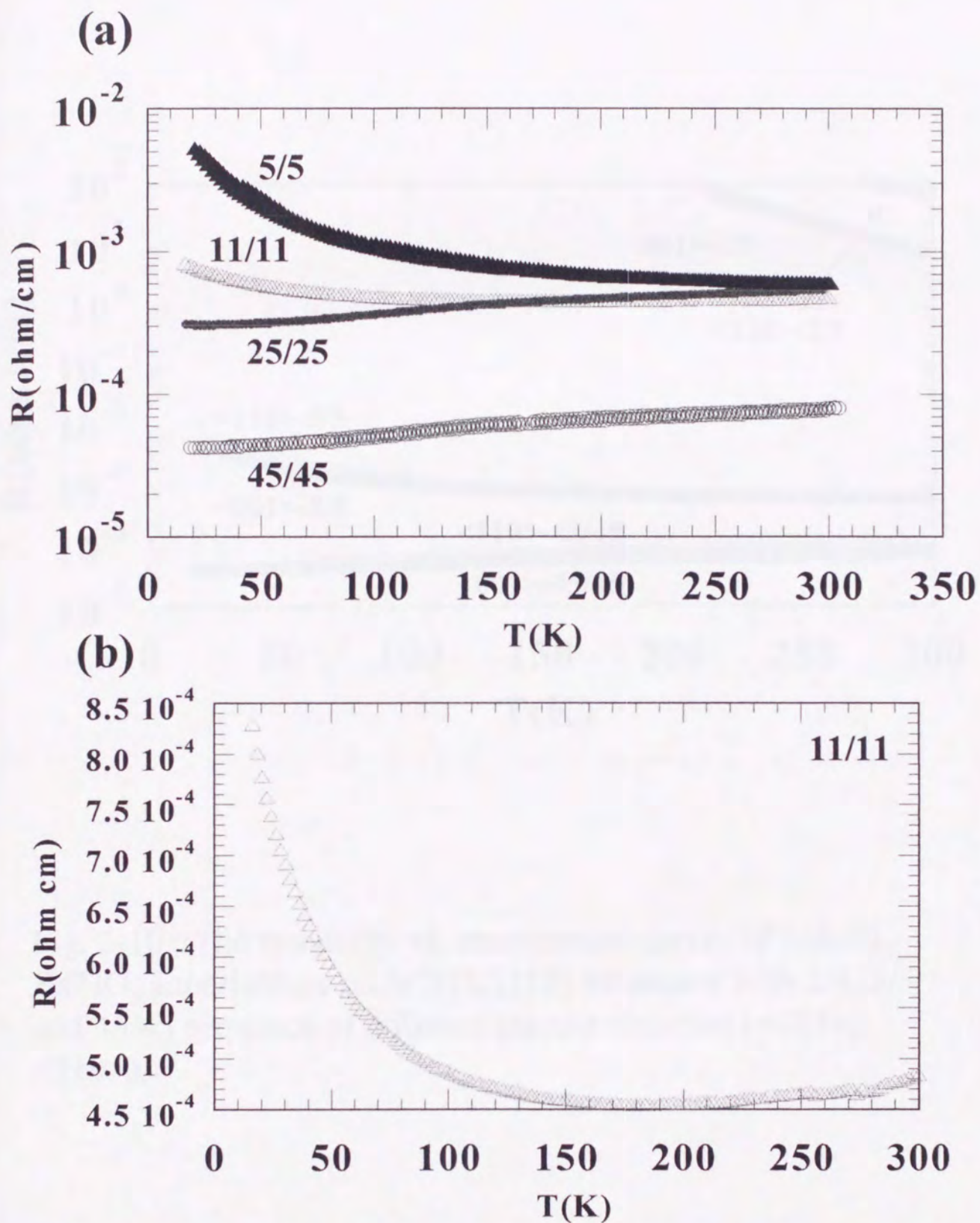


Fig. 5-9 : (a) The resistivity vs. temperature curves of SrRuO₃-BaTiO₃ superlattices on SrTiO₃ (110) substrates with various stacking sequences (5/5, 11/11, 25/25, 45/45). The current flow direction is $\langle 001 \rangle$. Figure (b) shows the enlargements of the figures of the 11/11 superlattice.

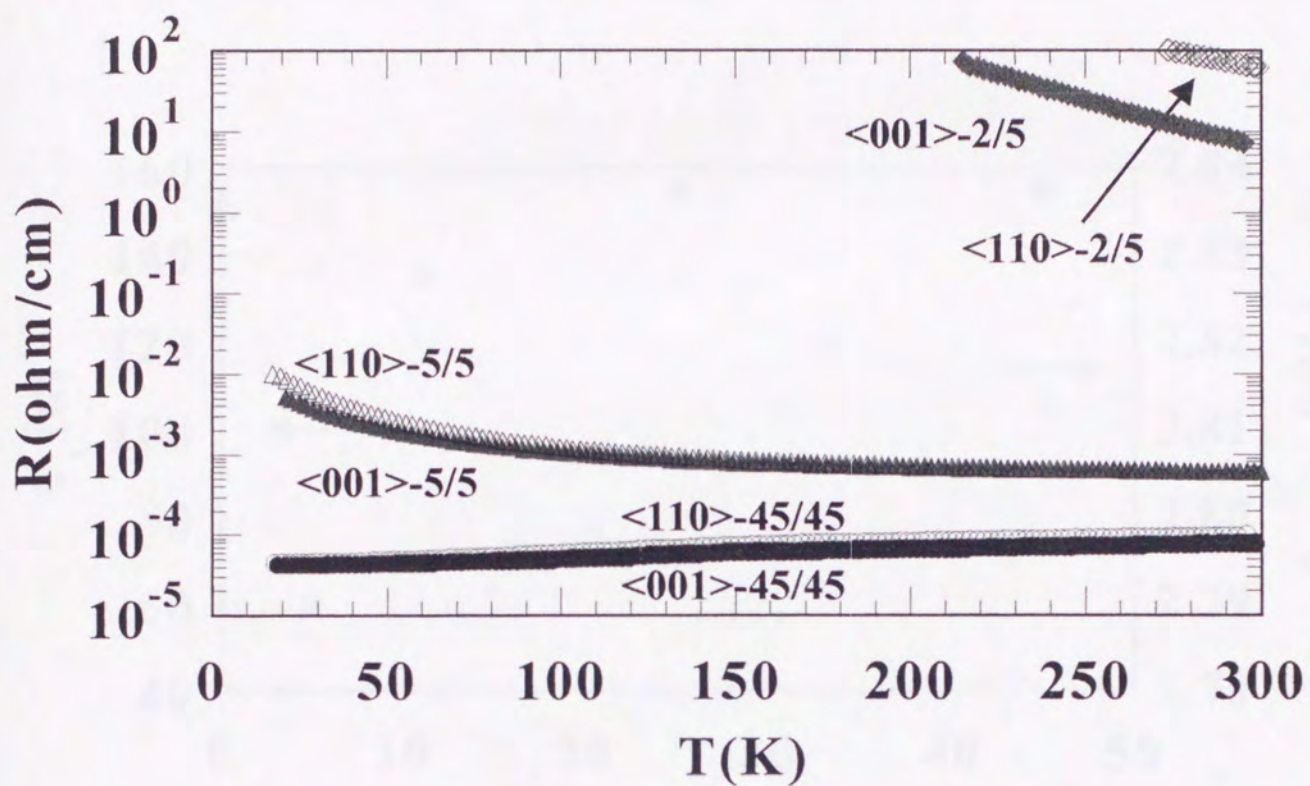


Fig. 5-10 : The resistivity vs. temperature curves of SrRuO_3 - BaTiO_3 superlattices on SrTiO_3 (110) substrates with 2/5, 5/5 and 45/45 sequence of different current direction ($\langle 001 \rangle$, $\langle 110 \rangle$).

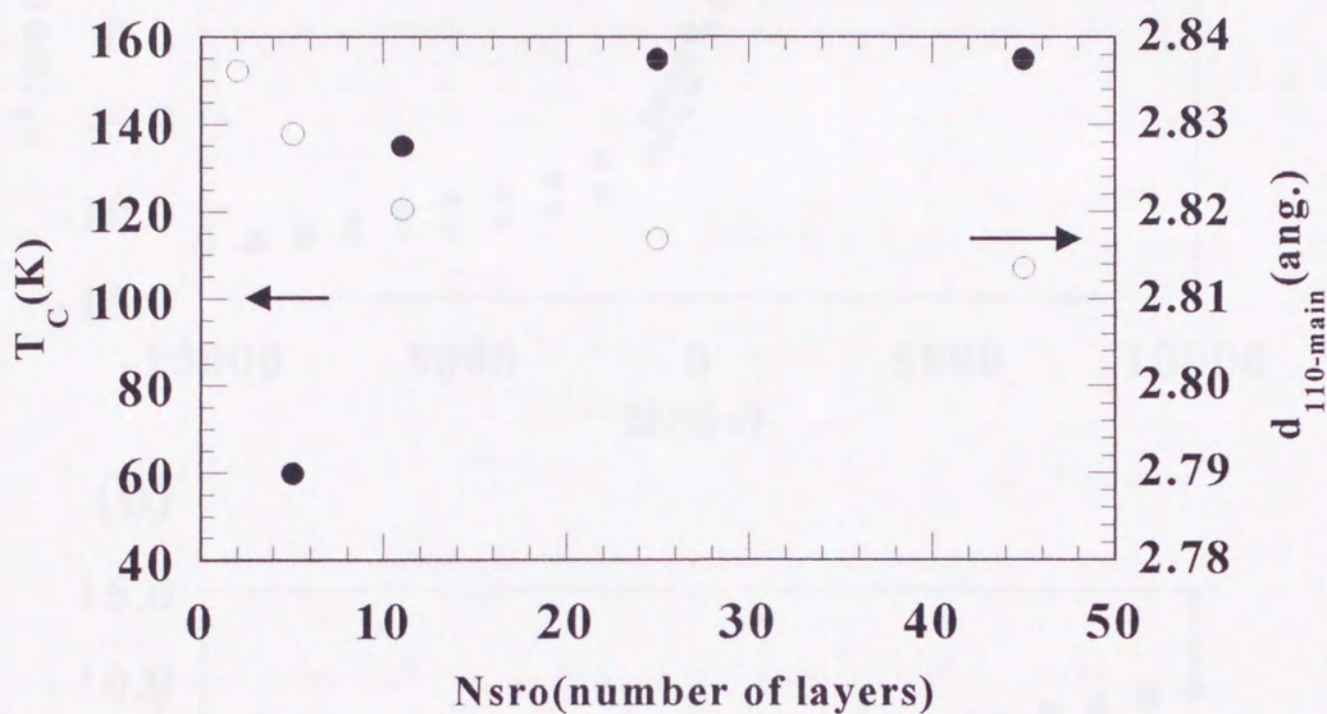


Fig. 5-11 : The lattice constants (d -value of (110)) and the Curie temperature (T_c) against the number of SrRuO_3 layers of each superlattice are plotted.

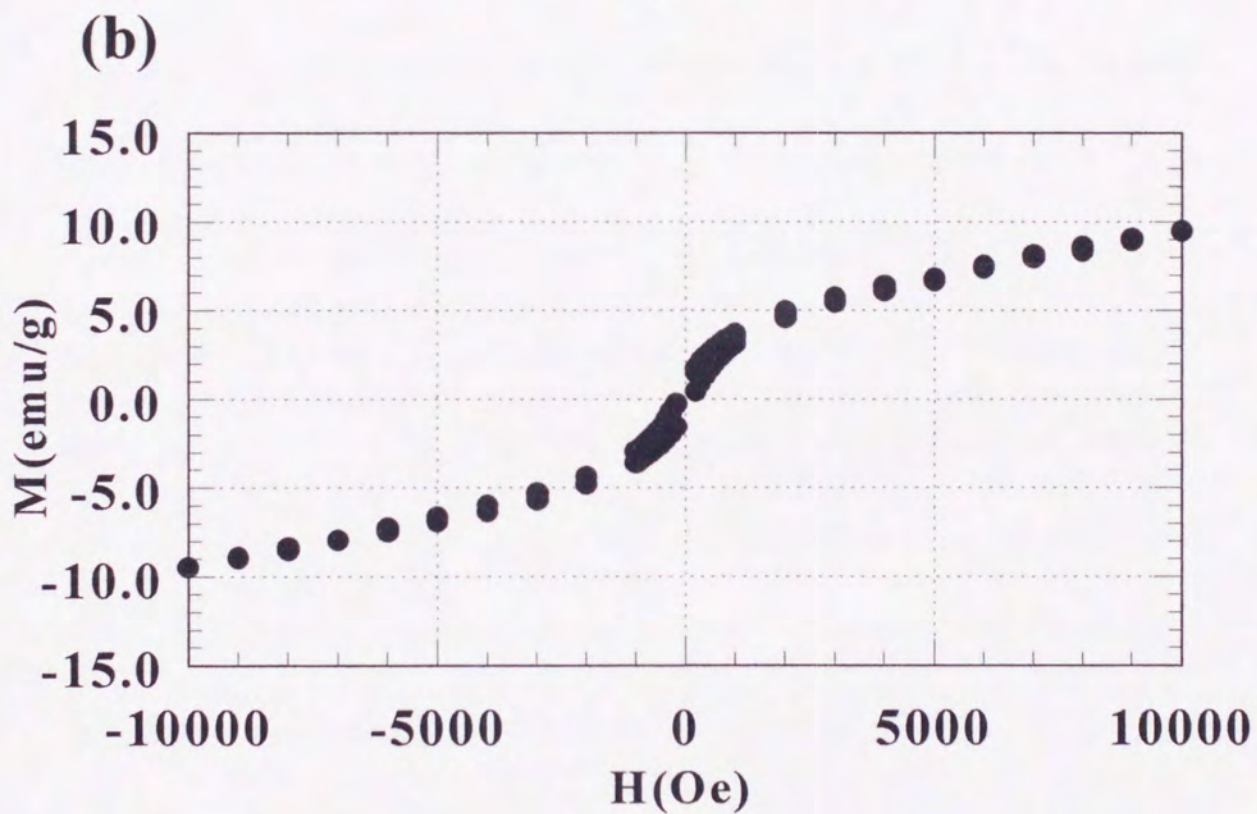
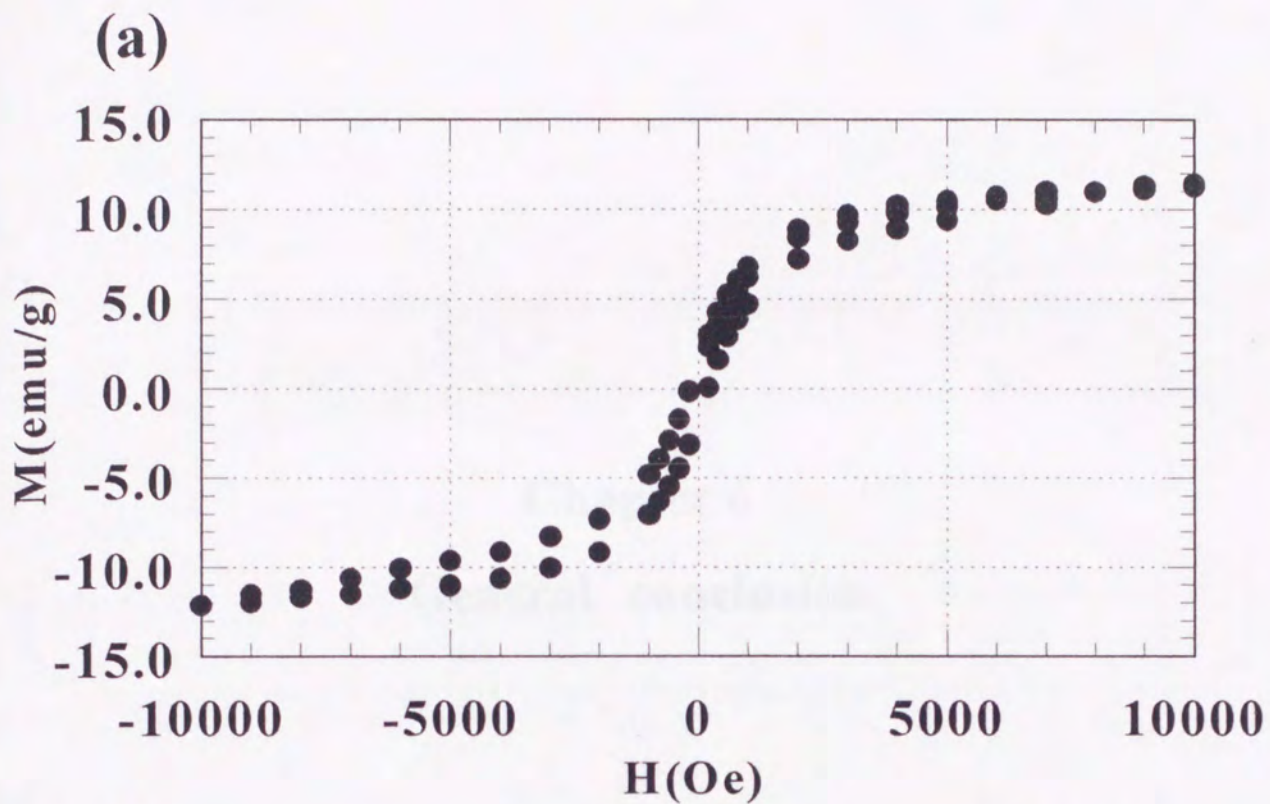


Fig. 5-12 Hysteresis curves of (a) SrRuO₃ and (b) SrRuO₃-BaTiO₃ superlattice with 5/5 sequence on SrTiO₃(110). The magnetic field is applied parallel to the <001> direction

Chapter 6

General conclusion

6 General Conclusion

The artificial superlattices of perovskite-type transition metal oxides (ABO_3) have been formed by a pulsed laser deposition (PLD) technique combined with the control of the stacking direction by the selection of the surface of the substrate [(100), (111) (110)]. Their physical properties can be controlled by managing the arrangement of B-site ions in my works. Especially, magnetic superlattices have been well studied in my works.

In chapter 3, the attempt to construct new magnetic materials ($LaFeO_3$ - $LaCrO_3$ superlattices) using the method of the artificial superlattice combined with the control of stacking directions was described. Antiferromagnetic behaviors were observed in all the films deposited on (100) and (110) substrates and the T_N changed systematically as the stacking periodicity changed. The superlattice on a (111) substrate with 1/1 sequence, on the other hand, exhibited ferromagnetic character. Though the total number of Fe and Cr ions are same in (100), (110) and (111) superlattices, quite different magnetic character can be created in the artificial superlattices.

In chapter 4, the concept of artificial introduction of spin frustration was proposed. The artificial superlattices of ferromagnetic $LaMnO_3$ and antiferromagnetic $LaFeO_3$ were constructed on $SrTiO_3$ (111), (100) and (110) substrates and their magnetic

properties were compared. The magnetization of superlattices constructed on the (111) plane increased as the stacking periodicity decreased, and the superlattice with 1/1 stacking periodicity exhibited ferromagnetic (or ferrimagnetic) behavior. In the case of the superlattices formed on the (100) and (110) surfaces, on the other hand, the spin frustration was introduced by the spin competition at the interface of ferromagnetic LaMnO_3 and antiferromagnetic LaFeO_3 layers. And spin-glass-like behaviors was observed in superlattices with a stacking periodicity of less than 3/3. The control of the strength of the spin frustration is possible by the control of stacking sequence and direction. In the case of (110) superlattices, the strength of the spin frustration effect was about roughly twice as large as that of the (100) superlattice.

In chapter 5, the proposal for its formation of low dimensional (one-dimensional) perovskite-type magnetic materials by means of the artificial superlattice on (110) substrate was given. The artificial superlattices of ferromagnetic SrRuO_3 and nonmagnetic BaTiO_3 were formed on SrTiO_3 (110) substrates with various stacking periodicity and their magnetic and electric properties were examined. The ferromagnetic and metallic features of SrRuO_3 collapsed from 11 layers. Specially, the antiferromagnetic behaviors and anisotropy of resistivity were observed in the 2/5 superlattice. It is thought that the behaviors are due to the complex effect of low

dimensionality of SrRuO₃ layers and lattice strain effects the interfaces of SrRuO₃ and BaTiO₃. I believe the low-dimensional magnetic materials will be formed by this method freely in the near future.

In my studies, various types of perovskite-type magnetic superlattices were formed using PLD method combined with the control of staking direction. The concept of the control of the staking direction has never been performed in perovskite-type superlattices in the previous reports. The variation of materials design in the field of perovskite-type superlattices have been enlarged by the method. It is thought that the novel materials with various atomic arrangements and physical properties are fabricated by the method successively.

3.1. Coexistence of ferroelectricity and ferromagnetism in BiFeO_3 -
 BaTiO_3 thin films at room temperature

(2001) BiFeO_3 thin films have been synthesized on SrTiO_3 (STO) by
the pulsed laser deposition technique and their structural properties have been investigated.

The ferroelectric hysteresis loops were measured at room temperature with

$\text{P} \sim \text{E}$ and $\text{M} \sim \text{H}$ characteristics. The ferroelectric
development of thin layers and the magnetic properties were studied in detail.

The dielectric constant of the films decreased with increasing film
thickness below 100 nm. The magnetic hysteresis loops of the films, on the other
hand, decreased with increasing thickness.

Chapter 7

Appendix

7.1. Introduction

Transition metal oxides have become focus for variety of physical
properties. MnO , TiO_2 , Fe_3O_4 , etc. have been well known for their ferroelectricity
and used as variously various applications. On the other hand, LaMnO_3 , NiMn_2O_4 ,
 TiMn_2O_4 , etc. have well studied for their colossal magnetoresistance (CMR) properties.
Unfortunately, however, these oxides have been studied independently so far. The
ferroelectric and ferromagnetic materials are very interesting not only for applications,
but also from the view point of material science. It will be expected to form a new
type material by combination of ferroelectric and ferromagnetic materials. For
example, if it possible to make the system where in which the magnetic properties

7.1 Coexistence of ferroelectricity and ferromagnetism in BiFeO₃-BaTiO₃ thin films at room temperature

(Bi_{0.7} Ba_{0.3}) (Fe_{0.7} Ti_{0.3})O₃ films have been constructed on Nb-doped SrTiO₃ (100) by the pulsed-laser deposition technique, and their physical properties have been examined. The films exhibit both ferroelectricity and ferromagnetism (weakferromagnetism) with $P_r=2.5 \mu\text{ C/cm}^2$ and $M_r=0.2 \text{ emu/g}$ at room temperature. The film-thickness dependence of their magnetic and electric properties (size effect) is also discussed simultaneously. The dielectric constants of the films decrease with reducing film-thickness below 1000 Å. The magnetic Curie temperature of the films, on the other hand, does not change at all down to 250 Å.

7.1-1 Introduction

Perovskite type transition metal oxides have treasure boxes for variety of physical properties. Pb(Zr, Ti)O₃, BaTiO₃, etc. have been well known for their ferroelectricity and used as nonvolatile memory applications. On the other hand, (La, Sr)MnO₃, Tl₂Mn₂O₇, etc. have well studied for their colossal magnetoresistance (CMR) properties. Unfortunately, however, these materials have been studied independently so far. The ferroelectric and ferromagnetic materials are very interesting not only for applications but also from the view point of material science. It will be expected to form a new type memory by combination of ferroelectric and ferromagnetic materials. For example, it is possible to make the memory device in which the magnetic properties

changed by lattice strain effect of ferroelectric materials.

It has been reported that perovskite type bulk materials, such as BiFeO_3 [1], shows ferroelectricity and ferromagnetism (ferrimagnetism, weakferromagnetism) simultaneously [2-3]. But, a few results on thin films which shows both ferromagnetism and ferroelectricity have been reported. Fujii et al. formed the solid solution film of BiFeO_3 , which shows both weakferromagnetism and ferroelectricity, and BaTiO_3 (or $\text{Pb}(\text{Zr}, \text{Ti})\text{O}_3$), one of typical perovskite type ferroelectric materials, and examined physical properties of the film [4-5]. As deposited BiFeO_3 - BaTiO_3 solid solution film was amorphous like and the film became polycrystalline after annealing treatment. Coexistence of ferromagnetism and ferroelectricity was observed in the film. Fe_2O_3 - Bi_2O_3 - PbTiO_3 solid solution amorphous films were formed by the same group and the coexistence of both ferromagnetism and ferroelectricity was also confirmed [6-7]. But, these films are amorphous like and the origin of ferromagnetism and ferroelectricity is not distinct for unclearness of their crystal structures.

In this study, (001) oriented $(\text{Bi}_{0.7}\text{Ba}_{0.3})(\text{Fe}_{0.7}\text{Ti}_{0.3})\text{O}_3$ films were formed on Nb doped SrTiO_3 (100) substrates by the pulsed-laser deposition technique and their physical properties were examined. Materials with crystalline phase such as oriented films are desirable to clarify the origin of ferromagnetic and ferroelectric properties. And, the film-thickness dependence of dielectric and magnetic properties (size effect) was also studied.

7.1-2 Experimental

All the films were formed on Nb-doped (0.5 wt%) SrTiO_3 (100) substrates by the pulsed-laser deposition technique. The laser was operated in ArF excimer

(wavelength : 193 nm) with an energy density of 0.5 J/cm². (Bi_{0.7} Ba_{0.3}) (Fe_{0.7} Ti_{0.3})O₃ targets were synthesized by mixing proper molar ratio of Bi₂O₃, Fe₂O₃ and BaTiO₃ powders (10-mol % of Bi₂O₃ with respect to bismuth in BiFeO₃ was supplemented to compensate the evaporation loss) and sintering at 670°C for 24 hours with intermediate grinding. BaTiO₃ powder was added into BiFeO₃ to reduce a leakage current of films. All films were formed at 570°C in an oxygen/ozone (8%) ambient pressure of 3mTorr with the deposition rate was 10-20 Å/min, and post annealed at 450°C for 1 hour under flowing O₂. The lattice parameters of the films were measured using 2θ - θ X-ray diffraction and four circle X-ray diffraction methods. Electric properties, such as the dielectric constant and loss tangent, were measured using impedance analyzer (Hewlett Packard; 4194A). Nb-doped SrTiO₃ (100) substrates are used as bottom electrode and the upper Ag electrode was formed by vacuum evaporation. Ferroelectric hysteresis loops were observed using Sawyer-Tower circuit of our own made. Magnetic measurements were performed using a SQUID magnetometer (Quantum design MPMS-5S) with the magnetic field applied parallel to the film plane.

7.1-3 Results and Discussion

Figure 7-1 shows X-ray diffraction pole figure scan and φ-scan for (111) planes of a (Bi_{0.7} Ba_{0.3}) (Fe_{0.7} Ti_{0.3})O₃ film with 1000 Å in thickness. Only four sharp peaks are observed showing the film has very good in-plane variation.

The frequency variation (100 Hz to 1 MHz) of the dielectric constants (ε_r) and loss tangent (tan δ) of the (Bi_{0.7} Ba_{0.3}) (Fe_{0.7} Ti_{0.3})O₃ film (2000 Å) are shown in Fig. 7-2. The ε_r and tan δ do not show remarkable change in the whole frequency range and

show almost constant value of 56 and 1.5 %, respectively.

Figure 7-3 (a) shows the dielectric hysteresis loop of $(\text{Bi}_{0.7}\text{Ba}_{0.3})(\text{Fe}_{0.7}\text{Ti}_{0.3})\text{O}_3$ film (3000 Å) at room temperature. Clear hysteresis behavior indicates ferroelectric character of the film. The remanant polarization (P_r) is $2.5 \mu\text{C}/\text{cm}^2$ and coercive field (E_C) is 533 kV/cm. (Ferroelectric properties of the BaTiO_3 film, prepared using the same technique to confirm the adequacy of the large E_C , were measured to be one-fifth of that of $(\text{Bi}_{0.7}\text{Ba}_{0.3})(\text{Fe}_{0.7}\text{Ti}_{0.3})\text{O}_3$ film. BiFeO_3 films also show clear hysteresis, and P_r is $4.0 \mu\text{C}/\text{cm}^2$ and E_C is 20 kV/cm, respectively [8].) The observed E_C is very large compared to other ordinary perovskite-type ferroelectric materials such as BaTiO_3 though the $(\text{Bi}_{0.7}\text{Ba}_{0.3})(\text{Fe}_{0.7}\text{Ti}_{0.3})\text{O}_3$ films have good crystallinity and no impurity phase. Therefore, it is speculated that the large E_C is caused by following two reasons. One is that the E_C of ferroelectric materials including Pb or Bi are generally large, and the other is that the increasing of the number of ferroelectric domain boundaries which restricts reversing of polarization.

Magnetic hysteresis curve of the film is shown in Fig. 7-3 (b). Clear hysteresis is observed at room temperature, too. The saturation magnetization (M_s) of the film is estimated to be 2 emu/g ($\approx 0.1 \mu_B/\text{site}$) from hysteresis curve measured at 6 K. The origin of small M_s is unclear.

It was tried to find the valence numbers of B-site ions, such as Fe and Ti, using the X-ray photoelectron spectroscopy (XPS) measurements. The valence number of Ti ions was found to be almost 4+ (binding energy : 458.4 eV). Two kinds of valence numbers, 2+ (binding energy : 709.4 eV) and 3+ (binding energy : 710.9 eV), were observed for Fe ions. It seems that Fe ions have two different valence numbers because of the

oxygen deficiency.

There are two possible explanations for the origin of spontaneous magnetization below 380K. One is magnetic interactions between Fe^{3+} - Fe^{2+} and the other is weakferromagnetism of BiFeO_3 . But, more experiments are needed to clarify the origin of ferromagnetism.

The results described above show that ferroelectricity and ferromagnetism (weakferromagnetism) coexist simultaneously in the film at room temperature. Coexistence of ferroelectricity and ferromagnetism in the same material give us the possibility to form a new type memory. Furthermore, we can discuss the physical properties such as ferroelectricity and ferromagnetism at the same time.

Thickness dependence of the ferroelectric and ferromagnetic properties (size effect) was also measured in the $(\text{Bi}_{0.7}\text{Ba}_{0.3})(\text{Fe}_{0.7}\text{Ti}_{0.3})\text{O}_3$ films. The thickness of the film is varied from 250 to 3000 Å. The dielectric constants (ϵ_r) and magnetic Curie temperatures (T_c) of the films with different thickness (250-3000 Å) were compared and the a and c-axis lattice constants were estimated from the X-ray measurements (2θ - θ scan and ϕ -scan). These results are exhibited in Fig. 7-4. The ϵ_r decreases remarkably with reducing the thickness when the film-thickness becomes thinner than 1000 Å (Fig. 7-4(a)). On the other hand, the ferromagnetic T_c keeps almost constant values in the whole thickness range (Fig. 7-4(b)). The a-axis lattice constant decrease and c-axis lattice constant increase with decreasing the thickness (Fig. 7-4(c)).

The size effect of ferroelectric films such as BaTiO_3 etc. were studied by many researchers from theoretical and experimental points of view [9-12]. Some possible explanations were proposed such as the lattice stress effects due to the lattice mismatch

in the interface [13] and the layer effects between a substrate and a film which has a low dielectric constant [14]. In bismuth-based layer-structured ferroelectric system, we have reported that the size effects also exist even in the case when the above-mentioned two effects were removed [15]. It was emphasized that the surface effect is also important in the paper.

In this letter, the size effect of ferroelectricity and ferromagnetism has been interpreted mainly from the viewpoint of the lattice stress effect. But, we think that the decreasing of ϵ_r and constant value of the magnetic Curie temperatures are originated from the both lattice stress and surface effect.

Yano et al. said that the size effect of BaTiO₃ thin film is caused by two-dimensional stress due to the lattice mismatch between substrate and film [13]. Behaviors of ϵ_r in our system are very similar to their results. We also think that the uniaxial lattice stress cause the size effect for ϵ_r . On the other hand, as for magnetic interactions, the effect for decrease of lattice constant *a* and increase of *c* are almost cancelled out and *T_C* show almost constant values.

7.1-4 Conclusion

In summary, we have fabricated (Bi_{0.7} Ba_{0.3}) (Fe_{0.7} Ti_{0.3})O₃ solid solution films by pulsed-laser ablation technique. The films exhibit both ferroelectricity and ferromagnetism (weakferromagnetism) above room temperature. Clear ferroelectric and ferromagnetic hysteresis loops were observed. The *P_r* is 2.5 μC/cm² and *E_C* is 533 kV/cm, and the residual magnetization (*M_r*) is 0.2 emu/g and coercive field (*H_C*) is 200 Oe, respectively. Film-thickness dependence of electric and magnetic properties

7.1-5 References

- [1] Yu. E. Roginskaya, Yu. N. Venevtsev and G. S. Zhdanov, *J. Exp. Theor. Phys.*, **44**, 1418 (1963).
- [2] Yu. E. Roginskaya, Yu. N. Venevtsev and G. S. Zhdanov, *Sov. Phys. JETP* **21**, 817 (1965).
- [3] G. A. Smolenskii and I. E. Chupis, *Sov. Phys. Usp.* **25**, 475 (1982).
- [4] S. Shimizu, S. Jinzenji, A. Kajima, T. Miyama and T. Fujii, *IEEE Trans. J. Mag. Jpn.* **10**, 912 (1987).
- [5] T. Fujii, S. Jinzenji, Y. Asahara, A. Kajima and T. Shinjo, *J. Appl. Phys.* **64**, 5434 (1988).
- [6] A. Kajima, T. Kaneda, H. Ito, T. Fujii and I. Okamoto, *J. Appl. Phys.* **70**, 3760 (1991).
- [7] A. Kajima, T. Kaneda, H. Ito, T. Fujii and I. Okamoto, *J. Appl. Phys.* **69**, 3663 (1991).
- [8] Extended Abstracts (The 58th Autumn Meeting 1997), The Japan Society of Applied Physics 558.
- [9] Y. Yano, K. Iijima, Y. Daitoh, T. Terashima, Y. Bando, Y. Watanabe, H. Kasatani and H. Terauchi, *J. Appl. Phys.* **76**, 7833 (1994).
- [10] T. Hayashi, N. Oji and H. Maiwa, *Jpn. J. Appl. Phys* **33**, 5277 (1994).
- [11] W. L. Zhong, Y. G. Wang, P. L. Zhang and B. D. Qu, *Phys Rev. B* **50**, 698 (1994).
- [12] W. L. Zhong, B. D. Qu, P. L. Zhang and Y. G. Wang, *Phys Rev. B* **50**, 12375 (1994).
- [13] Y. Yano, K. Iijima, Y. Daitoh, T. Terashima, Y. Bando, Y. Watanabe, H. Kasatani,

and H. Terauchi, J. Appl. Phys. **76**, 7833 (1994).

[14] N. Ichinose and T. Ogiwara, Jpn. J. Appl. Phys. **34**, 5198 (1995).

[15] M. Hamada, H. Tabata and T. Kawai, Jpn. J. Appl. Phys. **37**, 5174 (1998).



Fig. 7-1) XRD (a) pole figure and (b) θ -scans of $(\text{Bi}_{1-x}\text{Bb}_x)_2(\text{Ti}_{1-x}\text{Ti}_x)\text{O}_7$ film (1000 Å) on Nb-doped SrTiO_3 (100) substrate.

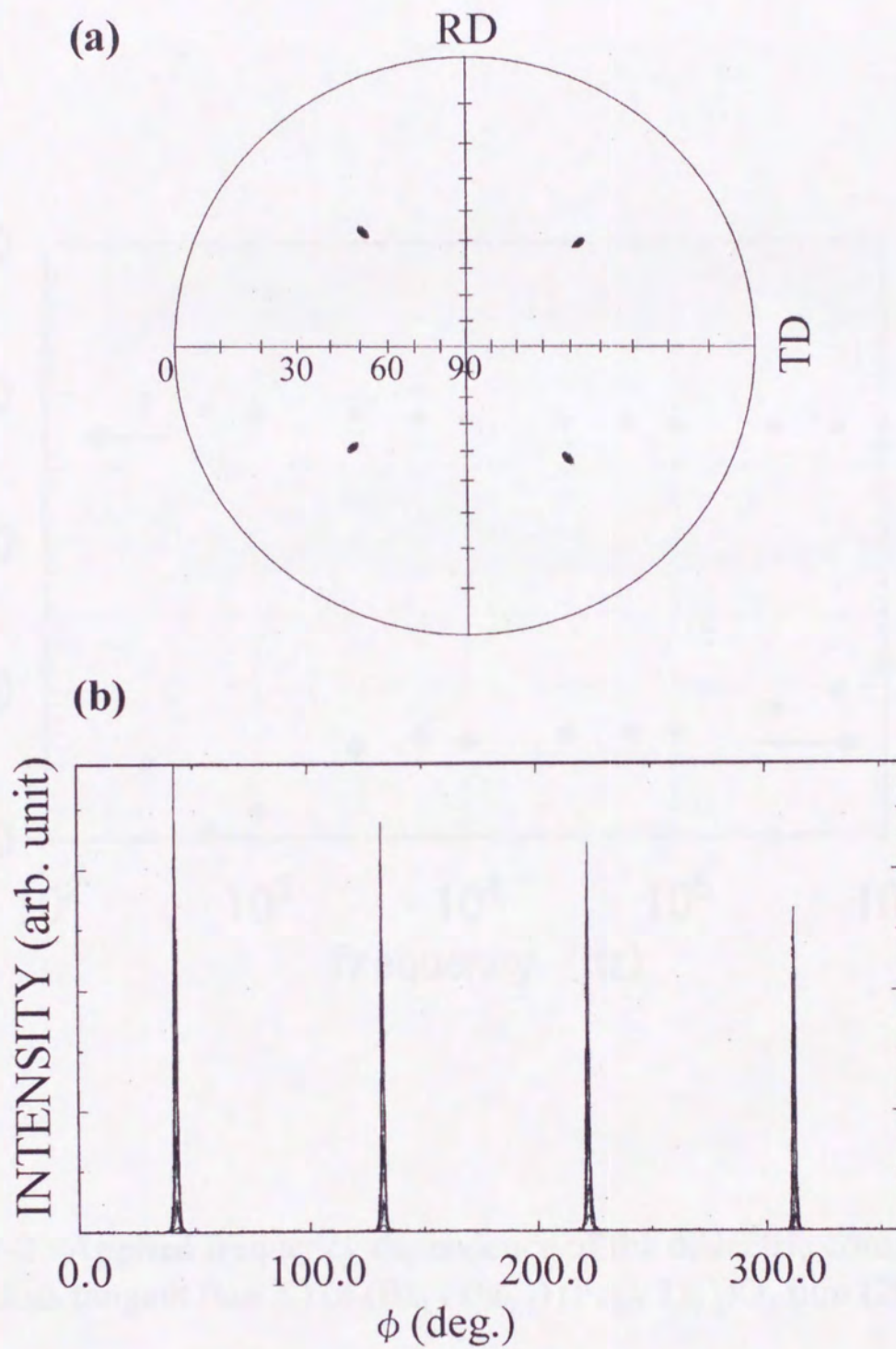


Fig. 7-1 : XRD (a) pole figure and (b) ϕ -scans of $(\text{Bi}_{0.7} \text{Ba}_{0.3})(\text{Fe}_{0.7} \text{Ti}_{0.3})\text{O}_3$ film (1000 \AA) on Nb doped $\text{SrTiO}_3(100)$ substrate.

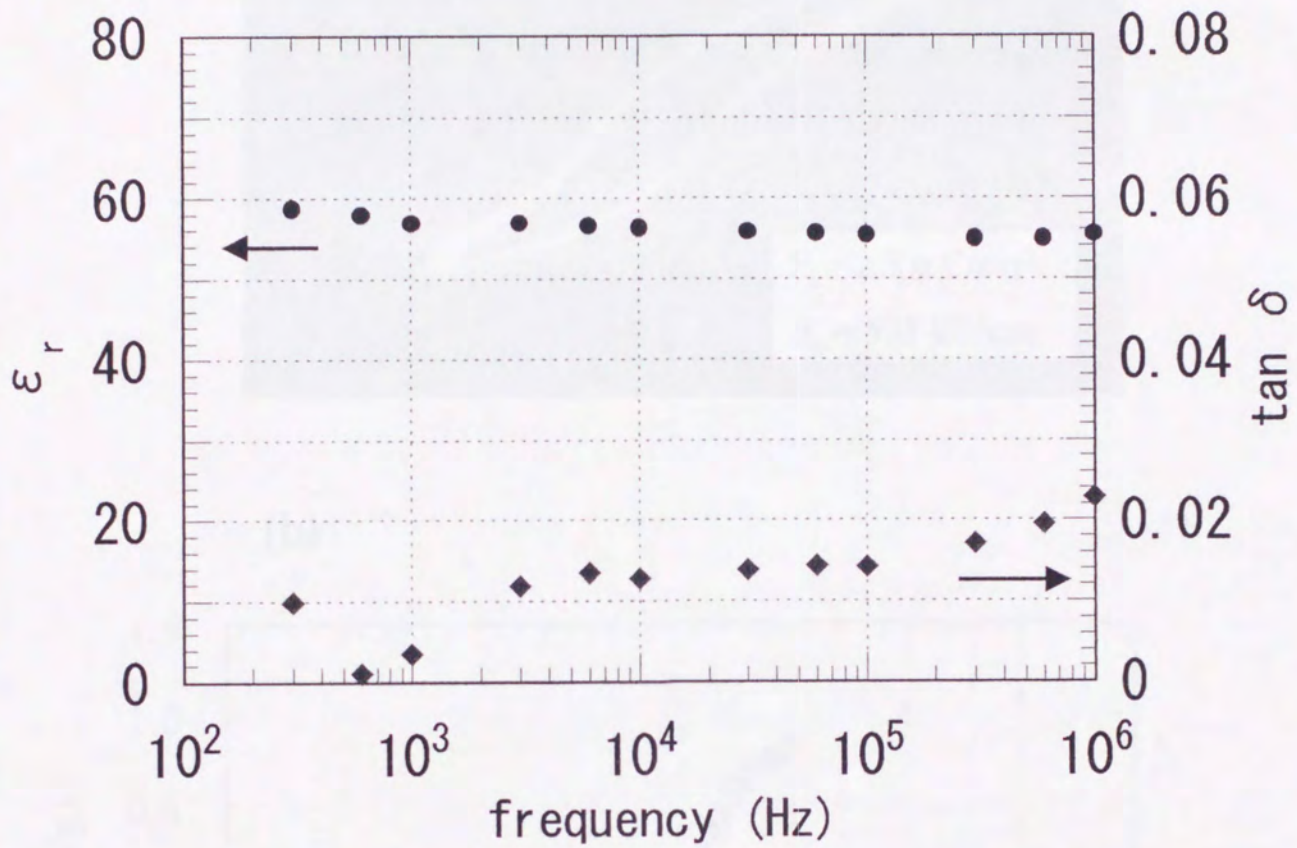
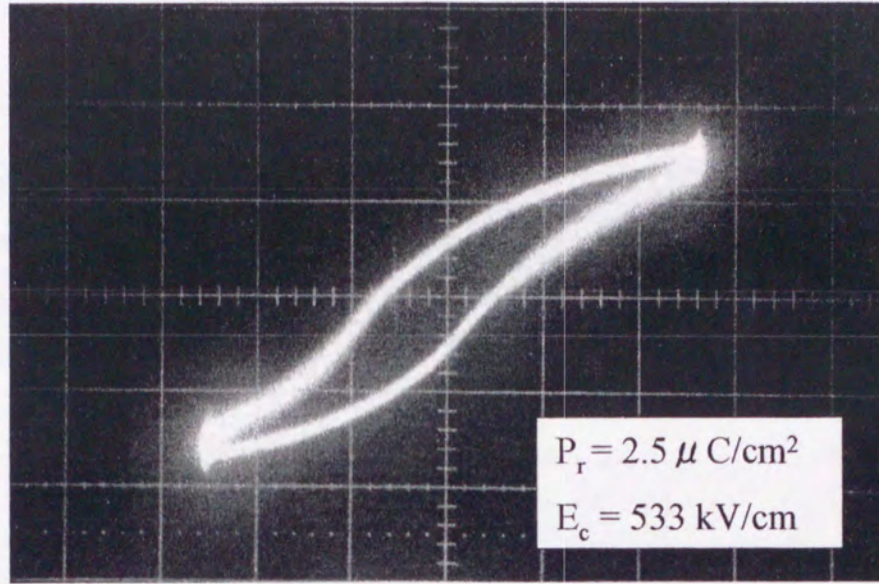


Fig. 7-2 : Applied frequency dependence of the dielectric constant (ϵ_r) and loss tangent ($\tan \delta$) of $(\text{Bi}_{0.7}\text{Ba}_{0.3})(\text{Fe}_{0.7}\text{Ti}_{0.3})\text{O}_3$ film (2000 Å).

(a)



(b)

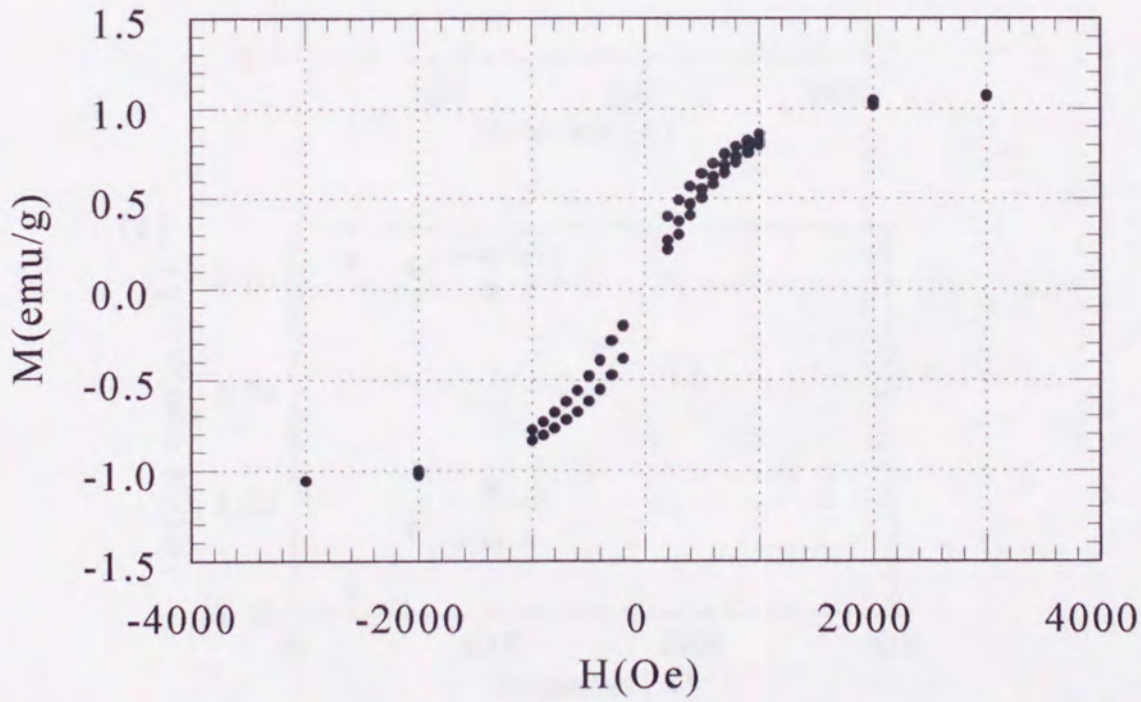


Fig. 7-3 : Electric-(a) and magnetic-(b) hysteresis curves of $(\text{Bi}_{0.7}\text{Ba}_{0.3})(\text{Fe}_{0.7}\text{Ti}_{0.3})\text{O}_3$ film (3000 Å) at room temperature. (a) $P_r=2.5 \mu \text{ C/cm}^2$, $E_c=533 \text{ kV/cm}$ (b) $M_r=0.2 \text{ emu/g}$, $H_C=200 \text{ Oe}$.

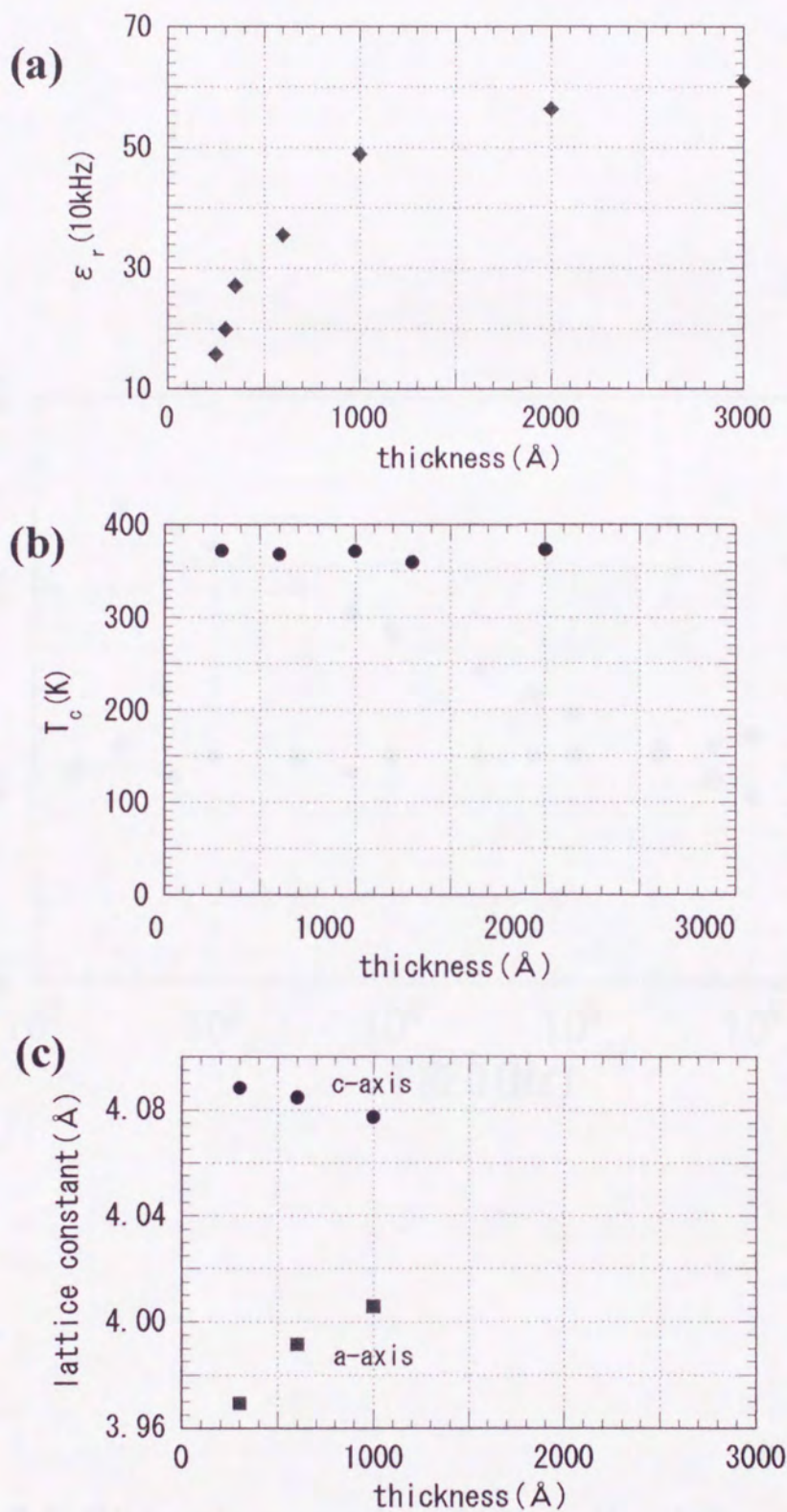


Fig. 7-4 : (a) Dielectric constant (ϵ_r), (b) magnetic Curie temperature (T_c) and (c) lattice constant (a-axis and c-axis) of $(\text{Bi}_{0.7}\text{Ba}_{0.3})(\text{Fe}_{0.7}\text{Ti}_{0.3})\text{O}_3$ film against the total film-thickness (250-3000 Å).

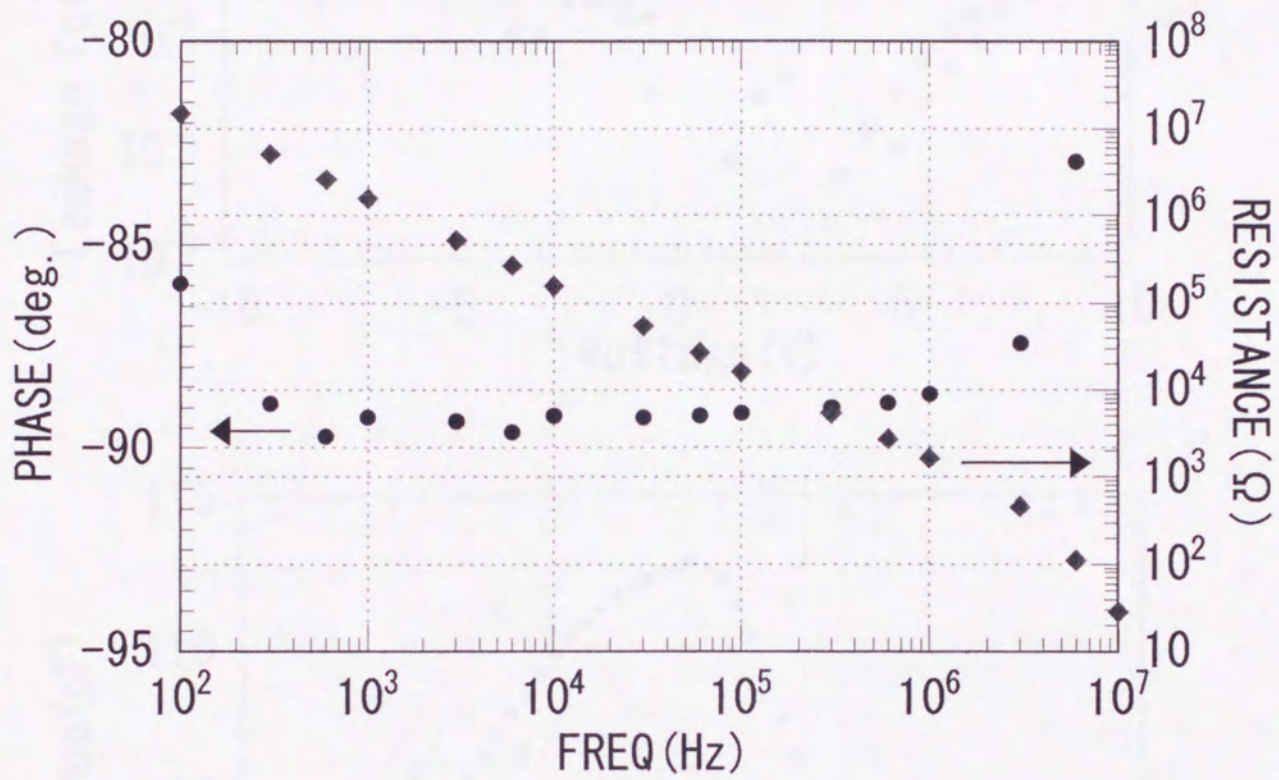


Fig. 7-5 Dielectric properties of $(\text{Bi}_{0.7}, \text{Ba}_{0.3})(\text{Fe}_{0.7}, \text{Ti}_{0.3})\text{O}_3$ film

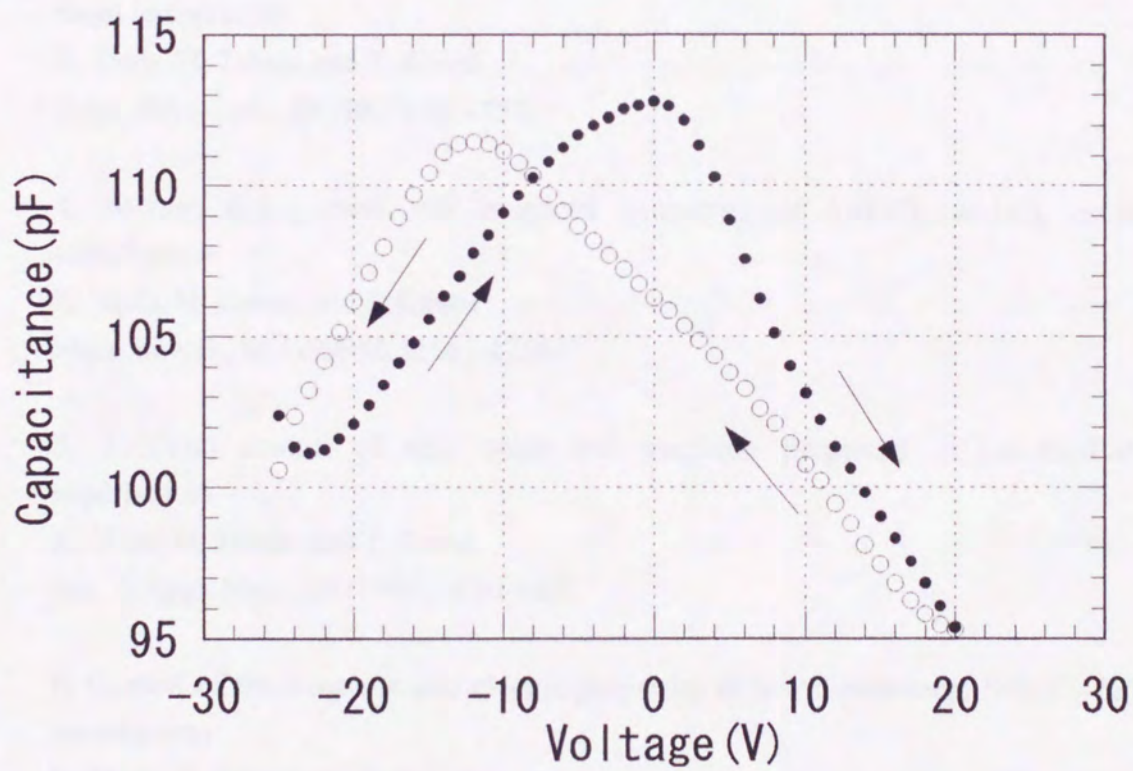
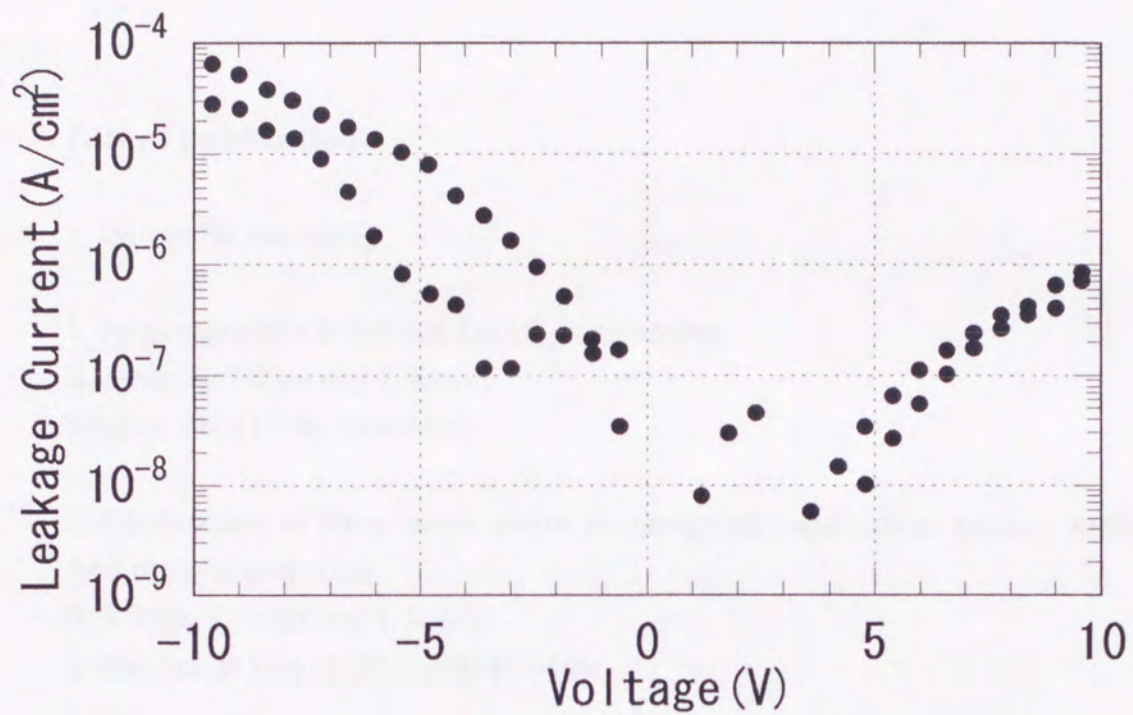


Fig. 7-6 I-V and C-V curves of $(\text{Bi}_{0.7}, \text{Ba}_{0.3})(\text{Fe}_{0.7}, \text{Ti}_{0.3})\text{O}_3$ film (2000 Å)

List of publications

[Scientific Journals]

1, Ferromagnetism in LaFeO_3 - LaCrO_3 superlattices

K. Ueda, H. Tabata and T. Kawai

Science, 280 (1998) 1064-1066.

2, Construction of ferroelectric and/or ferromagnetic superlattices by laser MBE and their physical properties

H. Tabata, K. Ueda and T. Kawai

J. Mat. Sci. & Eng. B, 56 (1998) 140-146.

3, Coexistence of ferroelectricity and ferromagnetism in BiFeO_3 - BaTiO_3 thin films at room temperature

K. Ueda, H. Tabata and T. Kawai

Appl. Phys. Lett., 75 (1999) 555-557.

4, Atomic arrangement and magnetic properties of LaFeO_3 - LaMnO_3 artificial superlattices

K. Ueda, H. Tabata and T. Kawai

Phys. Rev. B., 60 (1999) R12561-12564.

5, Artificial control of spin order and magnetic properties in LaCrO_3 - LaFeO_3 superlattices

K. Ueda, H. Tabata and T. Kawai

Jpn. J. Appl. Phys., 38 (1999) 6690-6693.

6, Control of the magnetic and electric properties of low dimensional SrRuO_3 - BaTiO_3 superlattices

K. Ueda, H. Tabata and T. Kawai

in submission

[Related works]

7, Magnetic properties of basic copper (II) formates

K. Ueda, S. Takamizawa, W. Mori and K. Yamaguchi

Mol. Cryst. Liq. Cryst., 286 (1996) 17-22

8, Calculation of magnetization by path integral method II

T. Kawakami, H. Nagao, K. Ueda, W. Mori and K. Yamaguchi

Mol. Cryst. Liq. Cryst., 286 (1996) 177-184.

9, Theoretical study and comparison with experiments for atacamite $\text{Cu}_2\text{Cl}(\text{OH})_3$

K. Ueda, S. Takamizawa, W. Mori S. Kubo and K. Yamaguchi

Mol. Cryst. Liq. Cryst., 306 (1997) 33-40.

[Proceedings]

1, Formation of ferroelectric/ferromagnetic functionally graded materials by Laser MBE and their physical properties

H. Tabata, H. Tanaka, K. Ueda and T. Kawai

Proc. of 9th Functionally Graded Materials Symp., (1997) 247-252.

2, Formation of ferromagnetic/ferroelectric superlattices by a laser MBE and their electric and magnetic properties

H. Tabata, K. Ueda and T. Kawai

Mater. Res. Soc. Proc., 494 (1998) 201-212.

3, Brain mimetic and the super five sense sensors formed by the combination of ferroelectric materials

H. Tabata, H. Matsui, K. Ueda and T. Kawai

The 4th Int. Conf. On Intelligent Materials Proc., (1998) 266-267

4, Size effect of ferroelectric and ferromagnetic properties of Bi-based perovskite type materials

H. Tabata, K. Ueda and T. Kawai

Mater. Res. Soc. Proc. in press (1999).

International meeting

1, Creation of a new spin ordered state on magnetic artificial superlattice

K. Ueda, H. Tabata, T. Kawai

American Physical Society March Meeting, March 16-20, 1998, Los Angeles, California, USA

2, Size effect of ferroelectric and ferromagnetic properties of $(1-x)\text{BiFeO}_3-x\text{BaTiO}_3$

K. Ueda, H. Tabata, T. Kawai

American Physical Society March Meeting, March 16-20, 1998, Los Angeles, California, USA

3, Discovery of atomic order in $\text{LaMn}_{0.5}\text{Fe}_{0.5}\text{O}_3$ film

K. Ueda, Y. Muraoka, H. Tabata, T. Kawai

American Physical Society March Meeting, March 20-26, 1999, Atlanta, Georgia, USA

4, Atomic scale control of magnetic order in $\text{LaFeO}_3\text{-LaCrO}_3$ and $\text{LaFeO}_3\text{-LaMnO}_3$ superlattices

K. Ueda, Y. Muraoka, H. Tabata, T. Kawai

American Physical Society March Meeting, March 20-26, 1999, Atlanta, Georgia, USA

5, Preparation and magnetic properties of $\text{LaMnO}_3/\text{LaFeO}_3$ superlattices on LaAlO_3 substrates

Y. Muraoka, K. Ueda, H. Tabata, T. Kawai

American Physical Society March Meeting, March 20-26, 1999, Atlanta, Georgia, USA

Acknowledgements

The author expresses his appreciation and gratitude to Professor T. Kawai of Institute of Scientific and Industrial Research of Osaka University for his encouragement and continuous guidance throughout the course of this investigation.

The author is very grateful to Prof. H. Tabata of ISIR-sanken, Osaka University for his valuable discussions and helpful suggestion during the study.

The author gratefully acknowledge Professor K. Yamaguchi and Professor M. Sorai of Department of Chemistry, Osaka University for their helpful guidance and fruitful discussion for the thesis.

The author is very grateful to Prof. T. Matsumoto and Dr. Hidekazu Tanaka of ISIR-sanken, Osaka University for their valuable discussions and helpful suggestions during this study.

I am very grateful to Mr. Makiyama of for helpful advises on the management of SQUID measurement.

Thanks are due to Dr. Hiroyuki Tanaka and Dr. Y. Muraoka for their helpful discussions and encouragement.

The author would like to thank all the members of Kawai Lab. of ISIR-sanken, Osaka-University.

The author is thankful to Professor W. Mori of Kanagawa University, Professor S. Takeda of Gunma University, Dr M. Nakano and Dr. H. Nagao for their support and encouragement in the author's master's course days.

Finally, the author thanks his family and friends for their understanding of the study and their affection.

